



JIMMA UNIVERSITY
SCHOOL OF GRADUATE STUDIES
JIMMA INSTITUTE OF TECHNOLOGY

FACULTY CIVIL AND ENVIRONMENTAL ENGINEERING
STRUCTURAL ENGINEERING STREAM

BEHAVIOR OF SHORT REINFORCED CONCRETE COLUMN WITH
NON-ORTHOGONAL BI-AXIAL MOMENT

A Thesis Submitted to Graduate Studies of Jimma University in Partial Fulfillment of the
Requirements for the Degree of Master Science in Structural Engineering.

By: HORA TEREFE

AUGUST, 2022

JIMMA, ETHIOPIA

JIMMA UNIVERSITY
SCHOOL OF GRADUATE STUDIES
JIMMA INSTITUTE OF TECHNOLOGY
FACULTY CIVIL AND ENVIRONMENTAL ENGINEERING
STRUCTURAL ENGINEERING STREAM

**BEHAVIOR OF SHORT REINFORCED CONCRETE COLUMN WITH
NON-ORTHOGONAL BI-AXIAL MOMENT**

A Thesis Submitted to Graduate Studies of Jimma University in Partial Fulfillment of the
Requirements for the Degree of Master Science in Structural Engineering.

By: HORA TEREFE

Main Advisor: Dr. Kabtamu Getachew (PhD)

Co-Advisor: Engr. Ibrahim Kedir (Msc)


AUGUST, 2022

JIMMA, ETHIOPIA

JIMMA UNIVERSITY
JIMMA INSTITUTE OF TECHNOLOGY
POST GRADUATE PROGRAM

This is to certify that the thesis prepared by Hora Terefe entitled: *“Behavior of short reinforced concrete column with non-orthogonal biaxial moment and axial load”* and submitted in partial fulfillment of the requirements for the degree of masters of Science in Structural Engineering complies with the regulations of the university and meets the accepted standards with respect to the originality and quality.

Approved by the Examining Committee:

_____	_____	_____
Advisor	Signature	Date
Dr. Binaya Patnaik		12/09/2022
External Examiner	Signature	Date
_____	_____	_____
Internal Examiner	Signature	Date
_____	_____	_____
Chairman	Signature	Date

DECLARATION

I, the undersigned, declare that this thesis is my own work and all sources of material used for the thesis have been duly acknowledged. And it is also approved by my advisors.

Name: Hora Terefe

Signature: _____

Date: _____

Place: Jimma University, Jimma Institute of Technology

Advisors

Main advisor: Dr. Kabtamu Getachew (PhD)

Signature: _____

Date: _____

Co- advisor: Engr. Ibrahim Kedir (Msc)

Signature: _____

Date: _____

ACKNOWLEDGEMENT

Firstly, I would like to thank God for making me strong and patient enough to finish the thesis.

Next, I would like to express my gratitude to Jimma University Institute of Technology for supporting me financially. Then I would like to express my special thanks to my advisors, Dr. Kabtamu Getachew and Engr. Ibrahim Kedir, for their continuous advice and motivation.

Finally, I would like to thank my family for supporting me in all respects throughout the thesis work.

ABSTRACT

Currently, the building structures are constructed in different shapes to keep the functionality of the building. Due to this, the reinforced concrete column may be subjected to two beams that run in non-orthogonal ways (other than 90 degrees). However, there hasn't been enough research done on the behavior of this type of column. The purpose of this study is to investigate the behavior of a short non-orthogonal biaxially loaded reinforced concrete column. The FEA software, which is Abaqus 6.14, was used for this study. Before modelling of the specimen, the experimental study, which was done by Wang G.G. and Thomas Hsu C.T., was used as a benchmark experiment and used for validation. The FEA results agreed with the experimental results up to 84%. The concrete and steel properties, which were used for software input, were prepared and modelling of the specimen was done. The Abaqus standard was used for modelling of 270 column specimens, and Concrete damage plasticity for concrete and plastic, for steel models, was used in the material property definition. Both tie and embedded region constraints were used in the interaction module. Eccentricity, concrete grade, angle between the axis of the moment, shape of the column, force, and displacement were variables considered in this study. In which force and displacement were considered, as dependent variables and the remaining were independent.

As eccentricity increases from 10 to 50mm along both directions for a short non-orthogonal biaxially loaded reinforced concrete column, the load-carrying capacity of the column reduces by an average value of 8.9% and the deflection increases by an average value of 12%. When the angle between the axis of moment increases from 15° to 90°, the axial load-carrying capacity of column reduces by an average value of 1.014% and its deflection increases by an average value of 0.7342%. As the concrete grade increases from fck 20 to 30Mpa, the axial load-carrying capacity of non-orthogonal RC columns, within interval, by an average value of 11.31% and the deflection reduces by an average value of 2.27%. The axial load-carrying capacity of the non-orthogonal square RC column is higher than the rectangular by 1.44%, but the deflection is smaller by 0.516%. For non-orthogonal biaxial moment, the circular column axial load-carrying capacity is higher than square and rectangular by 0.192% and 1.66%, respectively. Therefore, a circular column is preferable to other shapes of columns.

Key words: *Eccentricity, Non-orthogonal, Biaxially loaded column, concrete grade, shape of column.*

Table of content

Contents

ACKNOWLEDGEMENT	iv
ABSTRACT	v
Table of content	vi
LIST OF TABLES	viii
LIST OF FIGURES	ix
Acronyms	xii
List of Notations	xiii
CHAPTER ONE	1
INTRODUCTION	1
1.1 Background of the study	1
1.2 Statement of the problem	2
1.3 Objective of the study	3
1.3.1 General objective	3
1.3.2 Specific objective	3
1.4 Significance of the study	3
1.5 Scope of the study	3
1.6 Organization of papers	3
CHAPTER TWO	5
RELATED LITERATURE REVIEW	5
2.1 General Overview	5
2.2 Behavior of short Bi-axially loaded Reinforced Concrete column	6
2.3 Curvature mode of Reinforced concrete column	9
2.4 Method of analysis of short Bi-axially loaded Reinforced concrete column	13
CHAPTER THREE	24
RESEARCH METHODOLOGY	24
3.1 General	24
3.2 Research Design	24
3.3 Study Variables	24
3.3.1 Dependent study variables	24
3.3.2 Independent Variables	25

3.4 Specimen selection.....	25
3.5 Nonlinear Finite Element Software.....	34
3.6 Modeling of Short RC column.....	35
3.6.1 Geometry.....	36
3.6.2 Material property.....	39
3.6.3 Part assembly and their Interaction.....	52
3.6.4 Analysis step.....	55
3.6.5 Boundary condition and Loading.....	55
3.6.6 Meshing.....	55
CHAPTER FOUR.....	57
4.1 Validation of Finite Element Modelling.....	57
4.1.1 Bench mark experiment.....	57
4.1.2 FE result.....	59
4.2 Results and Discussion.....	62
4.2.1 Influence of both directions the same eccentricity on short biaxial non-orthogonal RC column.....	62
4.2.2 Influence of angle between axis of moment on short biaxial non-orthogonal RC column.....	65
4.2.3 Influence of concrete grade on short biaxial non-orthogonal RC column.....	67
4.2.4 Influence of shape of column on short biaxial non-orthogonal RC column.....	69
CHAPTER FIVE.....	73
CONCLUSION AND RECOMMENDATION.....	73
5.1 Conclusion.....	73
5.2 Recommendation.....	74
REFERENCES.....	75
APPENDIX-A.....	80
LOAD-DISPLACEMENT CURVE.....	80
APPENDIX-B.....	105
INPUT DATA OF MATERIAL PROPERTY.....	105

LIST OF TABLES

Table 3. 1: Column specimen	25
Table 4. 1: properties of hardened concrete at 28 days (Mean strength of three specimens)...	58
Table B. 1: Material properties for Longitudinal and lateral reinforcement	105
Table B. 2: Material properties for concrete fck 20Mpa	106
Table B. 3: Material properties for concrete fck 25Mpa	107
Table B. 4: Material properties for concrete fck 30Mpa	108
Table B. 5: Material properties of concrete with fck 26.9Mpa for validation.....	109

LIST OF FIGURES

Figure 2. 1: Curvature modes of RC columns under end eccentric loading.....	10
Figure 2. 2: Deformed shape of all tested columns	12
Figure 2. 3: Vertical load versus lateral deflection for all tested columns.	13
Figure 2. 4: A typical axial force-biaxial bending moment interaction surface.	21
Figure 2. 5: Idealized strain distribution for generation of interaction surface	22
Figure 2. 6: Idealized strain and stress distribution of rectangular RC section.	22
Figure 3. 1: Chart shows the procedure of modeling.....	36
Figure 3. 2: 3D plain concrete part	37
Figure 3. 3: Steel plate for end of the column.	38
Figure 3. 4: Compressive stress-strain diagram of concrete.....	43
Figure 3. 5: Compressive stress-crushing strain diagram of concrete.....	44
Figure 3. 6: Compressive damage-crushing strain diagram of concrete.	46
Figure 3. 7: Tensile stress-cracking strain diagram of concrete.....	49
Figure 3. 8: Tensile damage variables-cracking strain diagram of concrete.	50
Figure 3. 9: Tensile stress-strain of longitudinal reinforcement.....	51
Figure 3. 10: True stress-plastic strain of longitudinal steel reinforcement.	52
Figure 3. 11: Assembled short reinforced concrete column using Abaqus for SA2e5C1	53
Figure 3. 12: Assembled longitudinal and lateral reinforcement using Abaqus for SA2e5C1	53
Figure 3. 13: Assembled short reinforced concrete column using Abaqus for CA2e5C1.....	54
Figure 3. 14: Assembled longitudinal and lateral reinforcement using Abaqus for CA2e5C1	54
Figure 3. 15: Descriti reinforced concrete column using Abaqus for SA2e5C1	56
Figure 3. 16: Descriticized reinforced concrete column using Abaqus for CA2e5C1	56
Figure 4.1:Compressive stress-crushing strain diagram of $f_{ck}=26.9\text{Mpa}$ concrete	59
Figure 4.2:Compressive damage-crushing strain diagram of $f_{ck}=26.9\text{Mpa}$ concrete.....	60
Figure 4.3:Tensile stress-cracking strain diagram of $f_{ck}=26.9\text{Mpa}$ concrete	60
Figure 4.4:Tensile damage variables-cracking strain diagram of $f_{ck}=26.9\text{Mpa}$ concrete	61
Figure 4.5: Comparison of FE load-displacement curve with experimental and analysis.	62
Figure 4.6: Load displacement curve for illustration of eccentricity.....	64
Figure 4.7: Load displacement curve for illustration of angle.....	67
Figure 4.8: Load displacement curve for illustration of angle.....	69
Figure 4.9: Load displacement curve for illustration of shape of column.....	72

Figure A. 1: Load displacement curve for square, fck=20Mpa ($\alpha=30$ deg.)	80
Figure A. 2: Load displacement curve for square, fck=25Mpa ($\alpha=30$ deg.)	80
Figure A. 3: Load displacement curve for square, fck=30Mpa ($\alpha=30$ deg.)	81
Figure A. 4: Load displacement curve for square, fck=20Mpa ($\alpha=45$ deg.)	81
Figure A. 5: Load displacement curve for square, fck=25Mpa ($\alpha=45$ deg.)	82
Figure A. 6: Load displacement curve for square, fck=30Mpa ($\alpha=45$ deg.)	82
Figure A. 7: Load displacement curve for square, fck=20Mpa ($\alpha=60$ deg.)	83
Figure A. 8: Load displacement curve for square, fck=25Mpa ($\alpha=60$ deg.)	83
Figure A. 9: Load displacement curve for square, fck=30Mpa ($\alpha=60$ deg.)	84
Figure A. 10: Load displacement curve for square, fck=20Mpa ($\alpha=75$ deg.)	84
Figure A. 11: Load displacement curve for square, fck=25Mpa ($\alpha=75$ deg.)	85
Figure A. 12: Load displacement curve for square, fck=30Mpa ($\alpha=75$ deg.)	85
Figure A. 13: Load displacement curve for square, fck=20Mpa ($\alpha=90$ deg.)	86
Figure A. 14: Load displacement curve for square, fck=25Mpa ($\alpha=90$ deg.)	86
Figure A. 15: Load displacement curve for square, fck=30Mpa ($\alpha=90$ deg.)	87
Figure A. 16: Load displacement curve for rectangle, fck=20Mpa ($\alpha=15$ deg.)	87
Figure A. 17: Load displacement curve for rectangle, fck=25Mpa ($\alpha=15$ deg.)	88
Figure A. 18: Load displacement curve for rectangle, fck=30Mpa ($\alpha=15$ deg.)	88
Figure A. 19: Load displacement curve for rectangle, fck=20Mpa ($\alpha=30$ deg.)	89
Figure A. 20: Load displacement curve for rectangle, fck=25Mpa ($\alpha=30$ deg.)	89
Figure A. 21: Load displacement curve for rectangle fck=30Mpa ($\alpha=30$ deg.)	90
Figure A. 22: Load displacement curve for rectangle, fck=20Mpa ($\alpha=45$ deg.)	90
Figure A. 23: Load displacement curve for rectangle, fck=25Mpa ($\alpha=45$ deg.)	91
Figure A. 24: Load displacement curve for rectangle, fck=30Mpa ($\alpha=45$ deg.)	91
Figure A. 25: Load displacement curve for rectangle, fck=20Mpa ($\alpha=60$ deg.)	92
Figure A. 26: Load displacement curve for rectangle, fck=25Mpa ($\alpha=60$ deg.)	92
Figure A. 27: Load displacement curve for rectangle, fck=30Mpa ($\alpha=60$ deg.)	93
Figure A. 28: Load displacement curve for rectangle, fck=20Mpa ($\alpha=75$ deg.)	93
Figure A. 29: Load displacement curve for rectangle, fck=25Mpa ($\alpha=75$ deg.)	94
Figure A. 30: Load displacement curve for square, fck=30Mpa ($\alpha=75$ deg.)	94
Figure A. 31: Load displacement curve for rectangle, fck=20Mpa ($\alpha=90$ deg.)	95
Figure A. 32: Load displacement curve for rectangle, fck=25Mpa ($\alpha=90$ deg.)	95

Figure A. 33: Load displacement curve for rectangle, $f_{ck}=30\text{Mpa}$ ($\alpha=90$ deg.).....	96
Figure A. 34: Load displacement curve for rectangle, $f_{ck}=20\text{Mpa}$ ($\alpha=15$ deg.).....	96
Figure A. 35: Load displacement curve for circle, $f_{ck}=25\text{Mpa}$ ($\alpha=15$ deg.).....	97
Figure A. 36: Load displacement curve for circle, $f_{ck}=30\text{Mpa}$ ($\alpha=15$ deg.).....	97
Figure A. 37: Load displacement curve for circle, $f_{ck}=20\text{Mpa}$ ($\alpha=30$ deg.).....	98
Figure A. 38: Load displacement curve for circle, $f_{ck}=25\text{Mpa}$ ($\alpha=30$ deg.).....	98
Figure A. 39: Load displacement curve for circle, $f_{ck}=30\text{Mpa}$ ($\alpha=30$ deg.).....	99
Figure A. 40: Load displacement curve for circle, $f_{ck}=30\text{Mpa}$ ($\alpha=45$ deg.).....	99
Figure A. 41: Load displacement curve for circle, $f_{ck}=20\text{Mpa}$ ($\alpha=60$ deg.).....	100
Figure A. 42: Load displacement curve for circle, $f_{ck}=25\text{Mpa}$ ($\alpha=60$ deg.).....	100
Figure A. 43: Load displacement curve for circle, $f_{ck}=30\text{Mpa}$ ($\alpha=60$ deg.).....	101
Figure A. 44: Load displacement curve for circle, $f_{ck}=20\text{Mpa}$ ($\alpha=75$ deg.).....	101
Figure A. 45: Load displacement curve for circle, $f_{ck}=25\text{Mpa}$ ($\alpha=75$ deg.).....	102
Figure A. 46: Load displacement curve for circle, $f_{ck}=30\text{Mpa}$ ($\alpha=75$ deg.).....	102
Figure A. 47: Load displacement curve for circle, $f_{ck}=20\text{Mpa}$ ($\alpha=90$ deg.).....	103
Figure A. 48: Load displacement curve for circle, $f_{ck}=25\text{Mpa}$ ($\alpha=90$ deg.).....	103
Figure A. 49: Load displacement curve for circle, $f_{ck}=30\text{Mpa}$ ($\alpha=90$ deg.).....	104

Acronyms

ACI	American Concrete Institute
B31	first order three dimensional beam element
C3D8R	8 nodes linear brick, reduced integration hourglass control
CAE	Complete Abaqus Environment
CAeC	Circular with angle A, eccentricity e and concrete grade C
CFD	Computational Fluid Dynamics
EC-2	Euro code-2
Exp	Experimental
FE	Finite Element
FEA	Finite Element Analysis
FEM	Finite Element Method
R3D4	4 node 3D bilinear rigid quadrilateral element
RC	Reinforced Concrete
RCC	Reinforced Concrete Column
RP	Reference point
RAeC	Rectangular with angle A, eccentricity e and concrete grade C
SAeC	Square with angle A, eccentricity e and concrete grade C.
T3D2	First order three dimensional truss element
ULS	Ultimate Limit State

List of Notations

A1	Angle of 15degree
A2	Angle of 30degree
A3	Angle of 45degree
A4	Angle of 60 degree
A5	Angle of 75 degree
A6	Angle of 90degree
C	Circular
C1	Concrete grade with $f_{ck}=20\text{Mpa}$
C2	Concrete grade with $f_{ck}=25\text{Mpa}$
C3	Concrete grade with $f_{ck}=30\text{Mpa}$
e1	eccentricity with $e=10\text{mm}$
e2	eccentricity with $e=20\text{mm}$
e3	eccentricity with $e=30\text{mm}$
e4	eccentricity with $e=40\text{mm}$
e5	eccentricity with $e=50\text{mm}$
EI	Flexural rigidity of the column
L	Length of the column
n	Number of half sine in the deformed shape of the column
R	Rectangular
S	Square
ϵ_{c1}	Peak strain at peak stress
f_{cm}	Mean compressive strength at 28 days.
E_{cm}	Secant modulus of elasticity of concrete
ϵ_c^{ch}	Compressive crushing strain (inelastic strain)
l_{eq}	Characteristic length of the element
f_{ck}	Cylindrical compressive strength of concrete
G_{ch}	Crushing energies of concrete

G_F	Fracture energies of concrete
w_c	Critical crack opening
ε_t^{ck}	Tensile cracking strain (inelastic strain).
ε_{cm}	Compressive strain of concrete at the extreme fiber
ε_{c2}	Compressive strain of concrete at the peak stress
ε_{cu2}	Maximum compressive strain of concrete

CHAPTER ONE

INTRODUCTION

1.1 Background of the study

Nowadays, building has become a means of communication, especially to reflect a community's culture and social life. Different shapes of building may have been constructed to keep the aesthetic of the building. The design and construction of this kind of building may have a column that supports a beam running in a non-orthogonal way or crossing each other at some angle other than perpendicular.

A column is a vertical member used primarily to carry compressive loads. It is a structural part of the building that takes the load of the beam or slab directly and transfers it to the next consecutive lower floor column, which is finally transferred to the foundation. A column can be loaded with normal axial load with/without moments. A reinforced concrete column is a type of column in which its material consists of concrete and steel reinforcing bars. The reinforced concrete column can be short or slender (long) depending on the degree of slenderness. Short column is a column capable of withstanding axial forces and moments greater than or equal to the axial and moment capacity of the cross section of the column. But the slender column is a column whose sectional strength is reduced by second-order deformation (buckling) of the column. (Mac Gregor, et al. 1970).

According to Kwak H.J and Kim J.K. (2006), short RC columns, when overloaded, experience material failure prior to reaching a buckling mode of failure. Furthermore, the lateral deflections of short compression members subjected to bending moments are small and, thus, contribute little secondary bending moment by the $P-\Delta$ effect. Therefore, the ultimate resisting capacity of short reinforced concrete (RC) columns is generally determined on the basis of the assumption that the effects of buckling and lateral deflection on strength are negligibly small. Unlike a short RC column whose ultimate resisting capacity can be uniquely represented from a $P-M$ interaction diagram for a typical section, however, a slender RC column has a considerable reduction in strength because of a secondary bending moment caused by the lateral deflection, and its strength is dominantly affected by the slenderness ratio.

In this study, the behavior of short reinforced concrete columns under non-orthogonal biaxial moment and axial load will be investigated.

1.2 Statement of the problem

Mostly the reinforced concrete column, which is subjected to axial, uniaxial or bi-axial with orthogonal moments encountered. But now a reinforced concrete column of days with non-orthogonal bi-axial moments is also encountered in which its behavior is not studied. It is common in reinforced concrete structures for columns to be subjected to bending moments. These moments are generally invoked by the lateral forces induced by the earthquake and by the continuity of the frameworks in buildings. (Najmi A. and Tayem A., 1993).

According to Hamdy M.A. and El-Tony M. (2016), reinforced concrete columns with eccentric loading are generally available in practice because of the existence of certain bending moments. The eccentricity of the supporting beams and the unavoidable imperfections of the construction are the main sources of bending moments developed in columns subjected to gravitational loads. In addition, lateral loads caused by wind or earthquakes are another source of bending moments developed on the columns. Thus, the strength of the columns is controlled by the compression strength of the concrete, the tensile strength of the longitudinal reinforcements and the geometry of the cross-section of the column. Unlike reinforced concrete beams, compression failure cannot be avoided for eccentric load columns because the type of failure depends mainly on the axial load level.

In buildings, columns, especially corner columns, are subjected to biaxial bending, torsion, transverse and axial loads. The biaxial strength of reinforced concrete columns is often determined using the three-dimensional 3D interaction diagram, which is the axial load with respect to bending moments in two orthogonal directions. (Chang S.Y., 2010).

In this study column, where the source of moment is the supported beam and its crossing axis makes a non-orthogonal that is not perpendicular is considered. Thus, in this study, a short reinforced concrete column with non-orthogonal biaxial moments and axial load will be studied.

1.3 Objective of the study

1.3.1 General objective

The general objective of this study is to investigate the behavior of short reinforced concrete columns with non-orthogonal biaxial moments.

1.3.2 Specific objective

- To describe the effect of non-orthogonality of biaxial moment on the load-carrying capacity of reinforced concrete column.
- To determine the load-carrying capacity of reinforced concrete column with different eccentricities along both directions.
- To determine the load-carrying capacity of reinforced concrete column under non-orthogonal biaxial moments for different concrete grade.
- To recommend suitable shape of non-orthogonal biaxial reinforced concrete column by illustrating its behavior.

1.4 Significance of the study

This research is crucial for the professionals that are engaged in the design and construction of buildings, especially irregular buildings. This research enables the professionals to know the behaviors of the column under non-orthogonal bi-axial moments.

1.5 Scope of the study

This research will be limited to studying the behavior of the short reinforced concrete column under non-orthogonal biaxial moments. The study will be done using Finite Element Analysis software (ABAQUS 6.14).

1.6 Organization of papers

The first chapter of this report is the introduction, which includes the background of the study, statement of the problem, objective of the study, significance and scope of the study. Related

literature review is discussed in the second chapter of this report. Chapter three of this report deals with the methodology of this study, which include methods of modelling of the specimen. The fourth chapter is about the result and discussion of the study. The last chapter is about conclusion and recommendation.

CHAPTER TWO

RELATED LITERATURE REVIEW

2.1 General Overview

Columns are the vertical compression members, which transmit loads from the upper floors to the lower levels and to the soil through the foundations. Based on the position of the load on the cross section, columns are classified as concentrically loaded or eccentrically loaded columns. Eccentrically loaded columns are subjected to moments, in addition to axial force. Moments can be converted to a load P , and eccentricities e_x and e_y . Moments can be uniaxial, as in the case when two adjacent panels are not similarly loaded. A column is considered as biaxially loaded when the bending occurs about the x - and y -axis (Al-Ansari M.S. and Afzal M.S., 2020).

According to Kwak H.G. and Kim J.K. (2006), a reinforced concrete (RC) column, which is a primary structural member, is subjected to the axial force and bending moment which may be due to end restraint arising from the monolithic placement of floor beams and columns or due to eccentricity from imperfect alignment. Due to the combination of axial force and bending moment, the column section must be designed to ensure that the acting forces in a member exist inside the P - M interaction diagram representing the resisting capacity of the column.

According to Thomas Hsu C.T. (1986), reinforced concrete columns supporting slabs and beams and subject to eccentric compression belong to the most important structure elements. Their role still huge due to the increasing size of multi-storey high buildings. Structural members subjected to axial load and biaxial bending are encountered in design practice from time to time; a typical example is the corner column in a framed structure.

According to Abdel Rahman M.A., Mohammed F. and Mohammed M.A. (2010), reinforced concrete columns are generally subjected to eccentric compression as a result of their location in the structure, their cross-section or the type of forces they bear. Many columns are subjected to this kind of loads; the corner columns of a building or the piles of a bridge and column of frame structures.

Hashemi S.SH. and Vaghefi M., (2015) states that columns are the most critical part of any building or any structural skeletal frame system. A Reinforced Concrete (RC) column may be

subjected to biaxial bending, or to an axial load acting eccentrically, with respect to both principal axes of the cross section.

Eccentrically loaded reinforced concrete columns are commonly existing in practice due to the existence of some bending moments. The eccentricity of the supported beams as well as the unavoidable imperfections of construction are the main sources of the developed bending moments in the columns under gravity loads. In addition, lateral loads due to wind or earthquake loading are another source of the developed bending moments on the columns. Therefore, the strength of the columns is controlled by the compressive strength of concrete, the tensile strength of the longitudinal reinforcements and the geometry of the column cross-section contrasting to reinforced concrete beams, the compression failure cannot be avoided for eccentrically loaded columns since the type of failure is mainly dependent on the axial load level.

Reinforced concrete columns are classified as short columns while the slenderness effect can be neglected or slender columns where the slenderness effect has to be included in the design. In order to distinguish between these two types, there are two important limits for slenderness ratio/index which are the lower and the upper slenderness limits. Most of the limit expressions provided by codes were derived assuming a certain loss of the column ultimate capacity due to the second order effect. Lower slenderness limits may be defined as the slenderness producing a certain reduction, usually 5–10 %, in the column ultimate capacity compared to that of a non-slender column. In spite that the lower slenderness limit of short column is mostly dependent on the adopted design standards (Hamdy and el-tony,2016).

2.2 Behavior of short Bi-axially loaded Reinforced Concrete column

In buildings, columns, particularly corner columns, are subjected to biaxial bending, torsion, transverse, and axial loads. The biaxial strength of reinforced concrete columns is often determined using the three-dimensional 3D interaction diagram i.e., axial load versus the bending moments about two orthogonal directions. Many test results and analytical methods on the strength evaluation of columns have been reported Bresler 1960; Pannell 1963; Parme et al. 1966; Hsu 1988; Yen 1991; Wang and Hsu 1992; Ahmad and Weerakoon 1995; Rodriguez and Aristozabal-Ochoa 1999; Hong 2001; among many others. (Chang S.Y.,2010)

Reinforced concrete (RC) columns are subjected to eccentric vertical compression forces in general, and their failure is sudden and drastic, which can be a result of buckling, material failure, or a combination of both due to the interaction between the material and geometric nonlinearities. However, in most cases, a considerable portion of the total load acting on RC columns can be classified as sustained compression load. When this load is combined with the normal construction inaccuracies and load eccentricities, the column undergoes increasing out-of-plane deflection with time due to creep. This may consequently lead to loss of stability (creep buckling) under a sustained load that is significantly smaller than the short-term load carrying capacity. However, creep may not necessarily lead to buckling failure, but it may lead to premature creep rupture failures of the concrete or may reduce the residual strength of the column due to the increased internal stresses and strains with time (Hamed E. and Lai C., 2016).

Although methods available in the technical literature can provide reliable strength evaluation of reinforced concrete columns subject to static axial load and biaxial bending moments, it is still difficult to obtain the seismic responses of reinforced concrete columns through numerical methods. This is because the load displacement response is needed in their dynamic analysis. It is a difficult job to construct a mathematical model capable to reproduce the very complicated behavior of a reinforced concrete column subjected to biaxial bending and axial load since their hysteretic loops generally exhibit stiffness and strength degradations and pinching effects.

A mathematical model that describes the load-displacement relation is needed for determining the restoring force in the step by- step solution of the equation of motion, and the results are highly dependent on the reliability of the chosen model. The pseudo dynamic test method Chang (2001, 2002) is developed to overcome the difficulty arising from constructing a reliable mathematical model for the time history analysis. Thus, a test structure is needed to replace a mathematical model and then an experimentally measured restoring force is used instead of the one determined from an assumed load-displacement relation in performing a pseudo dynamic test. The specimen is often idealized as a discrete system and then the equations of motion are formulated through a finite element procedure. Furthermore, an integration method is needed to solve the equations of motion. It is worth noting that the inertial and damping properties in the equations of motion are analytically described while the restoring forces developed by the test specimen are experimentally measured (Chang S.Y.,2010).

In general buildings, short columns are designed as structural members having a high stiffness with low ductility. Due to their high stiffness, they are often subjected to relatively large lateral forces with small lateral displacements, resulting in brittle shear failure. Therefore, short columns usually dominate the seismic behavior of the buildings in earthquakes. Their lateral stiffness, shear strength, shear strength degradation, and collapse behavior significantly influence the seismic behavior of the whole structure. Due to aforementioned features, an inappropriate seismic evaluation on buildings containing short columns would result in expensive and inefficient retrofitting schemes.

Although the seismic response of short columns is dominated by shear force, it remains inconclusive whether the determining factor for column stiffness is primarily from shear deformation or from flexural deformation. Several researchers suggested that for columns with a shear-depth ratio larger than 5 (Sezen and Moehle¹) or larger than 2.5 (Brachmann et al.²), the contribution of shear deformation to the total lateral deformation of a column was less than the contribution of the flexural deformation. More experimental evidence is required, however, to study whether this observation is also applicable to short columns with a column height-depth ratio less than 2. An underestimation of shear deformation in short columns would cause an overestimation of their stiffness, leading to a false appearance of premature failure. Secondly, in general buildings, short columns belong in the category of short and deep members, the shear strength of which, according to specifications in ACI 318-11,³ should be determined based on strut-and-tie models (An Li Y., Huang Y.T. and Hwang S.J., 2014).

As shear failure of short or captive reinforced concrete columns is a common cause of building damage or collapse, large experimental research effort has been spent worldwide to assess the reinforced concrete short columns behavior under reversed lateral loading (Popa V., Cotofana D. and Vacareanu R., 2014)

According to Thomas Hsu C.T. (1986), the buckling behavior of reinforced concrete columns depends upon many different factors as column slenderness, load eccentricity, boundary conditions at ends, area and shape of the cross-section of concrete, area and spacing of the vertical and horizontal reinforcement, reinforcement ratio, compressive and tensile strength of concrete and the strength of a reinforcement.

The modes of concrete failure under fire exposure vary according to the nature of fire, loading system, and types of structure. Moreover, the failure could happen due to different reasons such

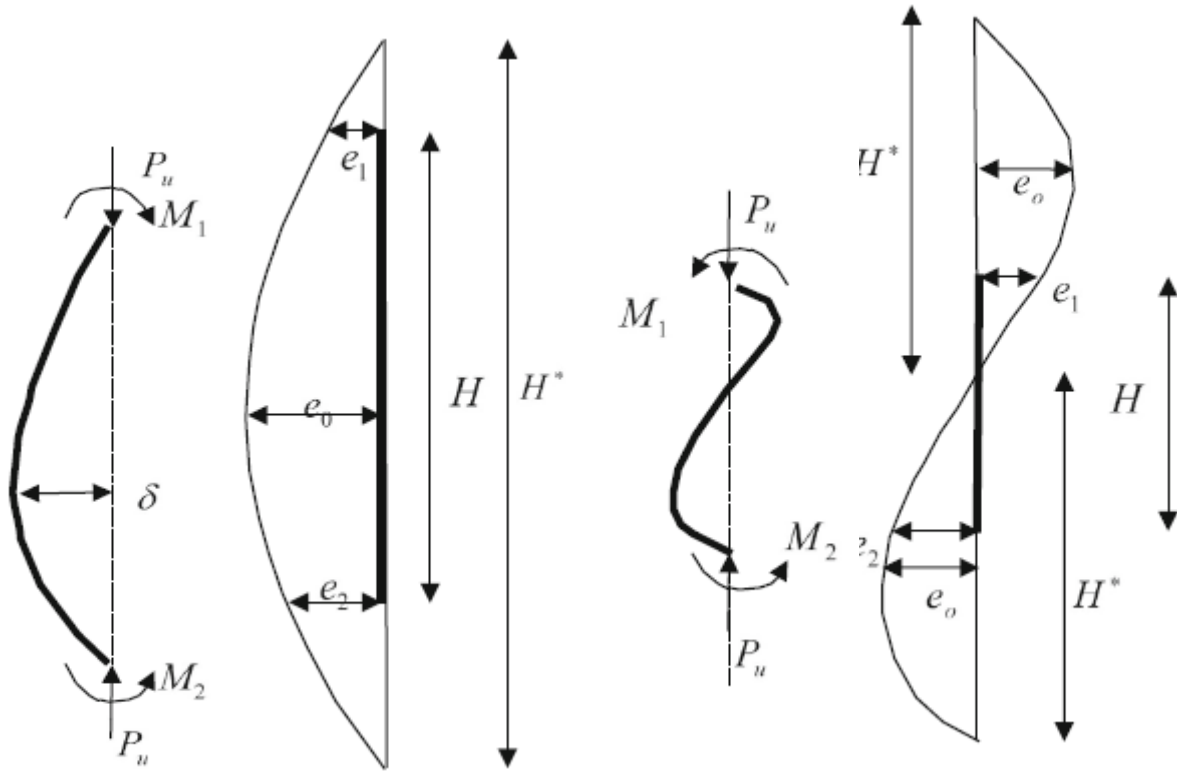
as a reduction of bending or tensile strength, loss of shear or torsional strength, loss of compressive strength, and more.

In order to extend the service life of reinforced concrete (RC) structures under rapidly increased loading requirements and severe environmental conditions, strengthening techniques have been developed for many years. Therefore, more economic and effective strengthening techniques for RC structures have been particularly needed to increase the capacities of structural members damaged by deterioration and overloads (Bikhiet M.M., El-Shafey N.F. and El-Hashimy H.M., 2014).

Current standards, such as the EN 1998, provide different methods of investigation to take into account the possible combination of bending actions in the two main directions of the structural element (Brecollotti M., Annibale L.M. and Bruno R.B., 2019).

2.3 Curvature mode of Reinforced concrete column

Hinged-ended columns braced against side-sway may be bent in either single or double curvature mode with loading depending on the direction of acting end moments as depicted in Fig.2.1 (Park and Paulay, 1975; Cranston, 1972). For both curvature modes, the bending deformations cause additional bending moments that can affect the primary end moments. If the additional moments are large, the maximum moments may move from ends to within the height of the columns. Since the lateral deformation for the case of single curvature mode is greater than that of the double curvature mode, the maximum bending moment in the single curvature case is higher than that in the double curvature one (Park and Paulay, 1975; Hamdy and el-tony,2016). Therefore, the greatest reduction in the ultimate load capacity will occur for the case of equal end eccentricities for columns bent in single curvature mode, while the smallest reduction will occur for the case of equal end eccentricities for columns bent in double curvature mode (Hamdy and el-tony,2016).



a) Single curvature

b) Double curvature

Figure 2. 1: Curvature modes of RC columns under end eccentric loading

It is accepted that the deflected axis of any column may be represented by a portion of the column deflected shape of axially loaded pin-ended column (Chen and Lui, 1987). Therefore, for a given column subjected to end moments, an equivalent column exists. Making use of Fig. 2.1, the column deflected shape of the equivalent pin-ended column can be represented by sinusoidal curve as illustrated in Eq. (2.1).

$$e = \frac{e_0 \sin(\pi x)}{H^*} \dots \dots \dots (2.1)$$

where e is the lateral deflection of the column at a distance x from one end of the column, H^* is the length of the equivalent pin-ended column and e_0 is the maximum deflection at the mid-height of the equivalent column that can be calculated using Eq. (2.2).

$$e = \phi_m \frac{H^{*2}}{\pi^2} \dots \dots \dots (2.2)$$

where ϕ_m is the curvature of the column based on the column's mode of failure.

This concept is adopted in order to reduce uni-axially loaded column to an axially loaded equivalent pin-ended column with greater length (El-Metwally 1994; Afefy et al. 2009; Afefy 2012).

For columns bent in double curvature mode, it can be noted that the columns showed un-symmetric deformed shape compared to initial center line of the column. However, when we consider the final deformed shape due to axial load as exhibited by column C-0-0, the final deformed shapes showed symmetric configuration with respect to the deformed shape of column C-0-0, for the case of equal end eccentricities as depicted in Fig. 2.2c. As for unequal end eccentricities, the maximum lateral deformations were shifted to the end having the higher end eccentricity as shown in Fig. 2.2d. Figure 2.3a shows the relationships between the vertical load and the developed lateral deflection at the mid-height section for all columns of Group No. 1. It can be noted that increasing the end eccentricity ratio resulted in decreasing the ultimate load carrying capacity and increasing the corresponding lateral deflection. The column S-5-5 showed the highest reduction in the ultimate capacity as well as the highest lateral deflection among all columns subjected to different end eccentricity combinations and bent in either single or double curvature modes as depicted in Figs. 2.3b, c. For columns having unequal end eccentricity combinations bent in single curvature modes and the columns bent in double curvature modes the maximum lateral deflections were noticed to be developed at the upper half of the columns as shown in Fig. 2.2. Therefore, the lateral deflections for those columns were presented at a distance 0.67 of the column height as depicted in Figs. 2.3b and 2.3c. It can be observed that the columns bent in double curvature modes showed higher ultimate capacity and lower lateral deflections than those of columns bent in single curvature modes and having the same end eccentricities combinations (Hamdy and el-tony,2016).

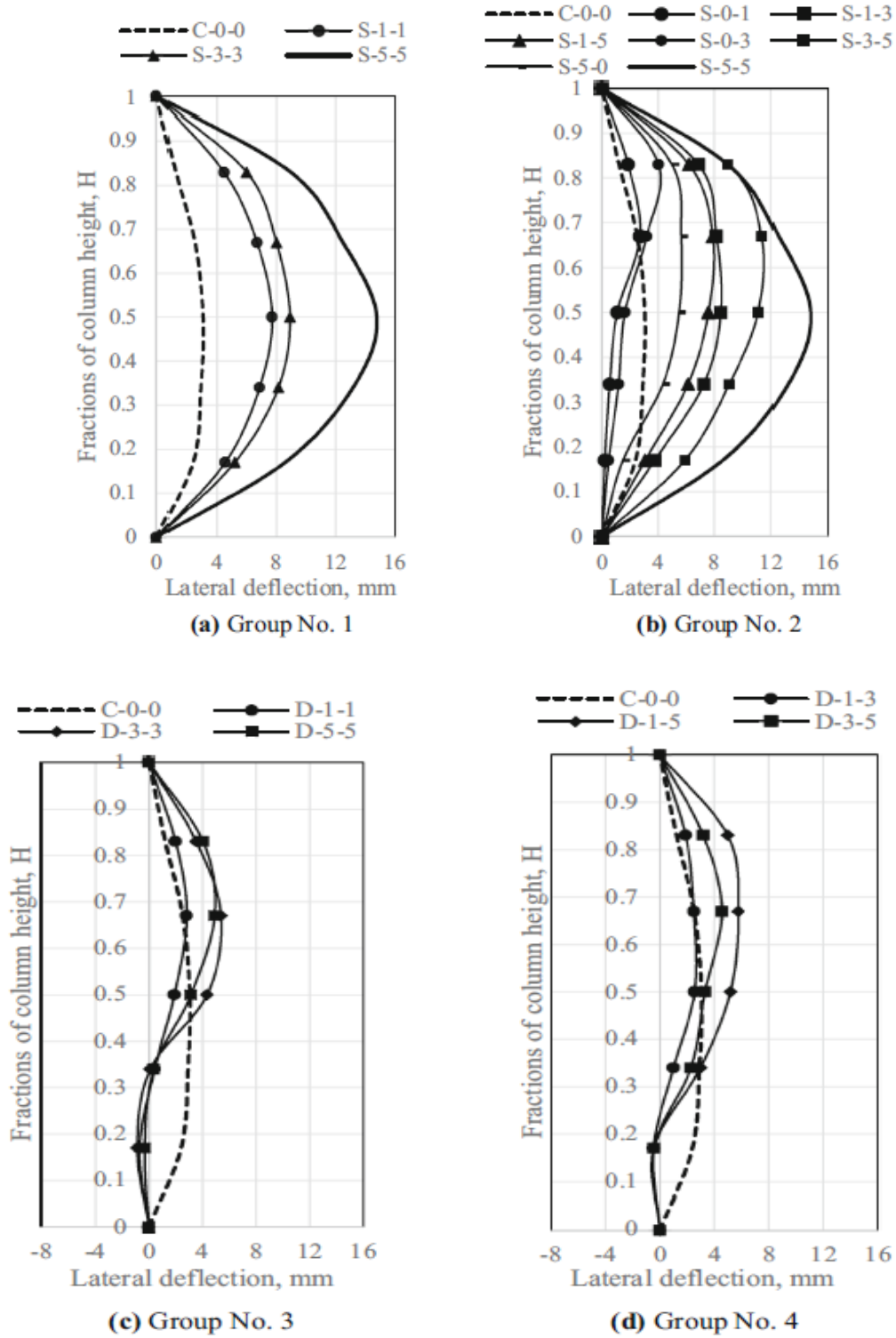


Figure 2. 2: Deformed shape of all tested columns

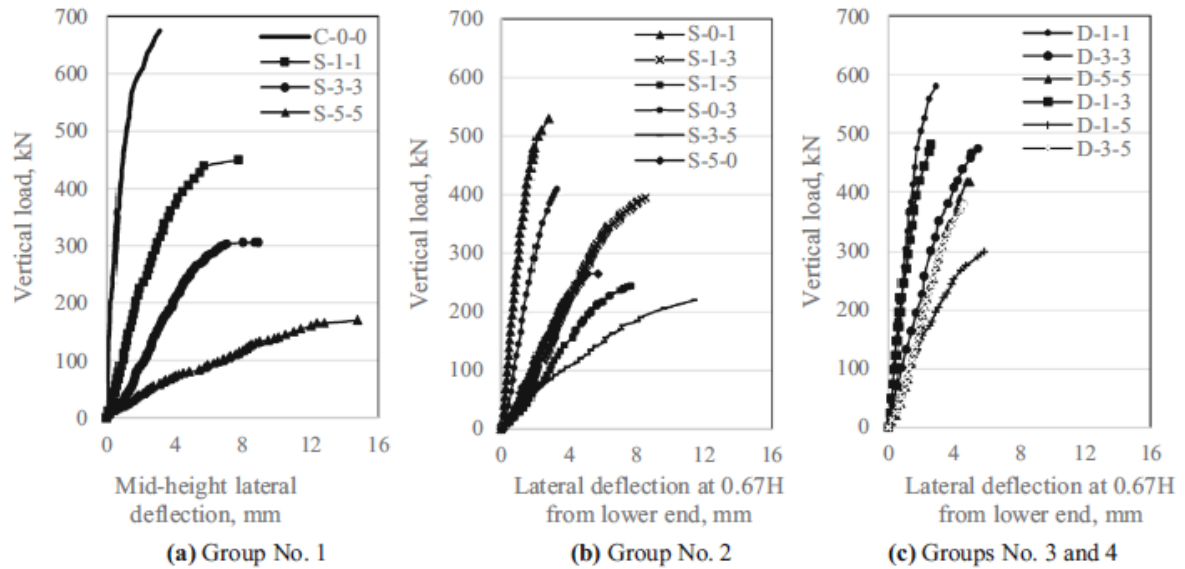


Figure 2. 3: Vertical load versus lateral deflection for all tested columns.

2.4 Method of analysis of short Bi-axially loaded Reinforced concrete column

Generally, the column is the most critical part of a building, bridge, or any structural skeletal frame system. A failure of one of these columns could lead to disastrous damage. These columns are usually loaded by biaxial bending, aside from axial compression or tension. However, most of the designs for reinforced concrete columns is based on unidirectional bending. This is understandable because most of the available design charts are for the unidirectional bending of reinforced concrete columns. These design charts can be extended to biaxial bending through the use of the load contour method and reciprocal load method developed by Bresler (1960) (Bernardo A.L.,2007).

Short reinforced concrete columns subjected to biaxial bending have received considerable attention. As a result, there are several empirical and approximate methods and design aids available for strength design of short column. A few studies have also emerged for the analysis of slender reinforced concrete columns subjected to biaxial bending. Chan (1982) developed a filament beam element with a rectangular cross section for the analysis of beam slab systems. Mari (1984) developed a similar element with arbitrary cross section and applied the proposed method to predict the behavior of reinforced concrete columns under biaxial bending. Although

unloading may take place at points adjacent to the curvature localization zone, they could not account for this phenomenon.

There have been many experimental studies on reinforced concrete columns, but they have mostly been limited to columns under uniaxial bending. There are a few tests about columns under biaxial bending in the past. However, only the behavior of columns until ultimate load was measured in these tests. The post peak behavior is important for determining ductility and energy absorption capacity. (Kim J.K and Lee S.S., 2000).

The load capacity equilibrium equations of RC columns under axial compression and biaxial bending were calculated based on the theory of “simplified rectangular block”, and load capacity of axial force and moment interaction relationship for different section forms have been carried out by Cengiz (1990). Di Ludovico *et al.* (2012) researched the experimental behavior of nonconforming RC columns with plain bars under constant axial load and biaxial bending (Z. Xu, Q. Han and C. Huang, 2016).

The capacity of a reinforced concrete column under biaxial bending and axial load is commonly represented by the interaction surface formed by the axial load, and two bending moments in two orthogonal directions. The evaluation of these quantities has been investigated extensively, especially for short RC columns with normal strength concrete, by many researchers including Bresler 1960, Ramamurthy 1966, Parme 1966, Hsu 1988, Wang 1988, Yen 1991, Rodriguez and Aristozabal- Ochoa 1999, and Hong 2000 (Wang W. and Hong H.P., 2002).

Most of the design charts available today are only for the uniaxial bending of columns. The development of design charts for biaxial bending of column sections will provide structural designers with an alternative way to analyze and design such column sections. This will not only make the design work easier but will also increase accuracy and, in turn, provide greater safety to the structure. In the course of developing the design charts, a better understanding of the behavior of biaxially-loaded columns will be achieved. The computer program that will be developed may be used as instructional material to help both students and practicing professionals understand and visualize what happens to a column subjected to biaxial bending. Over the past years, different approximation methods for the analysis and design of biaxial bending of reinforced concrete columns have been used by structural designers. The most popular among these are Besler’s (1960) Load Contour Method and the Reciprocal Load Method. Shown below is Besler’s equation:

$$\left(\frac{M_z}{M_{oz}}\right)^\alpha + \left(\frac{M_y}{M_{oy}}\right)^\alpha = 1 \dots\dots\dots(2.3)$$

Where: M_z = actual moment about z axis.

M_y = actual moment about y axis.

M_{oz} = Moment capacity about z-axis under uni-axial bending.

M_{oy} = Moment capacity about y-axis under uni-axial bending.

However, Nilson (1997), in his book entitled *Design of Concrete Structures.*, states the following: Although the load contour method and reciprocal load method are widely used in practice, each has serious shortcomings. With the load contour method, selection of the appropriate value of the exponent α is made difficult by a number of factors relating to the column shapes and bar distribution.

According to Park and Paulay (1975), the study of biaxial bending over the past years may be classified into the following: (a) methods of superposition; (b) methods of equivalent uniaxial eccentricity; and (c) methods based on approximation of shape interaction surface. Moran (1972) discussed simplified methods of superposition to reduce the inclined bending to bending about the major axes, thus allowing the uniaxial bending approach for the case of symmetrical reinforcement. This method has been used in the code of Venezuela. In the 1968 Spanish Code, an approximate analytical expression was adopted in order to be able to determine the equivalent uniaxial eccentricity of a section. Aside from Besler's popular methods, Pannell (1963), Furlong (1961), and Meek (1963) also made suggestions for the shape of the interaction surface. In the case of Weber (1966), he produced a series of design charts for square columns by linear interpolation between bending about the major axis and bending about a diagonal. A major drawback of these previous studies is the problem of finding an accurate model for the stress-strain relationship of concrete.

A new and simpler way, as compared to the Finite Element Method, is to study the behavior of reinforced columns, which may have been pioneered by Kaba and Mahin (1984). They presented the concept of the fiber method in their refined modeling of reinforced concrete columns for seismic analysis. The fiber method was found to be an effective method in predicting the flexural hysteretic response of reinforced concrete members, especially when bending and axial load dominate the behavior. Their work though was limited to the uniaxial bending of columns (Bernardo A.L.,2007).

To calculate the short RC column strength under biaxial bending accurately, several nonlinear equations involving several unknowns can be established. Some of these studies assumed that the capacity of concrete in compression can be calculated using an equivalent rectangular stress block ERSB model. Since the ERSB models were developed for rectangular compression zone, and the compression zone for the case of biaxial bending is commonly nonrectangular, this assumption can be inadequate for Kahn and Meyer (1995). Rodriguez and Aristozabal-Ochoa (1999) considered the nonlinear stress–strain relations of concrete and reinforcing steel for estimating the RC column capacity under biaxial bending and axial load.

In their approach, a limiting strain in the extreme compression fiber for concrete was assumed and the solution was obtained using the quasi-Newton method. An approach given by Hong (2000) considered the nonlinear stress–strain relations of concrete and reinforcing steel without imposing a limiting strain for concrete in compression. In that approach, the problem was formulated as a nonlinearly constrained optimization problem, and the solution was obtained using the sequential quadratic programming method.

It is noted that for design purpose, the method known as the reciprocal load RL method, which was proposed by Bresler (1960), has been suggested in the Concrete Design Handbook CPCA (1995) and in the commentary of ACI code ACI 318-99 1999. The RL method, which interpolates the interaction surface from the interaction curves obtained for the uniaxial bending cases, largely reduces the complexity in evaluating the capacity of RC columns under biaxial bending.

The adequacy of the RL method for short RC columns of normal strength concrete has been verified by Bresler (1960) And others using limited experimental results. However, its validity for high strength concrete is rarely discussed for ranges of values of the load eccentricities and reinforcement ratios. This validation is necessary since the shape of the stress–strain relation of normal strength concrete differs from that of high strength concrete Collins et al. 1993. It is noteworthy that for slender RC columns, the evaluation of the column capacity is further complicated with the interaction between the load and deformation (Mavichak and Furlong 1976; Wang and Hsu 1992; Hong 2001).

For an accurate estimate of the RC column capacity under axial load and biaxial bending, the method described in the following was adopted. Since it predicts well the short RC column strength of 85 test specimens found in the literature Hong (2000), and it also provides accurate estimation of the capacities of slender columns tested by Mavichak and Furlong (1979), Hong

(2001). The basic assumptions for the adopted method are that of plane sections before bending remain plane after bending; strain in the reinforcing steel equals the strain in the concrete at the same location; stress–strain curves of concrete and reinforcing steel are known; and the tensile strength of concrete can be neglected and the effects of shrinkage and creep can be ignored (MacGregor and Bartlett (2000). If the slenderness effect is of concern, it is further assumed that for a pin-ended column with an effective length of L , the deflection is a linear combination of the deflection about the x axis and the deflection about the y axis, which are assumed to be sinusoidal with maximum deflections at the mid-height of the column (Wang W. and Hong H.P., 2002).

Computer programs for designing reinforced concrete structures need to compute the internal forces through the integration of stresses over the concrete cross-section in order to obtain the interaction surface (N_u , M_{uy} , M_{uz}). This action is performed many times, and thus its optimization represents an important reduction in computing time. Romero et al. (2001) demonstrated that the runtime to obtain the internal forces of the section is mainly consumed during the evaluation of the internal equilibrium forces of concrete sections (N_c , M_{cy} , M_{cz}) and not in the steel bars.

Generally, the columns of such structures are subjected to axial loads and biaxial bending moments as a result of their geometry, the shape of the cross-section or the type of external forces exerted. In edification many examples follow this behaviour such as the columns in the corners of building and elements affected by seismic and wind forces. For this type of structures, the sections are typically rectangular or circular. The classical method of integrating the stresses in the concrete is usually performed by dividing the section into layers or fibers (also called cells). This technique is not numerically efficient due to the huge amount of information that is required to characterize the section and the large number of numerical operations needed to reach an acceptable level of error.

Moreover, this integration method could produce convergence problems for non-linear structural analysis.

Rodriguez and Aristizabal (2009) also proposed computing such integrals by decomposing the section into many trapezoids. In this case the constitutive equation is a parabola-rectangle diagram for the ascending branch and linear for the descending branch. They obtain the solution to the stresses integral analytically. Recently Barros et al. (2004) obtained the stress integral for the rectangular section analytically using the Heaviside functions. This method is valid for

ultimate loads, axial load and uniaxial bending and a parabola-rectangle diagram. Previously, the same authors, Barros et al. (2006), used the constitutive equation of Model Code 90 for a non-linear structural analysis under axial load and biaxial bending.

Fafitis (2001) developed a method for computing the internal forces of the concrete using Green's theorem. Use of this method allows the stress integral of the compressed area to be transformed into a path integral over the perimeter. This integral is solved numerically using the Gauss–Legendre quadrature. Bonet et al. (1999) also proposed two methods based on the Gauss quadrature. The first method was valid for a non-cylindrical stress field and the authors presented an automatic algorithm which subdivided the non-cracked concrete area with any polygonal shape (including holes) into a small number of quadrilateral areas.

The second method is suitable only for polygonal sections (including holes) in which the stress field is uniform over one direction (cylindrical stress fields) and it was decomposed the integration area into thick (or wide) layers parallel to the neutral axis. The integral of each layer was transformed into a path integral along the perimeter. This last method was termed the “Modified Thick Layer Integration” (MTLI) method. In this former paper, Bonet et al (1999) compared these two new methods based on the Gauss quadrature, the fiber method and the method proposed by Fafitis (2005) in terms of accuracy and speed (efficiency)(Bonet J.L., Barros M.H.F.M and Romero M.L.,2006).

In a recent study, Al-Ansari and Afzal (2020) also presented an analytical model for generating interaction diagram charts for biaxial columns. strength of reinforced concrete columns is normally expressed using interaction diagrams to relate the design axial load $2\phi P_n$ to the design bending moment ϕM_n . Each control point on the column interaction curve ($\phi P_n - \phi M_n$) represents one combination of design axial load, ϕP_n and design bending moment, ϕM_n , corresponding to a neutral-axis location.

Extensive studies have been carried out on the interaction diagrams (uniaxial and biaxial columns) of reinforced concrete (RC) rectangular columns. Several studies have also been performed on providing numerical approaches for the analysis and design of reinforced concrete columns. Furlong et al. (1961) provided an overview of the analysis and design of reinforced concrete columns subjected to biaxial bending. ,ey reviewed several methods of analysis that use traditional design methods and compared their results with the obtained data from physical tests of normal strength concrete columns subjected to short-term axial loads and biaxial

bending's, e_y concluded that the elliptic load contour equation and the reciprocal equation are the simplest to use, as they do not require complicated calculations (Al-Ansari M.S. and Afzal M.S., 2020).

Chen et al. (2010) proposed an iterative numerical method for rapid section analysis and design of short concrete composite columns subjected to biaxial bending. Wang and Hsu (2001) proposed the numerical method approach for the determination of load-moment curvature relationship for short and slender columns is numerical method approach is also applicable for columns, made of different materials, and shows good agreement with the different experimental results obtained in their study.

Whitney (1994) and Hsu et al. (1997) provided major research studies on numerical method approaches. Whitney suggested an approximate equation to estimate the nominal compressive strength of columns subjected to compression failure. Hsu in different research projects (1986) also presented the results of experimental and analytical studies on the strength and deformation of biaxially loaded short and tied columns with L-shaped, channel, and T-shaped cross sections. In another study, Hsu (1988) suggested a general equation for the analysis and design of reinforced concrete short and tied rectangular columns.

The inherent characteristic of quasi-brittle materials such as concrete creates cracking when the material is applied with external loading. Therefore, the failure mechanism of a concrete column with multiple loading conditions changes from an uncracked to a cracked condition. In the uncracked condition, axial force and bending moment applied to the column will have no coupling effects. However, in the cracked condition, axial force applied at the centroid of gross section may have an effect on curvature and bending moment about principal axis of gross section may also have an effect on axial strain at the sectional centroid. Furthermore, when biaxial bending occurs in a reinforced concrete column, curvature about each principal axis of gross section is affected by bending moments about both major and minor principal axes (Bikhiet M.M., El-Shafey N.F. and El-Hashimy H.M., 2014).

The design of the column then requires computation of the failure surface of the cross section, expressed in terms of the resisting axial load and of the components of the resisting bending moment about the principal axes. To date, many numerical methods have been proposed by researchers for calculating the bearing capacity of RC sections and for determination of the interaction diagram, which is commonly known as the P-M interaction curve or surface, under any uniaxial or biaxial bending conditions. Most design charts available today are only for the

uniaxial bending of columns. The development of design charts for the biaxial bending of columns will provide structural designers with an alternative way to analyze and design such column sections.

This will not only make the design easier, but will also increase accuracy, which, in turn, will provide greater structural safety. In the course of developing the design charts, a better understanding of the behavior of biaxially loaded columns will be achieved. It is possible to simplify the problem of biaxial design and analysis by generating the failure surface by means of suitable numerical formulations (Hashemi S.SH. and Vaghefi M., 2015).

Based on ACI criteria (1999), the column capacity interaction surface is numerically described by a series of discrete points that are generated on the three dimensional interaction failure surface. A typical interaction surface is shown in Figure 2.4. The coordinates of these points are determined by considering a suitable number of linear distributions of the normal strain on the section of the element, as shown in Figure 2.5.

The linear strain diagram is limited by the maximum concrete strain, ϵ_c , at the extremity of the section, to 0.003. This formulation is based consistently upon the general principles of ultimate strength design. The stress in the steel is given by the product of the steel strain and the steel modulus of elasticity, E_s , and is limited by the yield stress of the steel, f_y . The area associated with each reinforcing bar is assumed to be placed at the actual location of the center of the bar, and the algorithm does not assume any further simplifications, with respect to distributing the area of steel over the cross-section of the column.

The concrete compression stress block is assumed to be rectangular, according to Whitney's rectangular block, with a stress value of $0.85f_c$. Complementary parameters are described in ACI318-11. The interaction algorithm provides correction to account for the concrete area that is replaced by reinforcement in the compression zone. The effect of the reduction factor, β , is included in the generation of the interaction surface for calculating the ultimate capacity of the section. The value of β used in the interaction diagram varies between 0.65 and 0.90, under compression controlled to tension controlled conditions.

Following the indications of ACI318-11, P-M interaction curves are calculated on the basis of the following assumptions:

- ✓ The strain distribution on the reinforced concrete cross section is linear.
- ✓ The shear deformations are considered negligible.
- ✓ There is a perfect bond between the reinforcing bars and the surrounding concrete.

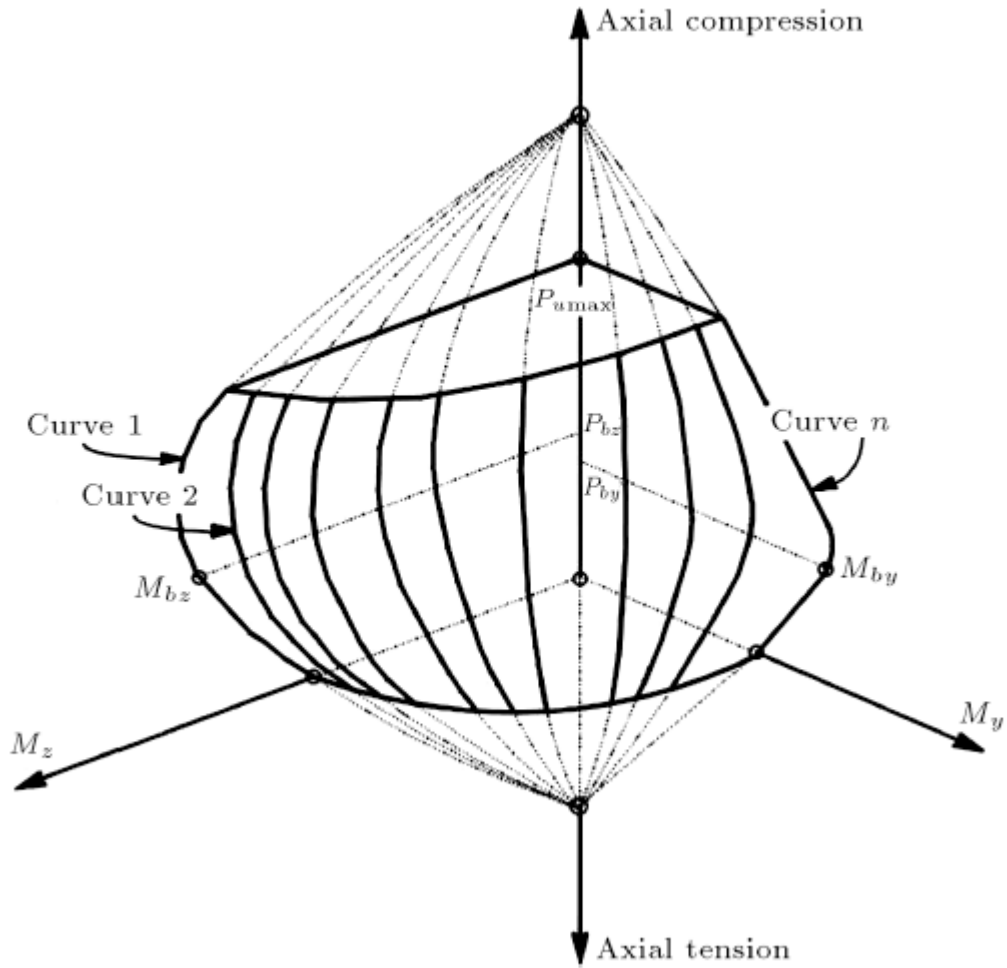


Figure 2. 4: A typical axial force-biaxial bending moment interaction surface.

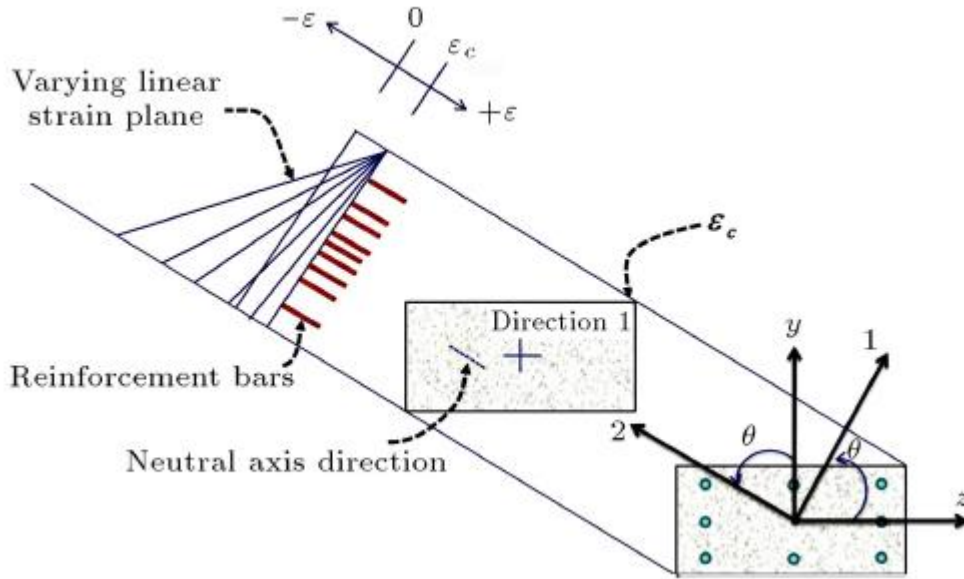
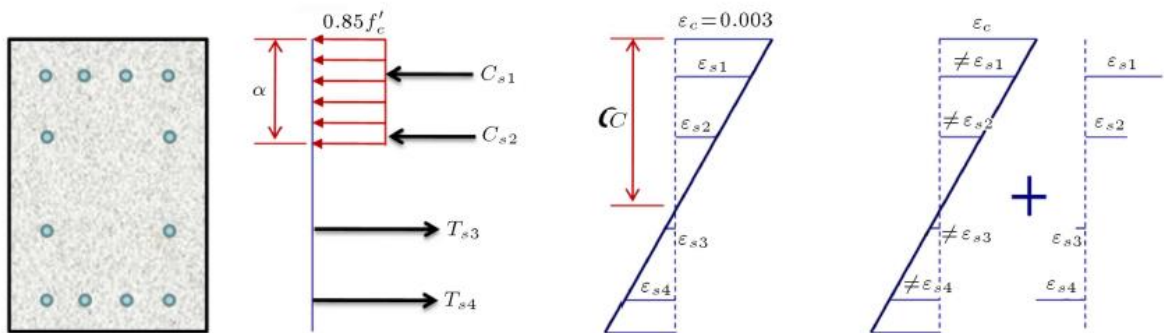


Figure 2. 5: Idealized strain distribution for generation of interaction surface

In this way, the P-M interaction surface, based on the perfect compatibility between concrete and bar deformations in an RC section, will be calculated (Figure 2.6(c)). In other words, the bond between the concrete and bars is assumed to be perfect and the slip is disregarded. In real columns, however, the bond between concrete and steel is not perfect, and the ensuring slip may affect bearing capacity estimation (Figure 2.6(d)) (Hashemi S.SH. and Vaghefi M., 2015).



a) Cross-section b) Stress distribution (ACI) c) Strain diagram d) Strain diagram
(Considering slip effect)

Figure 2. 6: Idealized strain and stress distribution of rectangular RC section.

The biaxial interaction diagrams of reinforced concrete (RC) rectangular columns have been investigated by numerous researchers. Gouwens (1975) developed simplified design aids for

rectangular columns that are included in many textbooks. For L-shaped columns, Marin (1979) presented design aids, Ramamurthy and Khan (1983) suggested two methods of design (the “failure surface” and the “equivalent” rectangular column), and Hsu (1985) presented theoretical and experimental results. Channel and box shaped columns have been reported by Hsu (1987) and Dundar (1990). T-shaped columns have also been reported by Hsu (1989). Most of the work developed by the aforementioned researchers was carried out using the Whitney’s rectangular stress block for the concrete in compression and integral methods to derive the overall equilibrium at the sectional level.

With the availability of powerful and inexpensive microcomputers, the analysis of RC columns and composite sections under biaxial bending and axial load became amenable using the “fiber” approach based on the finite element method (FEM) developed a computer program for practical design according to the American Concrete Institute code (1987) and Yen (1991) presented methods for the analysis of arbitrary cross sections. More recently, Barzegar and Erasito (1995) developed a computer algorithm for an arbitrary cross section using the Whitney’s rectangular stress block and integral methods. They used nonlinear stress-strain relationships: a second-degree parabola and a trapezoidal shape for the concrete, and a multilinear elastoplastic relationship for the reinforcements; however, their method is extremely difficult to implement into a computer program due to its complexities and lack of readily available information. Therefore, there is a real need for a general and simple approach (i.e., easy to program) that is fully available to designers to calculate the biaxial interaction diagrams of a column with any cross section (Rodriguez J.A. and Dario A.O., 1999).

CHAPTER THREE

RESEARCH METHODOLOGY

3.1 General

In this section, methods employed to model and analyze the short bi-axially loaded reinforced concrete column using finite element analysis software, which is known as ABAQUS, is discussed.

3.2 Research Design

Starting from the idea and proceeding to deciding the research area, which is the short RC column, the research topic was fixed first. Then groundwork was done before deciding on the title, and the problem was identified through reviewing the related literature. Consequently, the title was decided and planning was done to solve the identified problem. Before starting modelling, software training was held for three months to determine the method of modelling, the capability of the software, and related theories that were incorporated into the software. Based on the amount of work and time, the number of variables was decided. The specimen for a reinforced concrete column was prepared based on the variable which was studied in this thesis.

Currently, most of the buildings are constructed in irregular or regular shapes. Due to this, the beam intersection at the column may not be orthogonal and the behavior of this kind of column is not investigated and studied.

This study is numerical and it is modelled on ABAQUS 6.14 finite element software.

3.3 Study Variables

3.3.1 Dependent study variables

Dependent study variable is axial load, displacement.

3.3.2 Independent Variables

Independent study variables are eccentricity, angle between the axis of moment, concrete grade and shape of the column.

3.4 Specimen selection

A number of 270 column specimens were selected based on the above variables and taken randomly. The key parametric study was eccentricity, angle between the axis of the moment, concrete grade, shape of the column, axial load and lateral displacement of the column. The specimens are presented below in the Table-3.1.

Table 3. 1: Column specimen

S.NO.	Specimen	α (deg)	e_x'	e_y'	Shape of column	Concrete grade	Size of column	Bar
1	SA1e1C1	15	10	10	Square	20	400*400	4 ϕ 16
2	SA1e2C1	15	20	20	Square	20	400*400	4 ϕ 16
3	SA1e3C1	15	30	30	Square	20	400*400	4 ϕ 16
4	SA1e4C1	15	40	40	Square	20	400*400	4 ϕ 16
5	SA1e5C1	15	50	50	Square	20	400*400	4 ϕ 16
6	SA2e1C1	30	10	10	Square	20	400*400	4 ϕ 16
7	SA2e2C1	30	20	20	Square	20	400*400	4 ϕ 16
8	SA2e3C1	30	30	30	Square	20	400*400	4 ϕ 16
9	SA2e4C1	30	40	40	Square	20	400*400	4 ϕ 16
10	SA2e5C1	30	50	50	Square	20	400*400	4 ϕ 16
11	SA3e1C1	45	10	10	Square	20	400*400	4 ϕ 16
12	SA3e2C1	45	20	20	Square	20	400*400	4 ϕ 16
13	SA3e3C1	45	30	30	Square	20	400*400	4 ϕ 16
14	SA3e4C1	45	40	40	Square	20	400*400	4 ϕ 16
15	SA3e5C1	45	50	50	Square	20	400*400	4 ϕ 16
16	SA4e1C1	60	10	10	Square	20	400*400	4 ϕ 16
17	SA4e2C1	60	20	20	Square	20	400*400	4 ϕ 16
18	SA4e3C1	60	30	30	Square	20	400*400	4 ϕ 16
19	SA4e4C1	60	40	40	Square	20	400*400	4 ϕ 16
20	SA4e5C1	60	50	50	Square	20	400*400	4 ϕ 16
21	SA5e1C1	75	10	10	Square	20	400*400	4 ϕ 16
22	SA5e2C1	75	20	20	Square	20	400*400	4 ϕ 16
23	SA5e3C1	75	30	30	Square	20	400*400	4 ϕ 16

24	SA5e4C1	75	40	40	Square	20	400*400	4φ16
25	SA5e5C1	75	50	50	Square	20	400*400	4φ16
26	SA6e1C1	90	10	10	Square	20	400*400	4φ16
27	SA6e2C1	90	20	20	Square	20	400*400	4φ16
28	SA6e3C1	90	30	30	Square	20	400*400	4φ16
29	SA6e4C1	90	40	40	Square	20	400*400	4φ16
30	SA6e5C1	90	50	50	Square	20	400*400	4φ16
31	RA1e1C1	15	10	10	Rectangular	20	410*390	4φ16
32	RA1e2C1	15	20	20	Rectangular	20	410*390	4φ16
33	RA1e3C1	15	30	30	Rectangular	20	410*390	4φ16
34	RA1e4C1	15	40	40	Rectangular	20	410*390	4φ16
35	RA1e5C1	15	50	50	Rectangular	20	410*390	4φ16
36	RA2e1C1	30	10	10	Rectangular	20	410*390	4φ16
37	RA2e2C1	30	20	20	Rectangular	20	410*390	4φ16
38	RA2e3C1	30	30	30	Rectangular	20	410*390	4φ16
39	RA2e4C1	30	40	40	Rectangular	20	410*390	4φ16
40	RA2e5C1	30	50	50	Rectangular	20	410*390	4φ16
41	RA3e1C1	45	10	10	Rectangular	20	410*390	4φ16
42	RA3e2C1	45	20	20	Rectangular	20	410*390	4φ16
43	RA3e3C1	45	30	30	Rectangular	20	410*390	4φ16
44	RA3e4C1	45	40	40	Rectangular	20	410*390	4φ16
45	RA3e5C1	45	50	50	Rectangular	20	410*390	4φ16
46	RA4e1C1	60	10	10	Rectangular	20	410*390	4φ16
47	RA4e2C1	60	20	20	Rectangular	20	410*390	4φ16
48	RA4e3C1	60	30	30	Rectangular	20	410*390	4φ16
49	RA4e4C1	60	40	40	Rectangular	20	410*390	4φ16
50	RA4e5C1	60	50	50	Rectangular	20	410*390	4φ16
51	RA5e1C1	75	10	10	Rectangular	20	410*390	4φ16
52	RA5e2C1	75	20	20	Rectangular	20	410*390	4φ16
53	RA5e3C1	75	30	30	Rectangular	20	410*390	4φ16
54	RA5e4C1	75	40	40	Rectangular	20	410*390	4φ16
55	RA5e5C1	75	50	50	Rectangular	20	410*390	4φ16
56	RA6e1C1	90	10	10	Rectangular	20	410*390	4φ16
57	RA6e2C1	90	20	20	Rectangular	20	410*390	4φ16
58	RA6e3C1	90	30	30	Rectangular	20	410*390	4φ16
59	RA6e4C1	90	40	40	Rectangular	20	410*390	4φ16
60	RA6e5C1	90	50	50	Rectangular	20	410*390	4φ16
61	CA1e1C1	15	10	10	Circle	20	451.35	6φ12
62	CA1e2C1	15	20	20	Circle	20	451.35	6φ12
63	CA1e3C1	15	30	30	Circle	20	451.35	6φ12

64	CA1e4C1	15	40	40	Circle	20	451.35	6φ12
65	CA1e5C1	15	50	50	Circle	20	451.35	6φ12
66	CA2e1C1	30	10	10	Circle	20	451.35	6φ12
67	CA2e2C1	30	20	20	Circle	20	451.35	6φ12
68	CA2e3C1	30	30	30	Circle	20	451.35	6φ12
69	CA2e4C1	30	40	40	Circle	20	451.35	6φ12
70	CA2e5C1	30	50	50	Circle	20	451.35	6φ12
71	CA3e1C1	45	10	10	Circle	20	451.35	6φ12
72	CA3e2C1	45	20	20	Circle	20	451.35	6φ12
73	CA3e3C1	45	30	30	Circle	20	451.35	6φ12
74	CA3e4C1	45	40	40	Circle	20	451.35	6φ12
75	CA3e5C1	45	50	50	Circle	20	451.35	6φ12
76	CA4e1C1	60	10	10	Circle	20	451.35	6φ12
77	CA4e2C1	60	20	20	Circle	20	451.35	6φ12
78	CA4e3C1	60	30	30	Circle	20	451.35	6φ12
79	CA4e4C1	60	40	40	Circle	20	451.35	6φ12
80	CA4e5C1	60	50	50	Circle	20	451.35	6φ12
81	CA5e1C1	75	10	10	Circle	20	451.35	6φ12
82	CA5e2C1	75	20	20	Circle	20	451.35	6φ12
83	CA5e3C1	75	30	30	Circle	20	451.35	6φ12
84	CA5e4C1	75	40	40	Circle	20	451.35	6φ12
85	CA5e5C1	75	50	50	Circle	20	451.35	6φ12
86	CA6e1C1	90	10	10	Circle	20	451.35	6φ12
87	CA6e2C1	90	20	20	Circle	20	451.35	6φ12
88	CA6e3C1	90	30	30	Circle	20	451.35	6φ12
89	CA6e4C1	90	40	40	Circle	20	451.35	6φ12
90	CA6e5C1	90	50	50	Circle	20	451.35	6φ12
91	SA1e1C2	15	10	10	Square	25	400*400	4φ16
92	SA1e2C2	15	20	20	Square	25	400*400	4φ16

93	SA1e3C2	15	30	30	Square	25	400*400	4φ16
94	SA1e4C2	15	40	40	Square	25	400*400	4φ16
95	SA1e5C2	15	50	50	Square	25	400*400	4φ16
96	SA2e1C2	30	10	10	Square	25	400*400	4φ16
97	SA2e2C2	30	20	20	Square	25	400*400	4φ16
98	SA2e3C2	30	30	30	Square	25	400*400	4φ16
99	SA2e4C2	30	40	40	Square	25	400*400	4φ16
100	SA2e5C2	30	50	50	Square	25	400*400	4φ16
101	SA3e1C2	45	10	10	Square	25	400*400	4φ16
102	SA3e2C2	45	20	20	Square	25	400*400	4φ16
103	SA3e3C2	45	30	30	Square	25	400*400	4φ16
104	SA3e4C2	45	40	40	Square	25	400*400	4φ16
105	SA3e5C2	45	50	50	Square	25	400*400	4φ16
106	SA4e1C2	60	10	10	Square	25	400*400	4φ16
107	SA4e2C2	60	20	20	Square	25	400*400	4φ16
108	SA4e3C2	60	30	30	Square	25	400*400	4φ16
109	SA4e4C2	60	40	40	Square	25	400*400	4φ16
110	SA4e5C2	60	50	50	Square	25	400*400	4φ16
111	SA5e1C2	75	10	10	Square	25	400*400	4φ16
112	SA5e2C2	75	20	20	Square	25	400*400	4φ16
113	SA5e3C2	75	30	30	Square	25	400*400	4φ16
114	SA5e4C2	75	40	40	Square	25	400*400	4φ16
115	SA5e5C2	75	50	50	Square	25	400*400	4φ16
116	SA6e1C2	90	10	10	Square	25	400*400	4φ16
117	SA6e2C2	90	20	20	Square	25	400*400	4φ16
118	SA6e3C2	90	30	30	Square	25	400*400	4φ16
119	SA6e4C2	90	40	40	Square	25	400*400	4φ16
120	SA6e5C2	90	50	50	Square	25	400*400	4φ16

121	RA1e1C2	15	10	10	Rectangular	25	410*390	4φ16
122	RA1e2C2	15	20	20	Rectangular	25	410*390	4φ16
123	RA1e3C2	15	30	30	Rectangular	25	410*390	4φ16
124	RA1e4C2	15	40	40	Rectangular	25	410*390	4φ16
125	RA1e5C2	15	50	50	Rectangular	25	410*390	4φ16
126	RA2e1C2	30	10	10	Rectangular	25	410*390	4φ16
127	RA2e2C2	30	20	20	Rectangular	25	410*390	4φ16
128	RA2e3C2	30	30	30	Rectangular	25	410*390	4φ16
129	RA2e4C2	30	40	40	Rectangular	25	410*390	4φ16
130	RA2e5C2	30	50	50	Rectangular	25	410*390	4φ16
131	RA3e1C2	45	10	10	Rectangular	25	410*390	4φ16
132	RA3e2C2	45	20	20	Rectangular	25	410*390	4φ16
133	RA3e3C2	45	30	30	Rectangular	25	410*390	4φ16
134	RA3e4C2	45	40	40	Rectangular	25	410*390	4φ16
135	RA3e5C2	45	50	50	Rectangular	25	410*390	4φ16
136	RA4e1C2	60	10	10	Rectangular	25	410*390	4φ16
137	RA4e2C2	60	20	20	Rectangular	25	410*390	4φ16
138	RA4e3C2	60	30	30	Rectangular	25	410*390	4φ16
139	RA4e4C2	60	40	40	Rectangular	25	410*390	4φ16
140	RA4e5C2	60	50	50	Rectangular	25	410*390	4φ16
141	RA5e1C2	75	10	10	Rectangular	25	410*390	4φ16
142	RA5e2C2	75	20	20	Rectangular	25	410*390	4φ16
143	RA5e3C2	75	30	30	Rectangular	25	410*390	4φ16
144	RA5e4C2	75	40	40	Rectangular	25	410*390	4φ16
145	RA5e5C2	75	50	50	Rectangular	25	410*390	4φ16
146	RA6e1C2	90	10	10	Rectangular	25	410*390	4φ16
147	RA6e2C2	90	20	20	Rectangular	25	410*390	4φ16
148	RA6e3C2	90	30	30	Rectangular	25	410*390	4φ16

149	RA6e4C2	90	40	40	Rectangular	25	410*390	4φ16
150	RA6e5C2	90	50	50	Rectangular	25	410*390	4φ16
151	CA1e1C2	15	10	10	Circle	25	451.35	6φ12
152	CA1e2C2	15	20	20	Circle	25	451.35	6φ12
153	CA1e3C2	15	30	30	Circle	25	451.35	6φ12
154	CA1e4C2	15	40	40	Circle	25	451.35	6φ12
155	CA1e5C2	15	50	50	Circle	25	451.35	6φ12
156	CA2e1C2	30	10	10	Circle	25	451.35	6φ12
157	CA2e2C2	30	20	20	Circle	25	451.35	6φ12
158	CA2e3C2	30	30	30	Circle	25	451.35	6φ12
159	CA2e4C2	30	40	40	Circle	25	451.35	6φ12
160	CA2e5C2	30	50	50	Circle	25	451.35	6φ12
161	CA3e1C2	45	10	10	Circle	25	451.35	6φ12
162	CA3e2C2	45	20	20	Circle	25	451.35	6φ12
163	CA3e3C2	45	30	30	Circle	25	451.35	6φ12
164	CA3e4C2	45	40	40	Circle	25	451.35	6φ12
165	CA3e5C2	45	50	50	Circle	25	451.35	6φ12
166	CA4e1C2	60	10	10	Circle	25	451.35	6φ12
167	CA4e2C2	60	20	20	Circle	25	451.35	6φ12
168	CA4e3C2	60	30	30	Circle	25	451.35	6φ12
169	CA4e4C2	60	40	40	Circle	25	451.35	6φ12
170	CA4e5C2	60	50	50	Circle	25	451.35	6φ12
171	CA5e1C2	75	10	10	Circle	25	451.35	6φ12
172	CA5e2C2	75	20	20	Circle	25	451.35	6φ12
173	CA5e3C2	75	30	30	Circle	25	451.35	6φ12
174	CA5e4C2	75	40	40	Circle	25	451.35	6φ12
175	CA5e5C2	75	50	50	Circle	25	451.35	6φ12
176	CA6e1C2	90	10	10	Circle	25	451.35	6φ12

177	CA6e2C2	90	20	20	Circle	25	451.35	6φ12
178	CA6e3C2	90	30	30	Circle	25	451.35	6φ12
179	CA6e4C2	90	40	40	Circle	25	451.35	6φ12
180	CA6e5C2	90	50	50	Circle	25	451.35	6φ12
181	SA1e1C3	15	10	10	Square	30	400*400	4φ16
182	SA1e2C3	15	20	20	Square	30	400*400	4φ16
183	SA1e3C3	15	30	30	Square	30	400*400	4φ16
184	SA1e4C3	15	40	40	Square	30	400*400	4φ16
185	SA1e5C3	15	50	50	Square	30	400*400	4φ16
186	SA2e1C3	30	10	10	Square	30	400*400	4φ16
187	SA2e2C3	30	20	20	Square	30	400*400	4φ16
188	SA2e3C3	30	30	30	Square	30	400*400	4φ16
189	SA2e4C3	30	40	40	Square	30	400*400	4φ16
190	SA2e5C3	30	50	50	Square	30	400*400	4φ16
191	SA3e1C3	45	10	10	Square	30	400*400	4φ16
192	SA3e2C3	45	20	20	Square	30	400*400	4φ16
193	SA3e3C3	45	30	30	Square	30	400*400	4φ16
194	SA3e4C3	45	40	40	Square	30	400*400	4φ16
195	SA3e5C3	45	50	50	Square	30	400*400	4φ16
196	SA4e1C3	60	10	10	Square	30	400*400	4φ16
197	SA4e2C3	60	20	20	Square	30	400*400	4φ16
198	SA4e3C3	60	30	30	Square	30	400*400	4φ16
199	SA4e4C3	60	40	40	Square	30	400*400	4φ16
200	SA4e5C3	60	50	50	Square	30	400*400	4φ16
201	SA5e1C3	75	10	10	Square	30	400*400	4φ16
202	SA5e2C3	75	20	20	Square	30	400*400	4φ16
203	SA5e3C3	75	30	30	Square	30	400*400	4φ16
204	SA5e4C3	75	40	40	Square	30	400*400	4φ16
205	SA5e5C3	75	50	50	Square	30	400*400	4φ16
206	SA6e1C3	90	10	10	Square	30	400*400	4φ16
207	SA6e2C3	90	20	20	Square	30	400*400	4φ16
208	SA6e3C3	90	30	30	Square	30	400*400	4φ16
209	SA6e4C3	90	40	40	Square	30	400*400	4φ16
210	SA6e5C3	90	50	50	Square	30	400*400	4φ16
211	RA1e1C3	15	10	10	Rectangular	30	410*390	4φ16
212	RA1e2C3	15	20	20	Rectangular	30	410*390	4φ16
213	RA1e3C3	15	30	30	Rectangular	30	410*390	4φ16
214	RA1e4C3	15	40	40	Rectangular	30	410*390	4φ16
215	RA1e5C3	15	50	50	Rectangular	30	410*390	4φ16

216	RA2e1C3	30	10	10	Rectangular	30	410*390	4φ16
217	RA2e2C3	30	20	20	Rectangular	30	410*390	4φ16
218	RA2e3C3	30	30	30	Rectangular	30	410*390	4φ16
219	RA2e4C3	30	40	40	Rectangular	30	410*390	4φ16
220	RA2e5C3	30	50	50	Rectangular	30	410*390	4φ16
221	RA3e1C3	45	10	10	Rectangular	30	410*390	4φ16
222	RA3e2C3	45	20	20	Rectangular	30	410*390	4φ16
223	RA3e3C3	45	30	30	Rectangular	30	410*390	4φ16
224	RA3e4C3	45	40	40	Rectangular	30	410*390	4φ16
225	RA3e5C3	45	50	50	Rectangular	30	410*390	4φ16
226	RA4e1C3	60	10	10	Rectangular	30	410*390	4φ16
227	RA4e2C3	60	20	20	Rectangular	30	410*390	4φ16
228	RA4e3C3	60	30	30	Rectangular	30	410*390	4φ16
229	RA4e4C3	60	40	40	Rectangular	30	410*390	4φ16
230	RA4e5C3	60	50	50	Rectangular	30	410*390	4φ16
231	RA5e1C3	75	10	10	Rectangular	30	410*390	4φ16
232	RA5e2C3	75	20	20	Rectangular	30	410*390	4φ16
233	RA5e3C3	75	30	30	Rectangular	30	410*390	4φ16
234	RA5e4C3	75	40	40	Rectangular	30	410*390	4φ16
235	RA5e5C3	75	50	50	Rectangular	30	410*390	4φ16
236	RA6e1C3	90	10	10	Rectangular	30	410*390	4φ16
237	RA6e2C3	90	20	20	Rectangular	30	410*390	4φ16
238	RA6e3C3	90	30	30	Rectangular	30	410*390	4φ16
239	RA6e4C3	90	40	40	Rectangular	30	410*390	4φ16
240	RA6e5C3	90	50	50	Rectangular	30	410*390	4φ16
241	CA1e1C3	15	10	10	Circle	30	451.35	6φ12
242	CA1e2C3	15	20	20	Circle	30	451.35	6φ12
243	CA1e3C3	15	30	30	Circle	30	451.35	6φ12
244	CA1e4C3	15	40	40	Circle	30	451.35	6φ12
245	CA1e5C3	15	50	50	Circle	30	451.35	6φ12
246	CA2e1C3	30	10	10	Circle	30	451.35	6φ12
247	CA2e2C3	30	20	20	Circle	30	451.35	6φ12
248	CA2e3C3	30	30	30	Circle	30	451.35	6φ12
249	CA2e4C3	30	40	40	Circle	30	451.35	6φ12
250	CA2e5C3	30	50	50	Circle	30	451.35	6φ12

251	CA3e1C3	45	10	10	Circle	30	451.35	6φ12
252	CA3e2C3	45	20	20	Circle	30	451.35	6φ12
253	CA3e3C3	45	30	30	Circle	30	451.35	6φ12
254	CA3e4C3	45	40	40	Circle	30	451.35	6φ12
255	CA3e5C3	45	50	50	Circle	30	451.35	6φ12
256	CA4e1C3	60	10	10	Circle	30	451.35	6φ12
257	CA4e2C3	60	20	20	Circle	30	451.35	6φ12
258	CA4e3C3	60	30	30	Circle	30	451.35	6φ12
259	CA4e4C3	60	40	40	Circle	30	451.35	6φ12
260	CA4e5C3	60	50	50	Circle	30	451.35	6φ12
261	CA5e1C3	75	10	10	Circle	30	451.35	6φ12
262	CA5e2C3	75	20	20	Circle	30	451.35	6φ12
263	CA5e3C3	75	30	30	Circle	30	451.35	6φ12
264	CA5e4C3	75	40	40	Circle	30	451.35	6φ12
265	CA5e5C3	75	50	50	Circle	30	451.35	6φ12
266	CA6e1C3	90	10	10	Circle	30	451.35	6φ12
267	CA6e2C3	90	20	20	Circle	30	451.35	6φ12
268	CA6e3C3	90	30	30	Circle	30	451.35	6φ12
269	CA6e4C3	90	40	40	Circle	30	451.35	6φ12
270	CA6e5C3	90	50	50	Circle	30	451.35	6φ12

Note: a

- For shape of column square, rectangular and circular column which is designated by S,R and C respectively;
- For angle 15,30,45,60,75 and 90 degree which is designated by A1,A2,A3,A4,A5 and A6 respectively;
- For eccentricity 10,20,30,40 and 50mm which is designated by e1,e2,e3,e4 and e5, and

- For concrete grade $f_{ck}=20,25$ and 30Mpa which is designated by C1,C2 and C3 respectively;

Note: b

- SAeC...S=Square, A=Angle, e=eccentricity and C=Concrete grade
- RAeC...R=Rectangular, A=Angle, e=eccentricity and C=Concrete grade
- CAeC...C=Circular, A=Angle, e=eccentricity and C=Concrete grade.

3.5 Nonlinear Finite Element Software

In this research Nonlinear Finite element analysis software which is called ABAQUS 6.14 is used. The Abaqus finite element system includes Abaqus CAE, Abaqus viewer, Abaqus /standard, Abaqus/ explicit and Abaqus/CFD. Each of them is clearly described below.

- **Abaqus/CAE:** is a complete Abaqus environment that provides a simple, consistent interface for creating, submitting and evaluation results from Abaqus analysis products. Abaqus/CAE is divided into modules, where each module defines a logical aspect of the modeling process. As you move from module to module, you build the model from which Abaqus/CAE generates an input file that you submit to the Abaqus analysis product. The analysis product performs the analysis, sends information to Abaqus/CAE to allow you to monitor the progress of the job and generates an output database. Finally, using the visualization module of Abaqus/CAE to read the output database and view the results of analysis. (Abaqus/CAE userguides,2013).
- **Abaqus/Viewer:** provides graphical display of Abaqus finite element models and results. Abaqus/Viewer is incorporated into Abaqus/CAE as Visualization module.
- **Abaqus/Standard:** is general purpose analysis product. It can solve a wide range of linear and nonlinear problems involving the static, dynamic, thermal, electrical and electromagnetic response of components.
- **Abaqus/Explicit:** It is the other type of analysis product which provides nonlinear, transient, dynamic analysis of solids and structures using explicit time integration. Its powerful contact capabilities, reliability and computational efficiency on large models

also make it highly effective for quasi-static applications involving discontinuous nonlinear behavior.

- **Abaqus/CFD:** This product is a computational fluid dynamics program with extensive support for preprocessing, simulation and post processing in Abaqus/CAE. It provides scalable parallel CFD simulation capabilities to address a number of nonlinear coupled fluid-thermal and fluid structural problems. (Abaqus release note, 2013).

Therefore, a short bi-axially loaded reinforced concrete column is modeled and submitted to analysis product using Abaqus/ CAE.

3.6 Modeling of Short RC column.

Before modeling of the specimen the validation works which is described in the last portion of chapter four is done using method described in this chapter. The modeling procedure is described below and illustrated in Fig3.1.

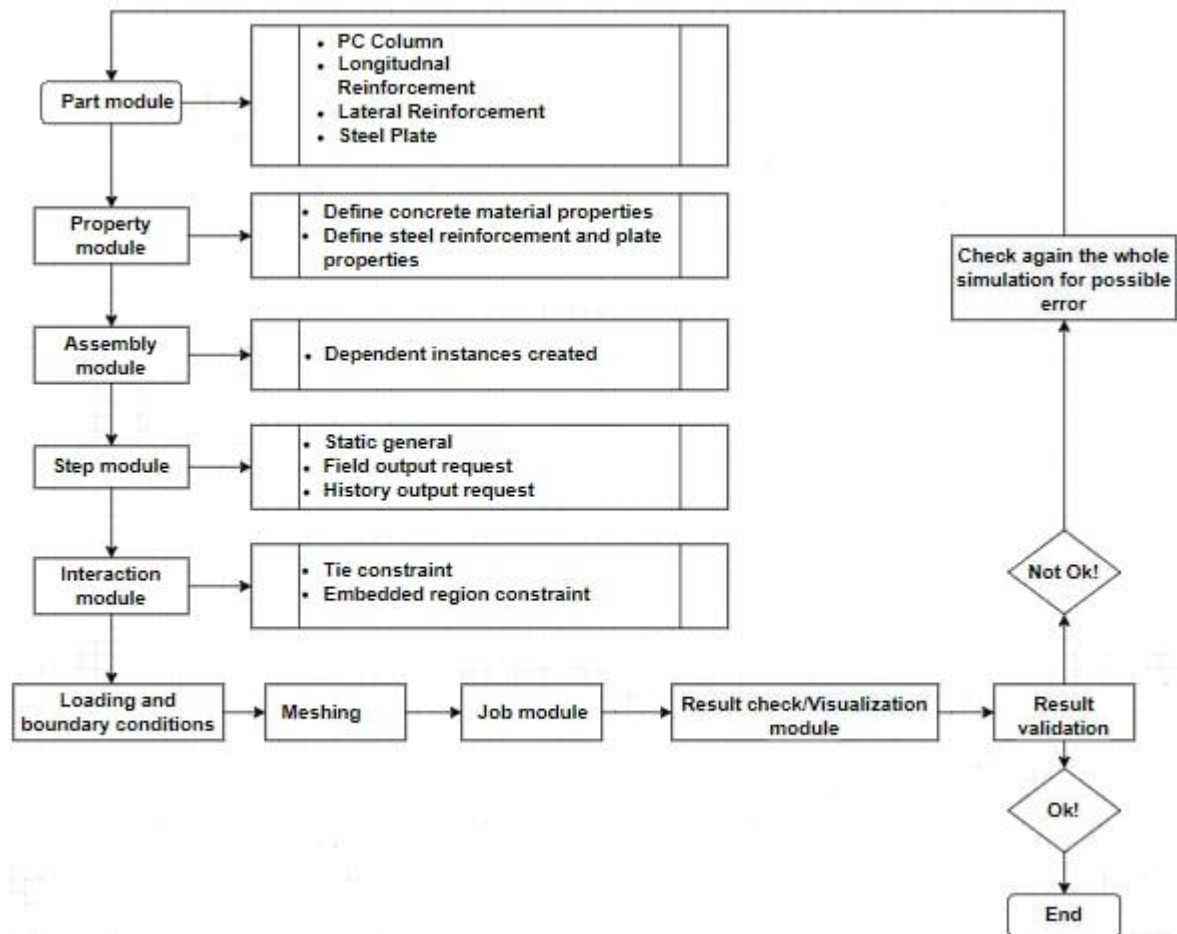
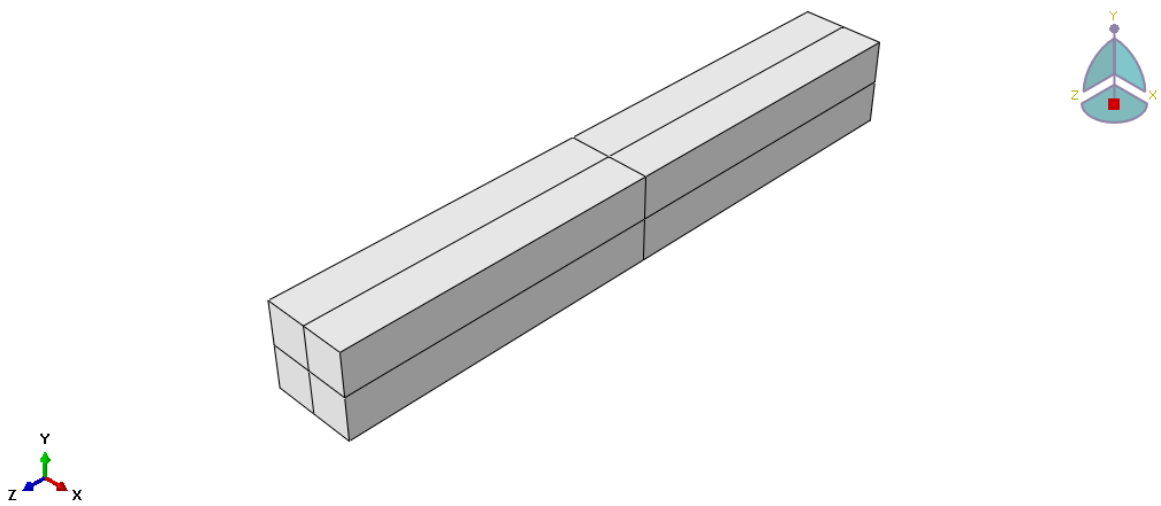


Figure 3. 1: Chart shows the procedure of modeling.

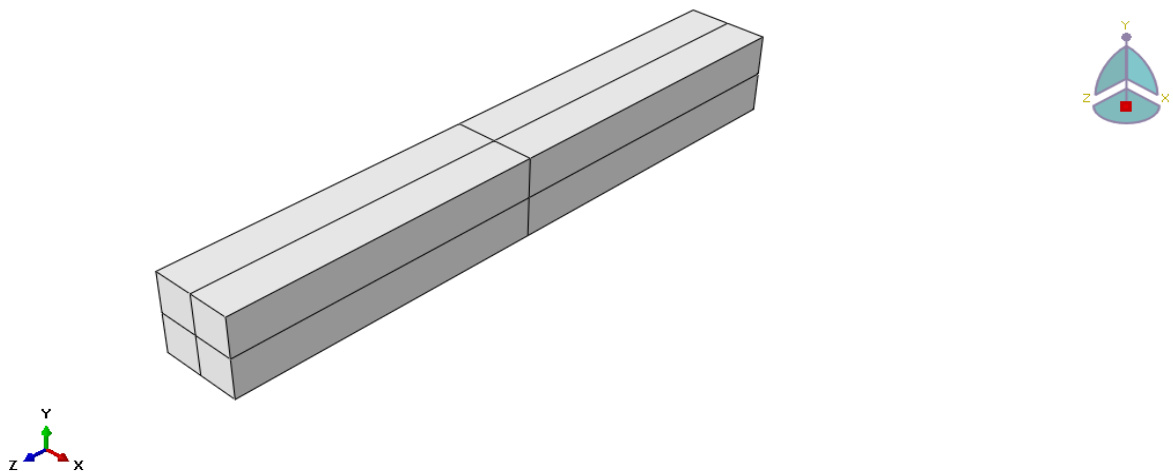
3.6.1 Geometry

a) Plain concrete column

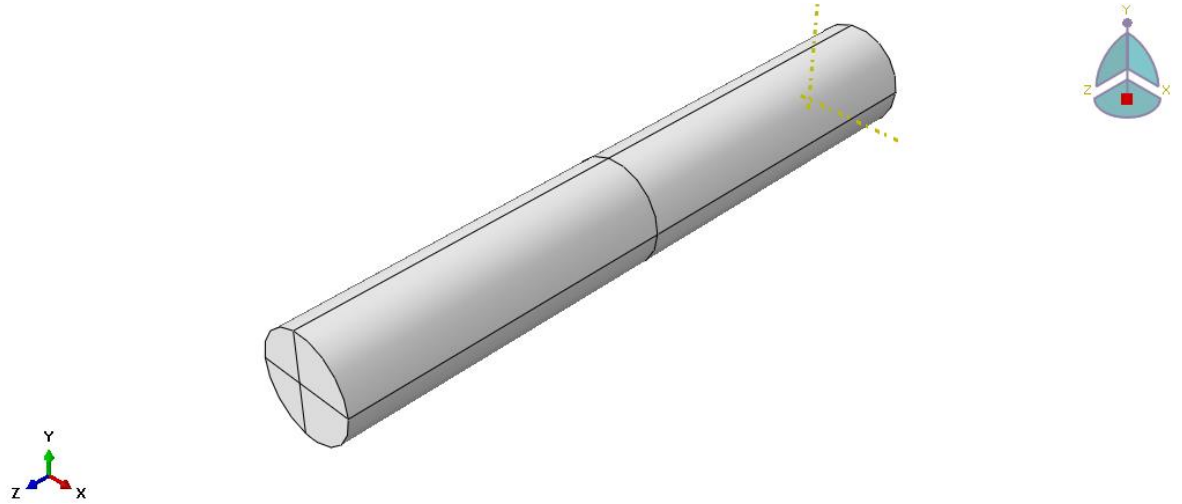
Square, rectangular and circular column with a height of 3000mm was modeled using 3D, deformable and extrusion method. It is shown in Fig 3.2. In order to keep the compatibility between steel plate and RC column the partition was created. This also enables us to refine the mesh and get better result.



a) Specimen SA1e1C1 for square



b) Specimen RA1e1C1 for Rectangular.



c) Specimen CA1e1C1 for Circular

Figure 3. 2: 3D plain concrete part

b) Longitudinal Reinforcement

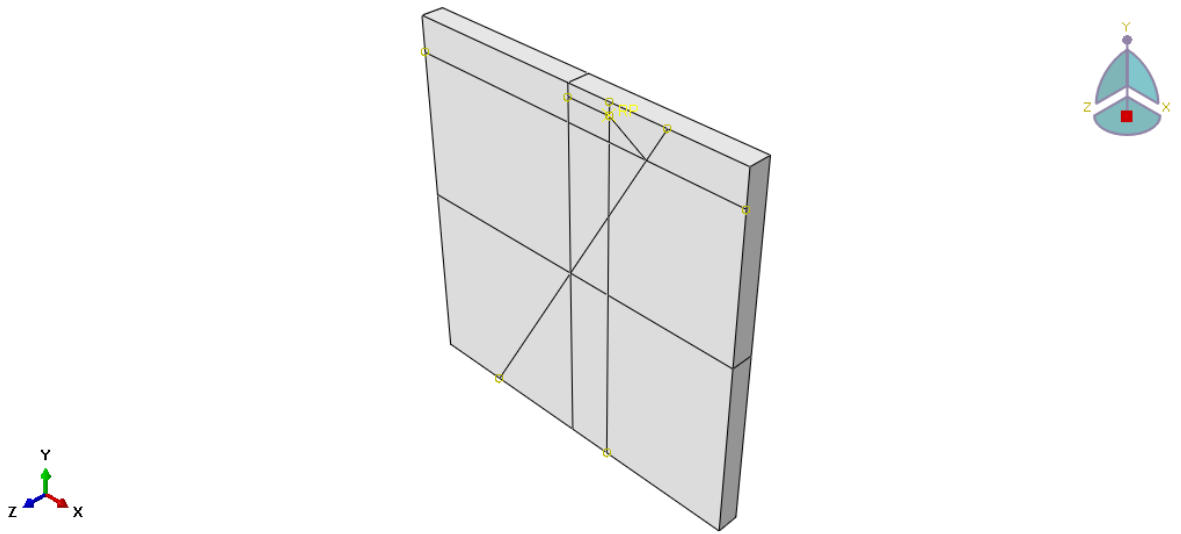
It was modeled using 3D, deformable and wire method.

c) Lateral reinforcement

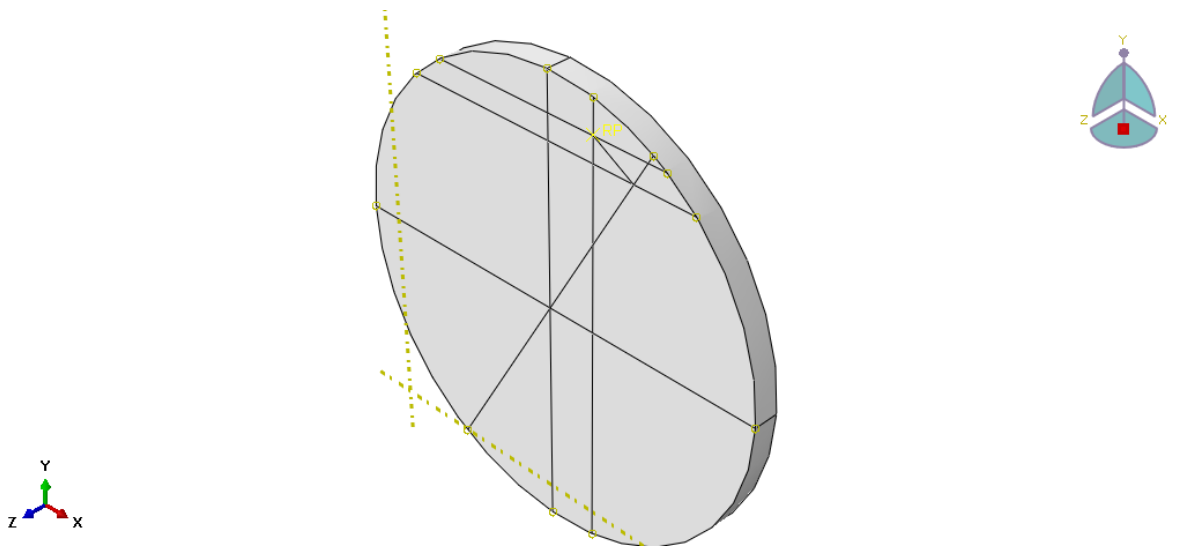
It was modeled using 3D, deformable and wire method.

d) Steel Plate

Steel Plate was used at the top end and bottom end of the column. It was modeled using 3D, discrete rigid and extrusion method. Thickness of 25mm was used. The non-orthogonal axis was modelled on this plate and presented in the following Figure 3.3.



a) Steel plate for square sample for specimen SA2e5C1



b) Steel plate for circular sample for specimen CA2e5C1

Figure 3. 3: Steel plate for end of the column.

3.6.2 Material property

Material property for the modelling of the specimen is taken randomly based on the concrete grade used on the site by keeping the variation of concrete grade constant for the purpose of study.

a) Concrete

Three different constitutive models are offered in Abaqus for the analysis of concrete at low confining pressures. These constitutive models are:

- Smearred crack concrete model
- Brittle cracking model
- Concrete damaged plasticity model

From the above mentioned model, smeared crack model is available only in Abaqus/Standard and Brittle cracking model is available only in Abaqus/Explicit. But concrete damaged plasticity is available in both Abaqus/Standard and Abaqus/Explicit. Each model is designed to provide a general capability for modeling plain and reinforced concrete in all types of structures. Brittle cracking model assumes that compressive behavior is always linear elastic. (Abaqus Analysis 3,2013). Since Abaqus/Standard was selected and compressive behavior is nonlinear concrete damage plasticity model was chosen.

➤ Concrete damage plasticity model

Alfarah et al. state that concrete exhibit nonlinear stress-strain response mainly because of micro-cracking. Cracks are oriented as the stress field and generate the failure modes. In tension, failure localized in a narrow band; stress-strain behavior is characterized by sudden softening accompanied with reduction in the unloading stiffness. In compression, failure begins usually in the outside and is more complex, involving volumetric expansion, strain localization, crushing, and inclined slipping and spalling; stress-strain behavior involves ductile hardening followed by softening and reduction in the unloading stiffness. (Alfarah B., et al., 2017). Concrete damage plasticity model have shown good performance in capturing concrete behavior which is mentioned above in tests on full-scale structures. (Nguyen G., et al., 2008). This model is particularly well suited for reproducing failure modes that are based on tensile cracking and compression crushing. (Alfarah B., et al., 2017).

When the concrete specimen is unloaded from any point on the strain softening branch of the stress-strain curves, the unloading response is observed to be weakened: the elastic stiffness of the material appears to be damaged (or degraded). The degradation of the elastic stiffness is significantly different between tension and compression tests. In either case, the effect is more pronounced as the plastic strain increases. The degraded response of concrete is characterized by two independent uniaxial damage variables d_t and d_c which are assumed to be functions of the plastic strain, temperature and field variables. The uniaxial degradation variables are increasing functions of the equivalent plastic strains. They can take values ranging from zero, for the undamaged material to one for the fully damaged material. If E_o is the initial (undamaged) elastic stiffness of the material, the stress-strain relations under uniaxial tension and compression loading are, respectively: (Abaqus Theory,2013).

$$\sigma_c=(1-d_c)E_o(\epsilon_c-\epsilon_c^{pl}) \dots\dots\dots(3.1)$$

$$\sigma_t=(1-d_t)E_o(\epsilon_t-\epsilon_t^{pl})\dots\dots\dots(3.2)$$

The parameters which were used in this model that was input for the software was discussed below:

For dilation angle, eccentricity, ratio of compressive biaxial to compressive uniaxial ($\frac{\sigma_{bo}}{\sigma_{co}}$), Constant K_c and viscosity the default value was used. The default values are listed below.

Table 3.2: Property of Concrete

Modulus of elasticity	29.962Gpa for C1; 31.476Gpa for C2; 32.84Gpa for C3 (Eqn.3.3)
Poisson ratio	0.2 (EC-2,2004)
Dilation angle	36 (default)
Eccentricity	0.1 (default)
f_{bo}/f_{co}	1.16 (default)
Constant, K_c	0.6667 (default)
Viscosity	0 (default)

i) Uniaxial Compressive strength of concrete

Cylindrical compressive strength of the concrete which was used in this thesis is 20Mpa, 25Mpa, 30Mpa. Uniaxial compressive stress-strain diagram which is provided on Euro code for nonlinear analysis was used. It was drawn from Equation which is provided on EC-2, Sec3.1.5 and also discussed below:

$$\frac{\sigma_c}{f_{cm}} = \frac{k\mu - \mu^2}{1 + (k-2)\mu} \dots\dots\dots(3.3), EC-2, (3.14)$$

Where:

$$\mu = \frac{\epsilon_c}{\epsilon_{c1}}$$

$$k = \frac{1.05 E_{cm} |\epsilon_{c1}|}{f_{cm}}$$

$$0 < |\epsilon_c| < |\epsilon_{cu1}|$$

ϵ_{c1} is peak strain at peak stress

f_{cm} is the mean compressive strength at 28 days.

E_{cm} is secant modulus of elasticity of concrete.

Equation which is provided in EC-2, Table 3.1 was used for, ϵ_{c1} , E_{cm} , f_{cm} and ϵ_{cu1} and also listed below.

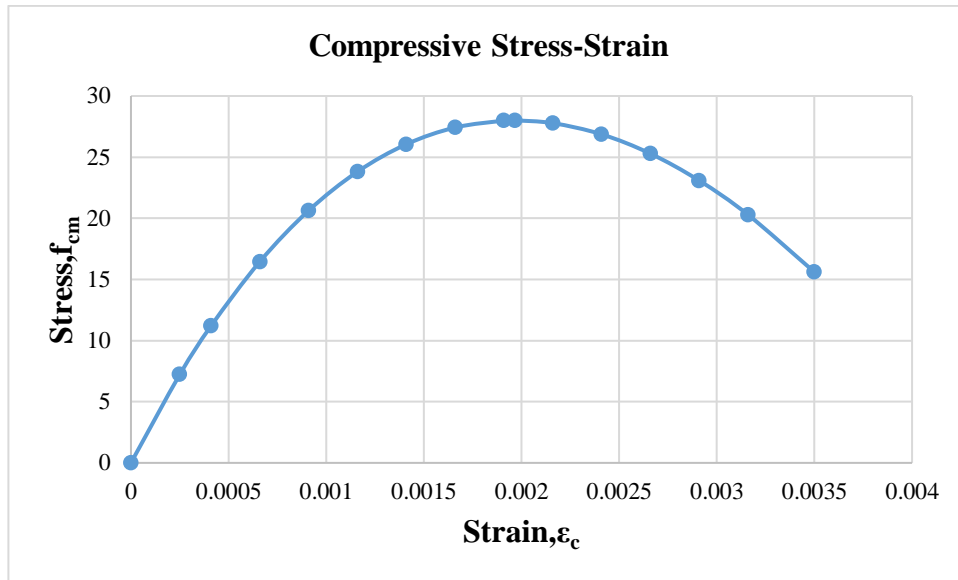
$$f_{cm} = f_{ck} + 8 \text{ (Mpa)} \dots\dots\dots(3.4)$$

$$E_{cm} = 22 \left[\frac{f_{cm}}{10} \right]^{0.3} \text{ where } f_{cm} \text{ (Mpa)} \dots\dots(3.5)$$

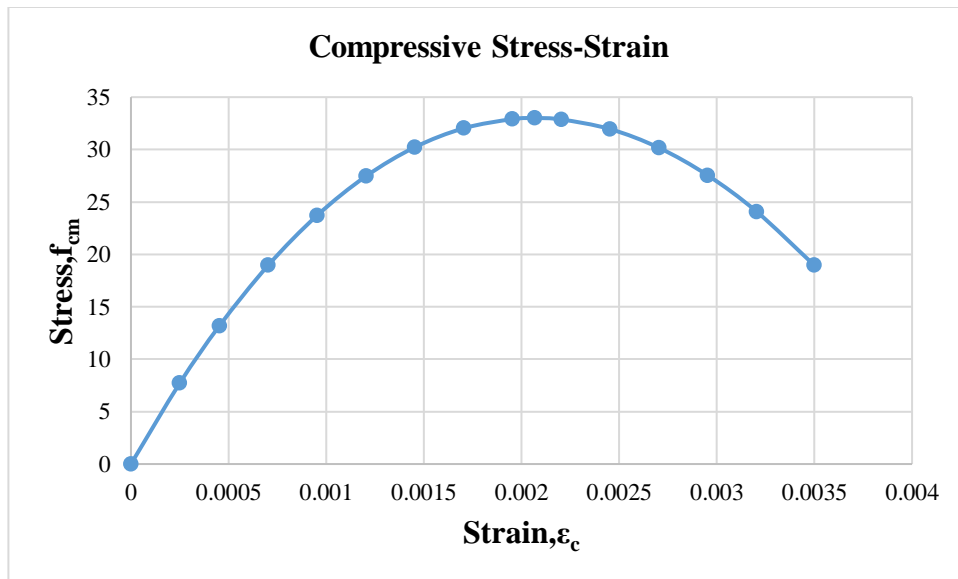
$$\epsilon_{c1} (\text{‰}) = 0.7 f_{cm}^{0.31} < 2.8 \dots\dots\dots(3.6)$$

$$\epsilon_{cu1} (\text{‰}) = 3.5$$

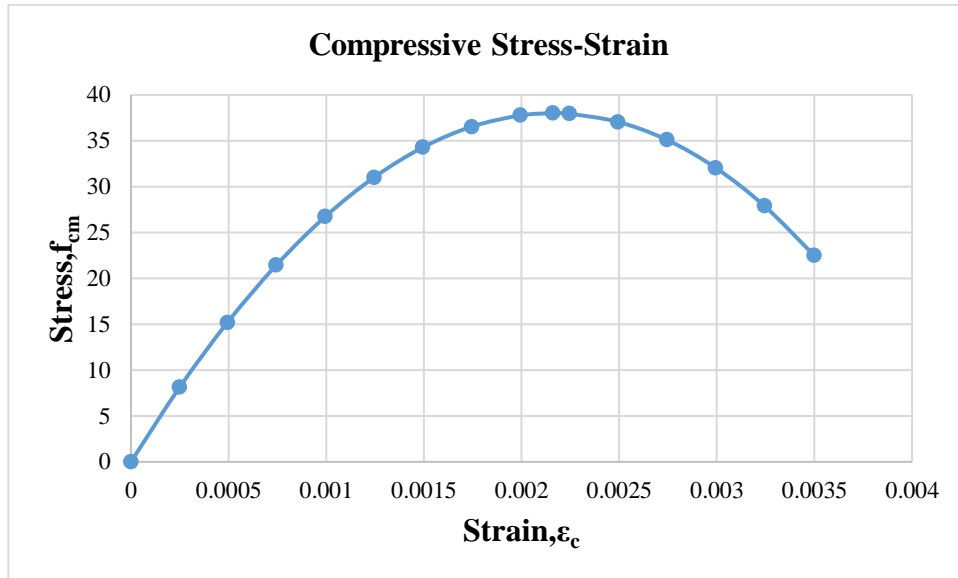
So, $0 < |\epsilon_c| < 3.5$ was considered. Using the above mentioned compressive cylindrical strength each point of the curve was determined and plotted as follows: But the tabulated result is presented in appendix B, Table B.1.



a) Compressive stress-strain diagram $f_{ck}=20\text{Mpa}$ (C1) concrete



b) Compressive stress-strain diagram $f_{ck}=25\text{Mpa}$ (C2) concrete

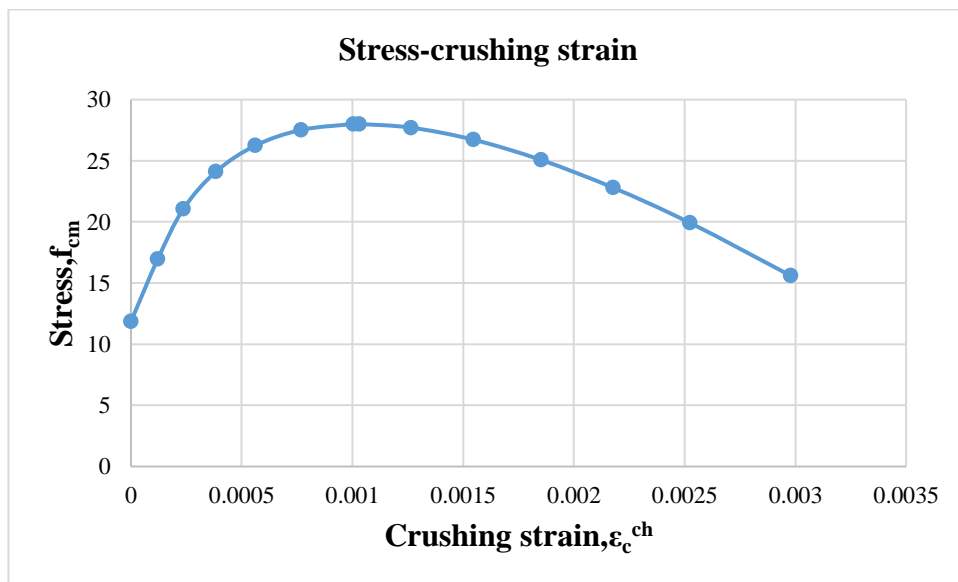


c) Compressive stress-strain diagram fck=30Mpa (C3) concrete

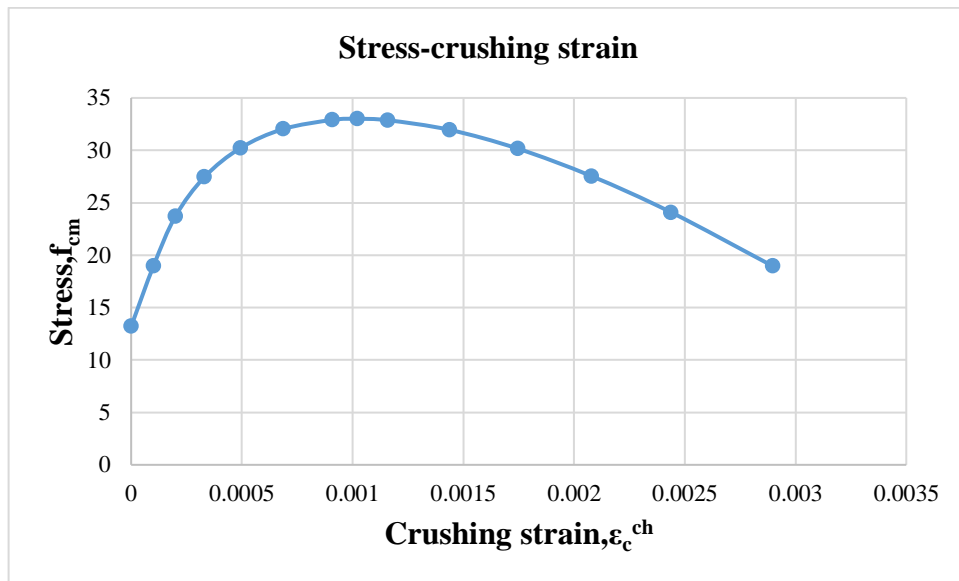
Figure 3. 4: Compressive stress-strain diagram of concrete

But the input which was used for Abaqus is Compressive stress-crushing strain. Crushing strain was calculated by deducting elastic strain from total strain. The diagram is plotted below but the table is presented in appendix B.

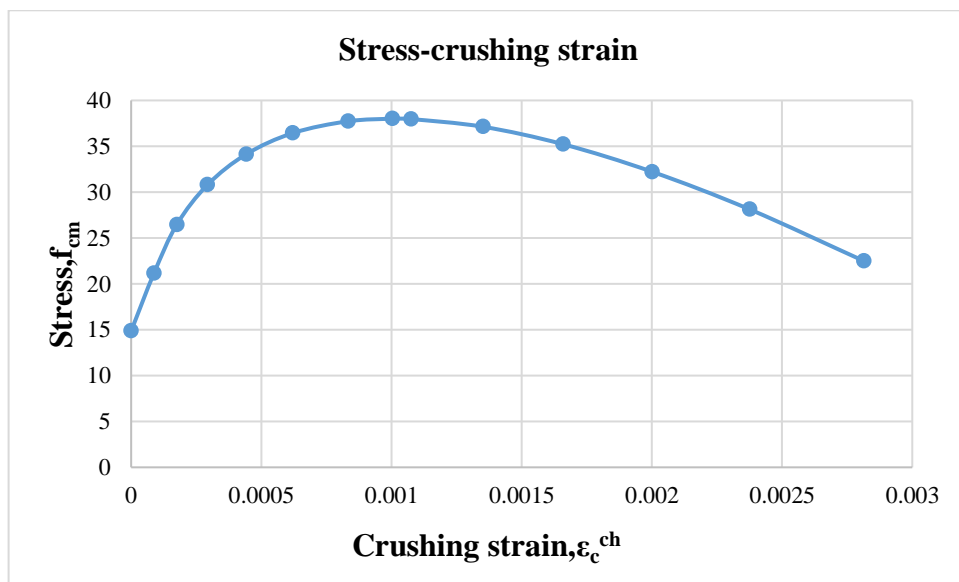
$$\epsilon_c^{ch} = \epsilon_{tot} - \frac{\sigma_c}{E_c} \dots\dots\dots (3.7)$$



a) Compressive stress-crushing strain diagram of fck=20Mpa (C1) concrete



b) Compressive stress-crushing strain diagram of fck=25Mpa (C2) concrete



c) Compressive stress-crushing strain diagram of fck=30Mpa (C3) concrete

Figure 3. 5: Compressive stress-crushing strain diagram of concrete.

ii) Compressive damage variables

The damage variables were prepared based on Alfarah B., et al. proposed methodology and equation. This equation is described as follows: (Alfarah B.,et al.,2017).

$$d_c = 1 - \frac{1}{2+a_c} [2(1+a_c) \exp(-b_c \epsilon_c^{ch}) - a_c \exp(-2b_c \epsilon_c^{ch})] \dots\dots\dots (3.8)(19)$$

Where: ϵ_c^{ch} is compressive crushing strain (inelastic strain).

$$a_c = 7.873, \quad b_c = \frac{1.97(f_{ck} + 8)l_{eq}}{G_{ch}} \dots\dots\dots (3.9)(34)$$

Where: l_{eq} is the characteristic length of the element.

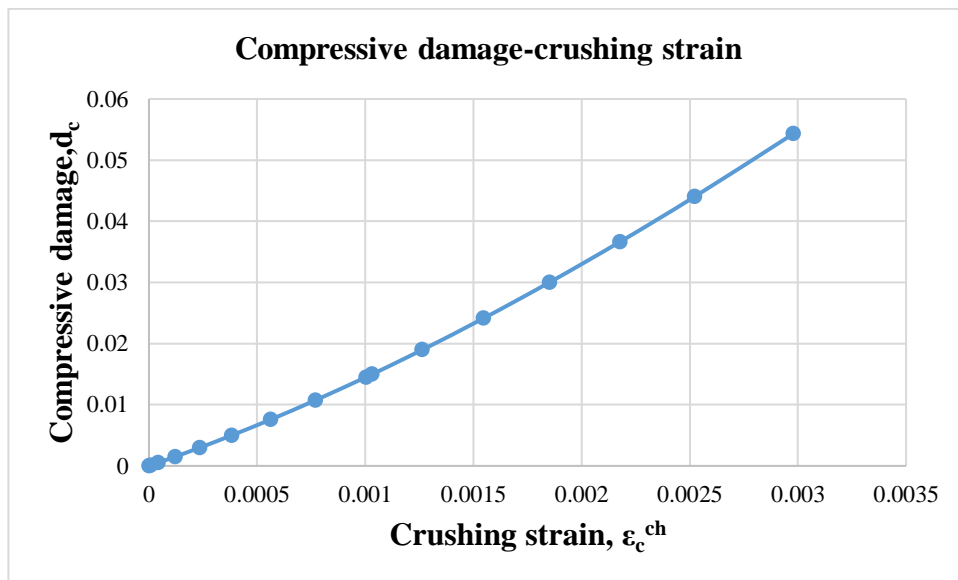
f_{ck} is cylindrical compressive strength of concrete.

G_{ch} is crushing energies, G_F is fracture energies.

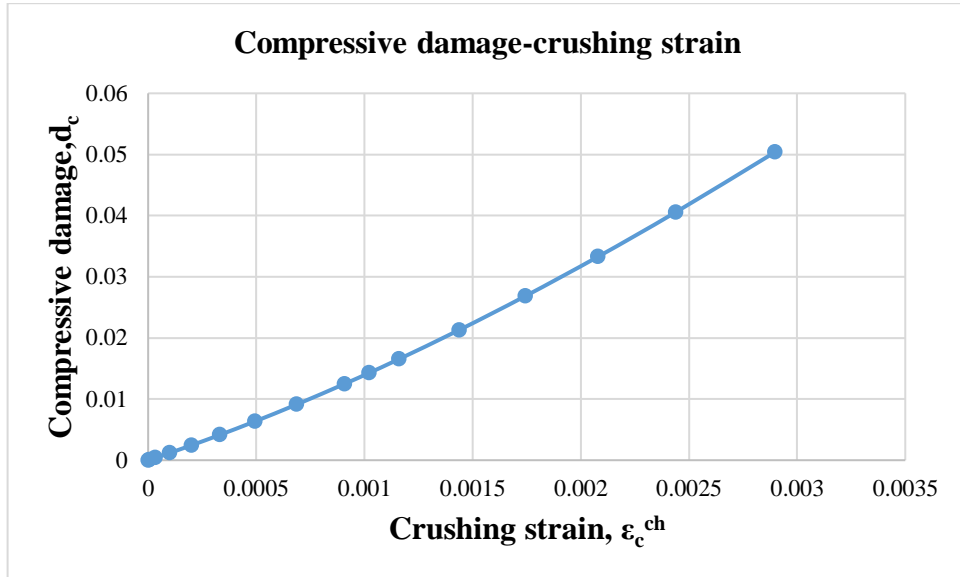
$$G_{ch} = \left(\frac{f_{cm}}{f_{tm}}\right)^2 G_F \dots\dots\dots (3.10)(32)$$

$$G_F \text{ (N/mm)} = 0.073 f_{cm}^{0.18}, \quad f_{cm} \text{ (Mpa)} \dots\dots\dots (3.11)(31)$$

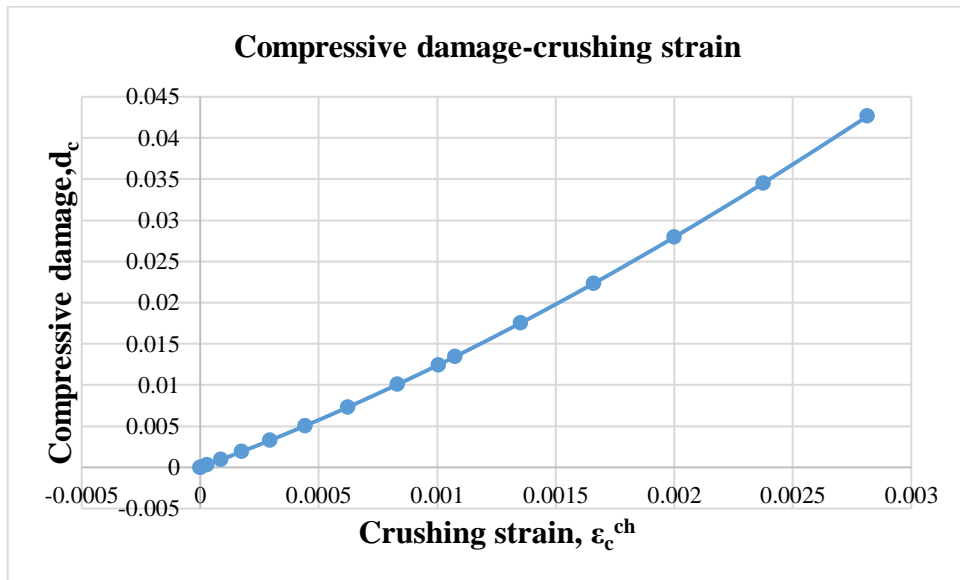
Using these equation damage variables were computed and tabulated. Compressive damage variable-crushing strain is illustrated below but the table is presented in appendix B.



a) Compressive damage-crushing strain diagram of $f_{ck}=20\text{Mpa}$ (C1) concrete.



b) Compressive damage-crushing strain diagram of fck=25Mpa (C2) concrete.



c) Compressive damage-crushing strain diagram of fck=30Mpa (C3) concrete.

Figure 3. 6: Compressive damage-crushing strain diagram of concrete.

iii) Tensile strength of concrete

For tensile behavior, the equation which is provided on Hordijk was used (Hordijk, 1992). The ratio of tensile stress $\sigma_t(w)$ (for crack width w) and maximum tensile strength f_{tm} is given as follows:

$$\frac{\sigma_t(w)}{f_{tm}} = \left[1 + \left(c_1 \left(\frac{w}{w_c} \right) \right)^3 \right] e^{-c_2 \left(\frac{w}{w_c} \right)} - \left(\frac{w}{w_c} \right) (1 + c_1^3) e^{-c_2} \dots \dots \dots (3.12)(29)$$

In equation 3.8, $c_1=3$, $c_2=6.93$ (Hordijk,1992); and w_c is the critical crack opening. The equation 3.12 shows that; $\sigma_t(0)=f_{tm}$ and $\sigma_t(w_c) = 0$. Therefore, w_c can be considered as the fracture crack opening.(Alfarah,2017).

$$w_c = \frac{5.14G_F}{f_{tm}} \dots \dots \dots (3.13)(30)$$

$$f_{tm} = 0.3016f_{ck}^{\frac{2}{3}} \dots \dots \dots (3.14)$$

In this proposed method the actual crack spacing was not studied but single crack per element has been assumed. Alfarah et al. agree that the assumption is suitable for global-purpose simulation. After this assumption, in the descending segment of the tensile stress-strain curve, the strain can be obtained in terms of the crack opening from the following kinematic relation. (Alfarah et al.,2017):

$$\epsilon_t = \epsilon_{tm} + \frac{w}{l_{eq}} \dots \dots \dots (3.15)(33)$$

Based on the above discussed method tensile stress-strain of concrete was computed and tabulated and plotted in appendix B. But stress-cracking strain which was used as input data for the software is plotted in Fig 3.7. Cracking strain was calculated by deducting elastic strain from total strain.

iii) Tensile damage variables

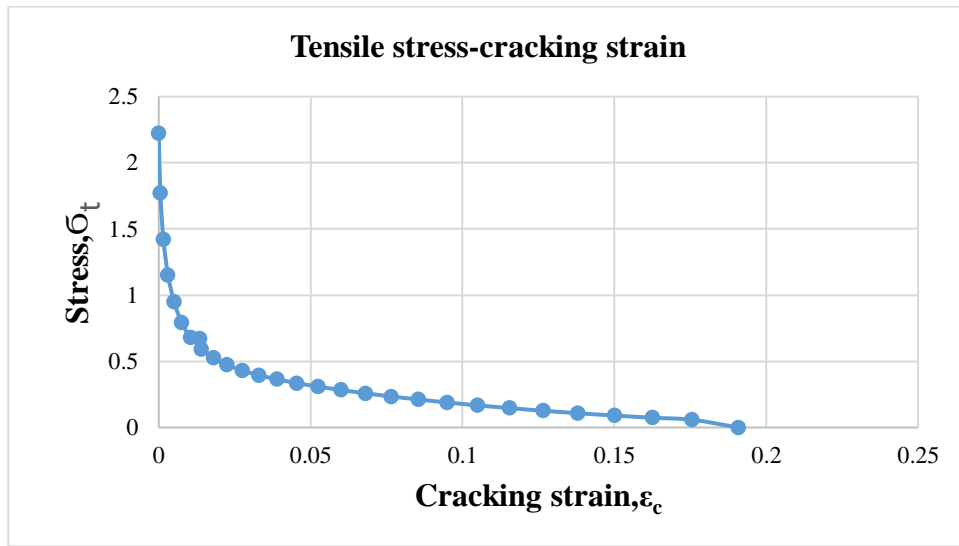
As it is discussed in compressive damage variables the same method was employed also for tensile damage variables and it is described as follows:

$$d_t = 1 - \frac{1}{2+a_t} [2(1+a_t) \exp(-b_t \varepsilon_t^{ck}) - a_t \exp(-2b_t \varepsilon_t^{ck})] \dots \dots \dots (3.16)(20)$$

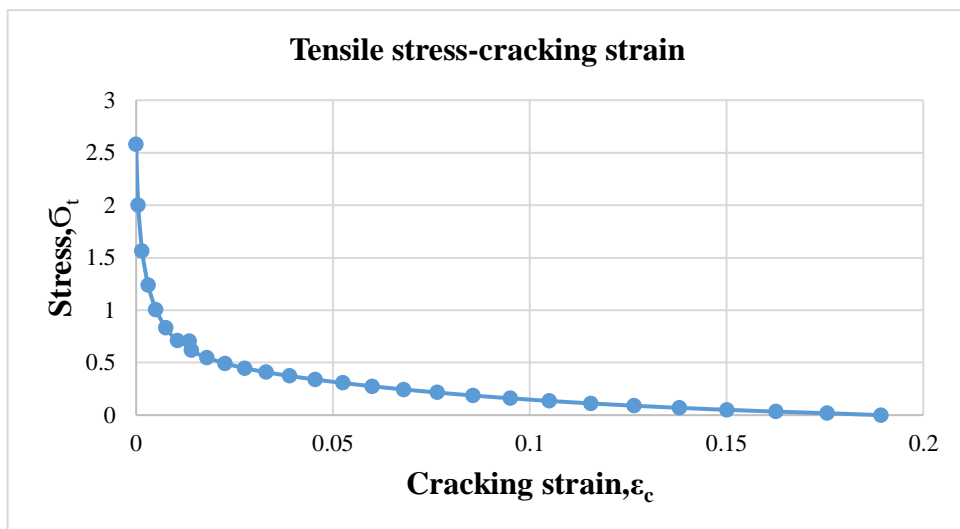
Where: ε_t^{ck} is tensile cracking strain (inelastic strain).

$$a_t = 1, \quad b_t = \frac{0.453(f_{ck})^{\frac{2}{3}} I_{eq}}{G_F} \dots \dots \dots (3.17)(34)$$

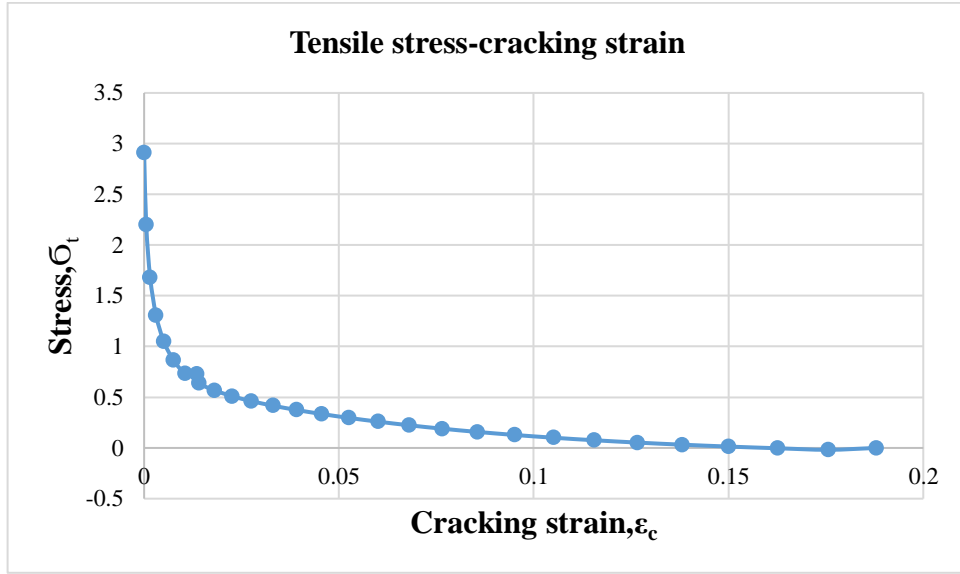
Using equation 3-16, tensile damage variables were computed and tabulated. Tensile damage variables-cracking strain is plotted in Fig3.8. But the table is presented in appendix B.



a) Tensile stress-cracking strain diagram of fck=20Mpa (C1) concrete.

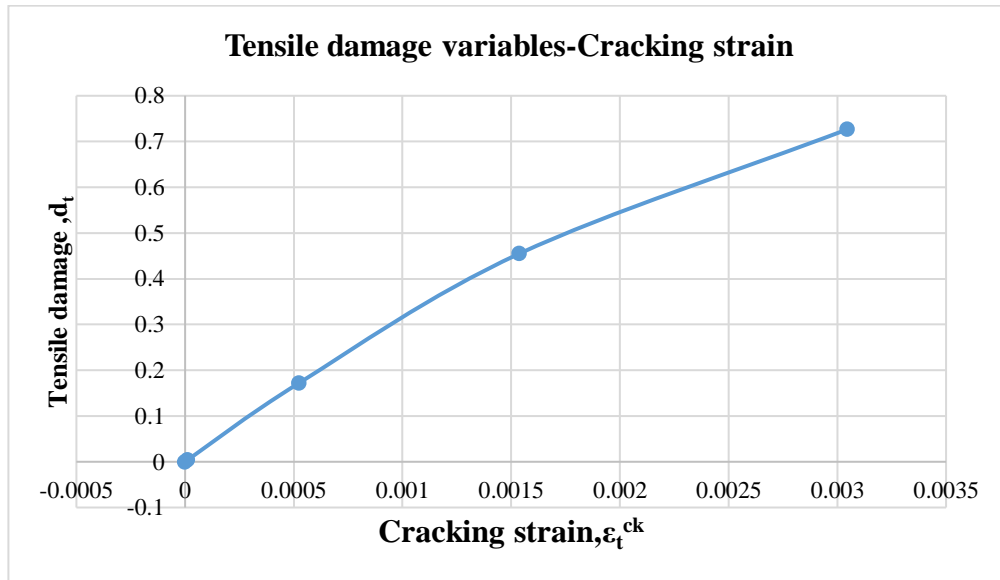


b) Tensile stress-cracking strain diagram of fck=25Mpa (C2) concrete

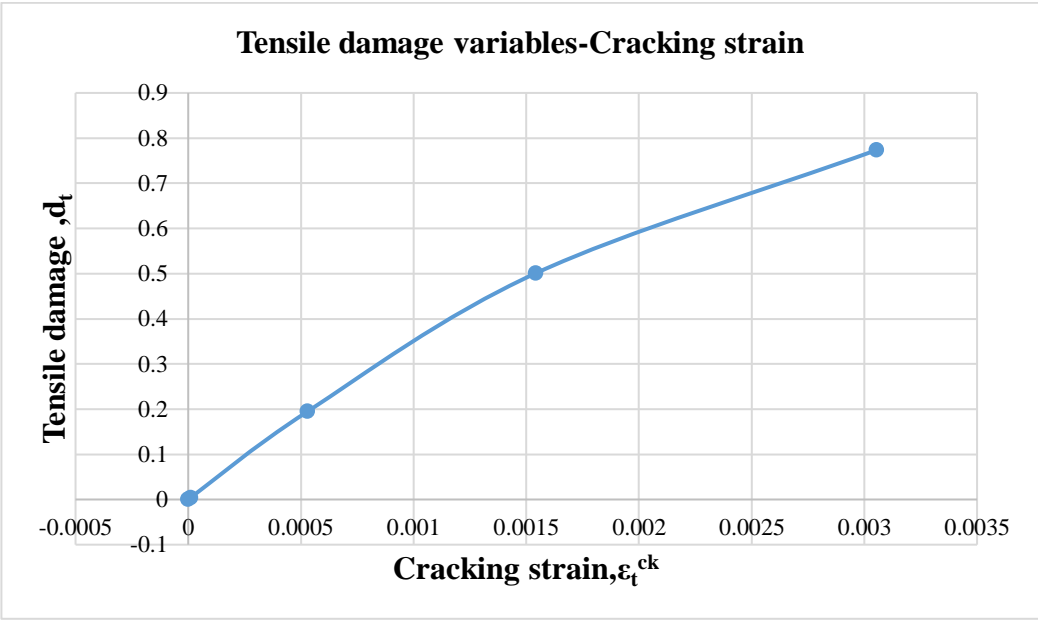


c) Tensile stress-cracking strain diagram of $f_{ck}=30\text{Mpa}$ (C3) concrete

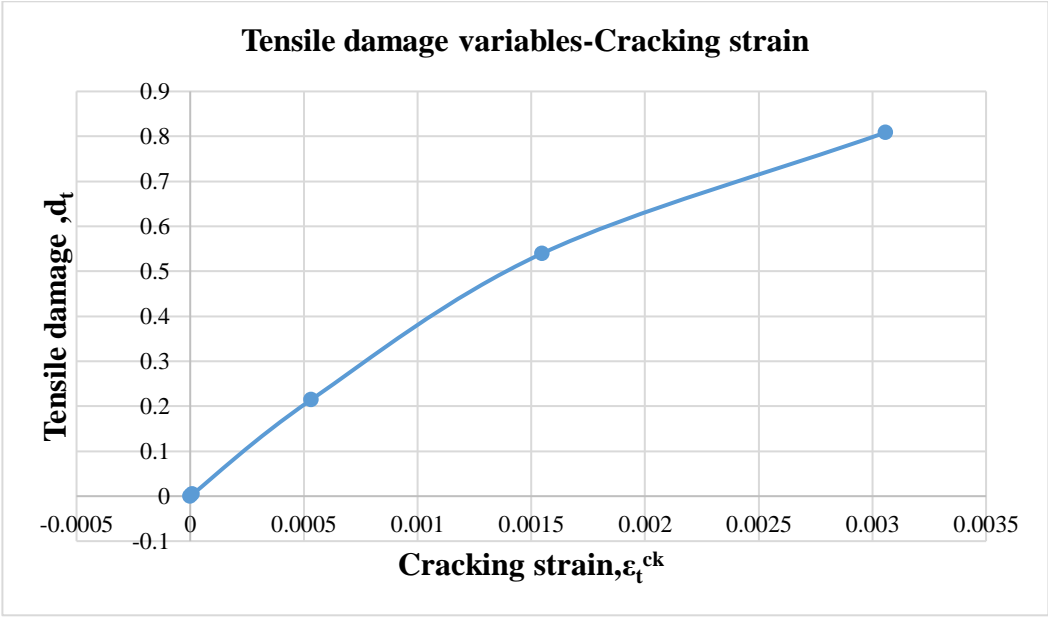
Figure 3. 7: Tensile stress-cracking strain diagram of concrete.



a) Tensile damage variables-cracking strain diagram of $f_{ck}=20\text{Mpa}$ (C1) concrete



b) Tensile damage variables-cracking strain diagram of fck=25Mpa(C2) concrete



c) Tensile damage variables-cracking strain diagram of fck=30Mpa(C3) concrete

Figure 3. 8: Tensile damage variables-cracking strain diagram of concrete.

b) Steel

For all of the following steel Poisson ratio of 0.3 were used.

i) Reinforcement bar

Stress-strain data for steel was taken from Wang G.G. and Thomas Hsu C.T. (1992) study. The mechanical properties of steel reinforcement are presented by the following graph for longitudinal reinforcement.

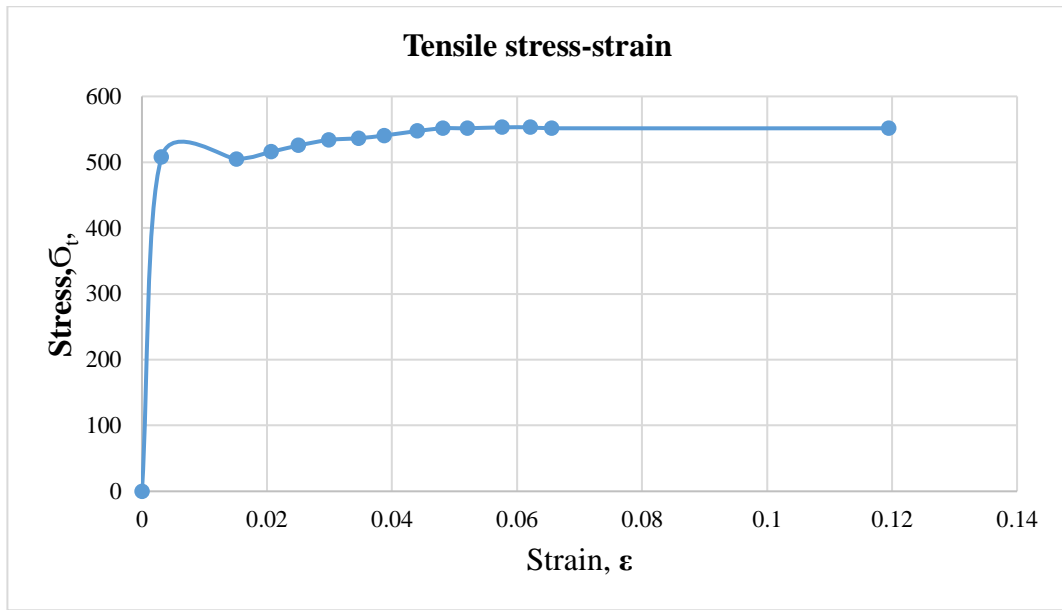


Figure 3. 9: Tensile stress-strain of longitudinal reinforcement.

For lateral reinforcement with yield strength of 350Mpa and elastic modulus of 203Gpa was used. The data is tabulated in Appendix B. But true stress-logarithmic plastic strain was used as input data for the software which was computed based on true stress and logarithmic strain equation. The equation which was used to compute true stress and logarithmic plastic strain from nominal stress and nominal strain is presented as follows (Abaqus Analysis-3,2013):

$$\sigma_{\text{true}} = \sigma_{\text{nom}}(1 + \epsilon_{\text{nom}}) \dots \dots \dots (3.20)$$

$$\epsilon_{\text{ln}}^{\text{pl}} = \ln(1 + \epsilon_{\text{nom}}) - \frac{\sigma_{\text{true}}}{E} \dots \dots \dots (3.21)$$

Using nominal stress and strain, true stress and logarithmic plastic strain was computed and tabulated in appendix B but the diagram is plotted in fig3.10.

For Longitudinal reinforcement

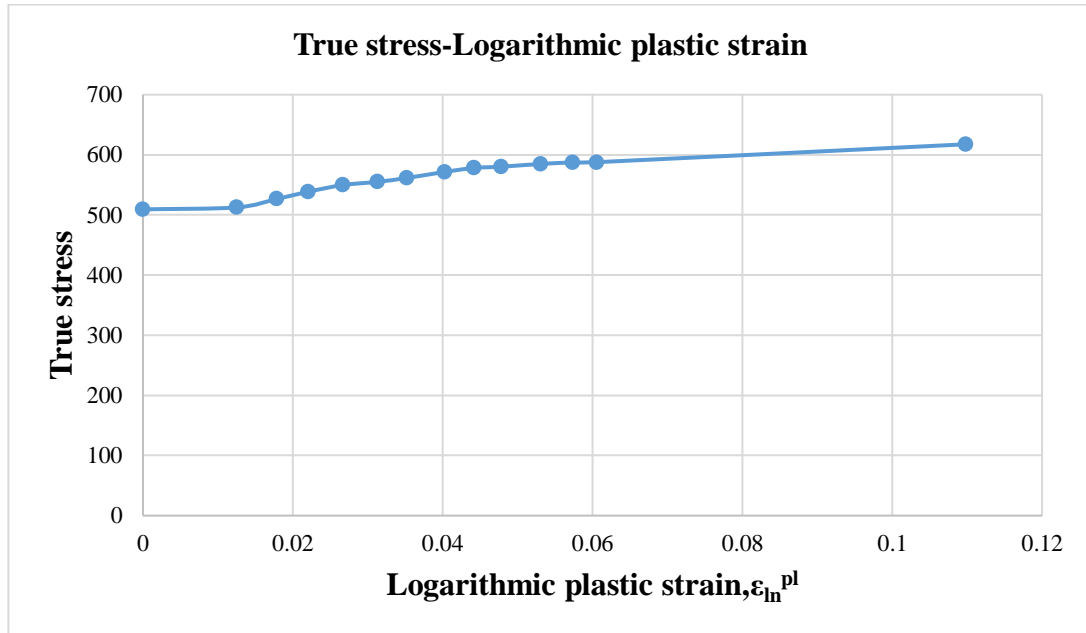


Figure 3. 10: True stress-plastic strain of longitudinal steel reinforcement.

For Lateral reinforcement the true stress is 351.116Mpa which is used as input for the software.

ii) Steel plate

Since the steel plate was discrete rigid the material property was not defined.

3.6.3 Part assembly and their Interaction

Instances were created for each part which was created at beginning of modeling and all instances were assembled to their relative position. Dependent instance was used. Spacing for lateral reinforcement that is used in the modeling was 75mm and 150mm at the end and mid of the column respectively in which they were used in validation. So the assembled reinforced concrete column and steel reinforcement frame is presented for both square and circular in fig

3.11 and fig 3.12 respectively. Since the procedure and arrangement for square and rectangular column is the same, it is not presented here for rectangular.

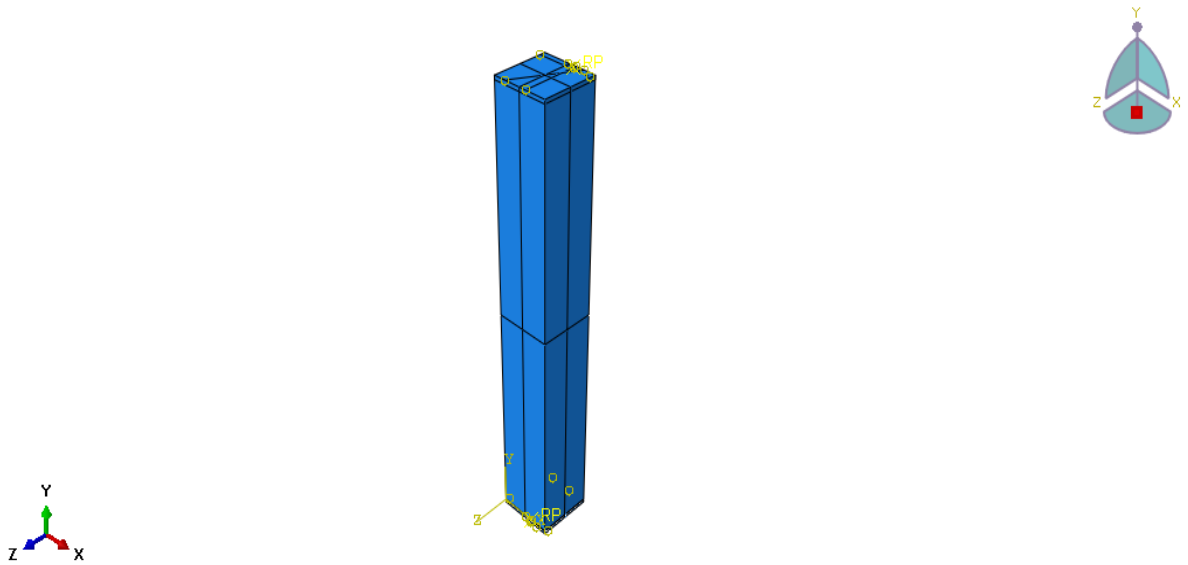


Figure 3. 11: Assembled short reinforced concrete column using Abaqus for SA2e5C1

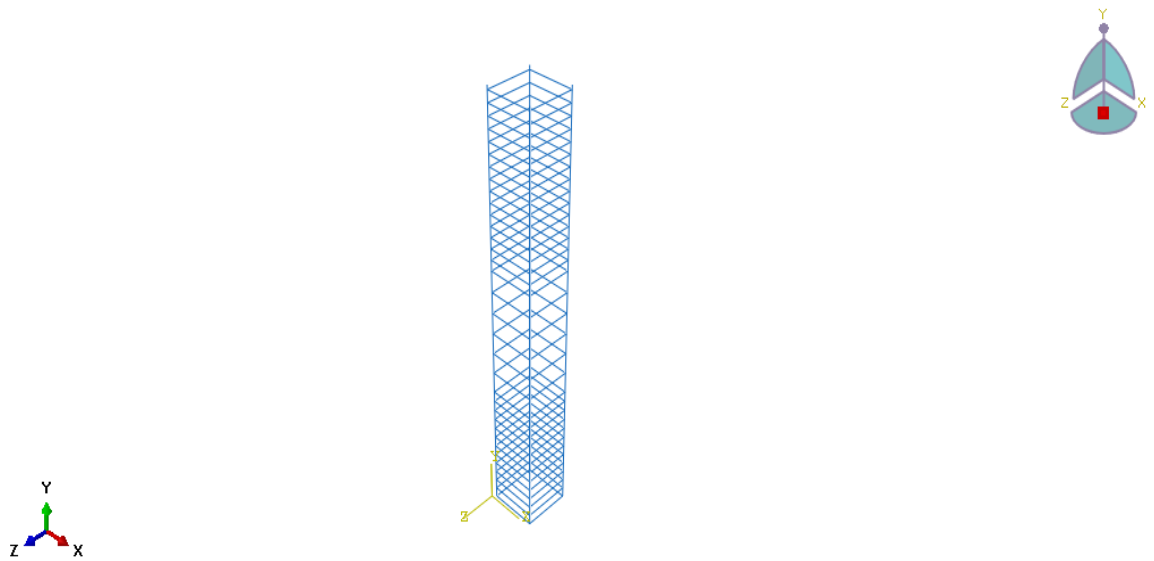


Figure 3. 12: Assembled longitudinal and lateral reinforcement using Abaqus for SA2e5C1

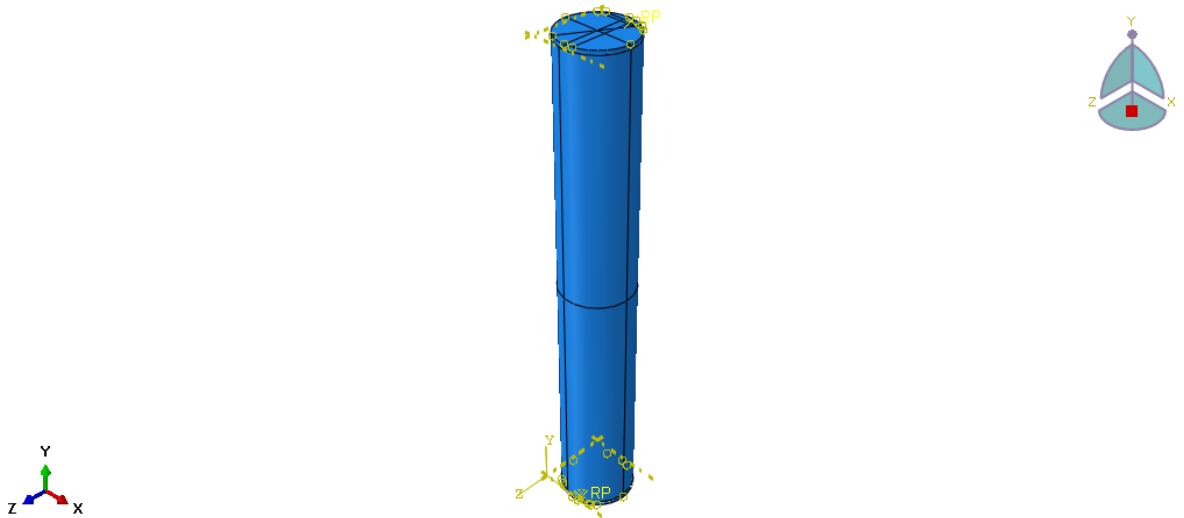


Figure 3. 13: Assembled short reinforced concrete column using Abaqus for CA2e5C1

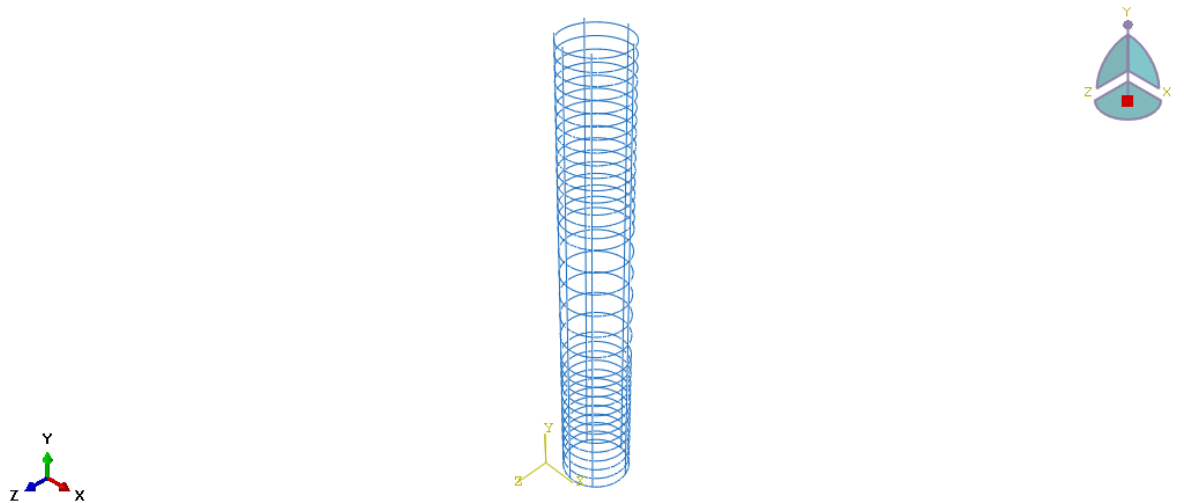


Figure 3. 14: Assembled longitudinal and lateral reinforcement using Abaqus for CA2e5C1

For reinforcement bar embedded region constraint was used by considering reinforcement as embedded part and concrete as a host. This type of constraint was used to create the strong bond between reinforcement and concrete. But for the region between column end and steel plate, tie constraint was used by taking column surface as a master and plate surface as slave. This constraint enables both column and steel plate to act as one body.

3.6.4 Analysis step

In addition to initial step only one step was created. In the created step static general method was selected. Static general method includes material nonlinearity. For initial increment 0.1 and for maximum 1 was used. Finally, the required field output and history output was selected.

3.6.5 Boundary condition and Loading

At both ends pin support which is not constrained in longitudinal direction of the column was used. Loading was done for each specimen at different eccentricity, angle with in axis of moment, for concrete grade and column shape. To consider the rate of loading on the column amplitude is defined with smooth step amplitude type.

3.6.6 Meshing

i) Mesh size

Different analysis was done in validation work using different mesh size until the analysis result was conforming to experimental result. So 0.02m mesh size gave the best result which conforms to experimental result and takes reasonable running time for the model. Since dependent instances were used mesh was done for parts.

ii) Element type

For Plain concrete column part C3D8R was used which is an 8 nodes linear brick, reduced integration hourglass control and B31 element which is first order three dimensional beam element was used for reinforcement. But T3D2 which is first order three dimensional truss element was used for lateral reinforcement. For steel plate R3D4 in which 4 node 3D bilinear rigid quadrilateral element was used. Meshing of square and circular RC column are shown in fig 3.15 and fig 3.16 respectively.

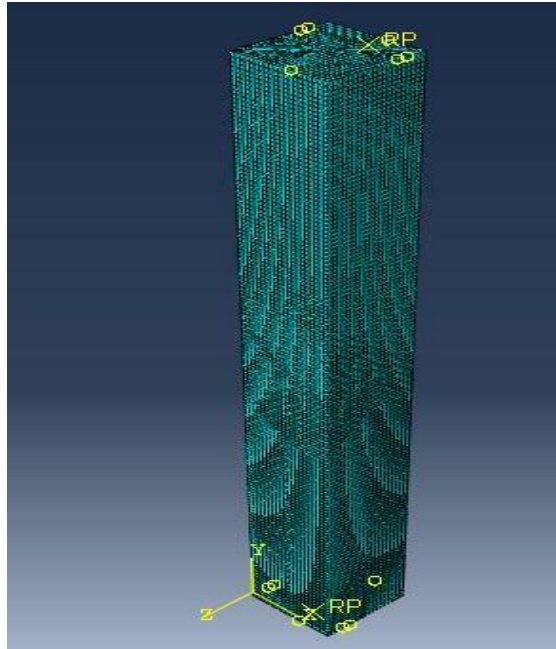


Figure 3. 15: Descriticized reinforced concrete column using Abaqus for SA2e5C1

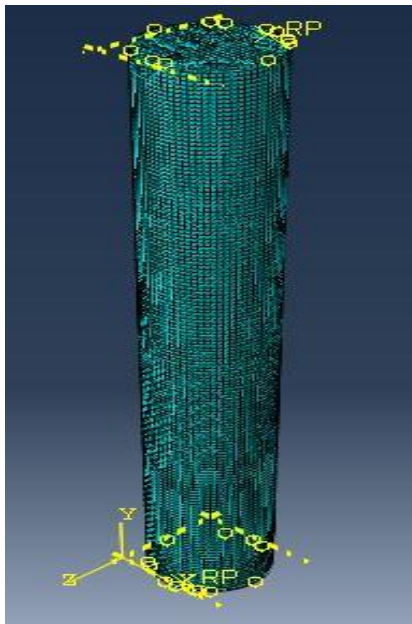


Figure 3. 16: Descriticized reinforced concrete column using Abaqus for CA2e5C1

Finally, job was created and the result was taken when the analysis was completed. Though stress-strain was checked, only load and displacement curve was collected for each specimen analysis.

CHAPTER FOUR

4.1 Validation of Finite Element Modelling

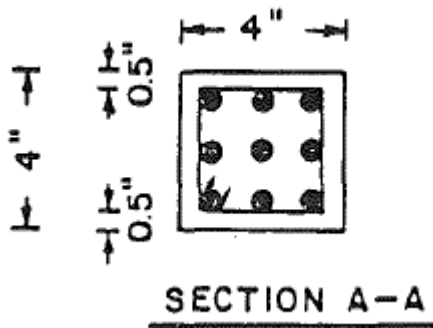
4.1.1 Bench mark experiment

Wang G.G. and Thomas Hsu C.T. (1992), which was done on the complete biaxial load-deformation behavior of RC columns, was used as a benchmark experiment. Specimen U-3 was selected for this thesis to use as a benchmark.

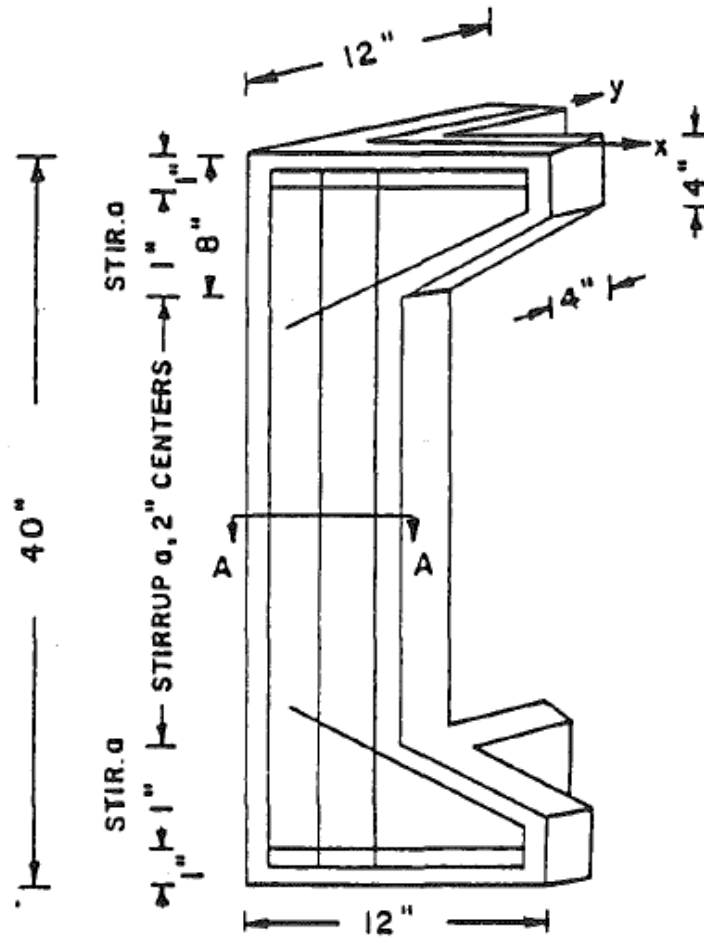
i) Geometrical property

The dimension of the specimen is 101.6mm (4 in) by 101.6mm (4 in) and its concrete cover is 12.7 mm. There are nine longitudinal reinforcements, which are D-5(6mm) bar and D-2(4mm) for lateral reinforcement.

The length of the column is 1016mm (40 in) and it is pinned at both ends of the column. The eccentricity for axial load is 88.9mm (3.5in) in the x-direction and 88.9mm (3.5in) in the y-direction. The lateral reinforcement is spaced at 25.4mm (1 in) around the support for 203.2mm (8 in) and 50.8mm (2 in) around the column's midpoint. For the purpose of eccentricity, the horizontal members with a length of 304.8mm (12in) are cast together. It is shown below in Figure 4.5.



a) Cross-section of the specimen column



b) Longitudinal of specimen column.

Figure 4. 1: Detail of benchmark experiment specimen

ii) Concrete property

The normal strength of concrete was used for the specimen. The property of concrete, which is used in the column specimen, is described as follows:

Table 4. 1: properties of hardened concrete at 28 days (Mean strength of three specimens)

Specimen	Size (sq.in.)	Height/breadth	fy (ksi)	$E_s \cdot 10^6$ (psi)	f_c (psi)	ex(in)	ey (in)
U-3	4*4	10	73	29.2	3894	3.5	3.5

iii) Steel property

The property of steel reinforcement was illustrated in Chapter 3, Research Methodology, and Figure 3.9.

iv) Experimental result

The maximum load-carrying capacity of the column is 35,585.6N and its corresponding deflection is 8.0518mm. A load displacement curve is also plotted together with finite element results in Figure 4.6. In this paper, the section analysis was also done, and the maximum axial load-carrying capacity and deflection are 35,763.53N and 7.112mm, respectively.

4.1.2 FE result

Material data

The concrete material which was used for modelling was illustrated with the following graph.

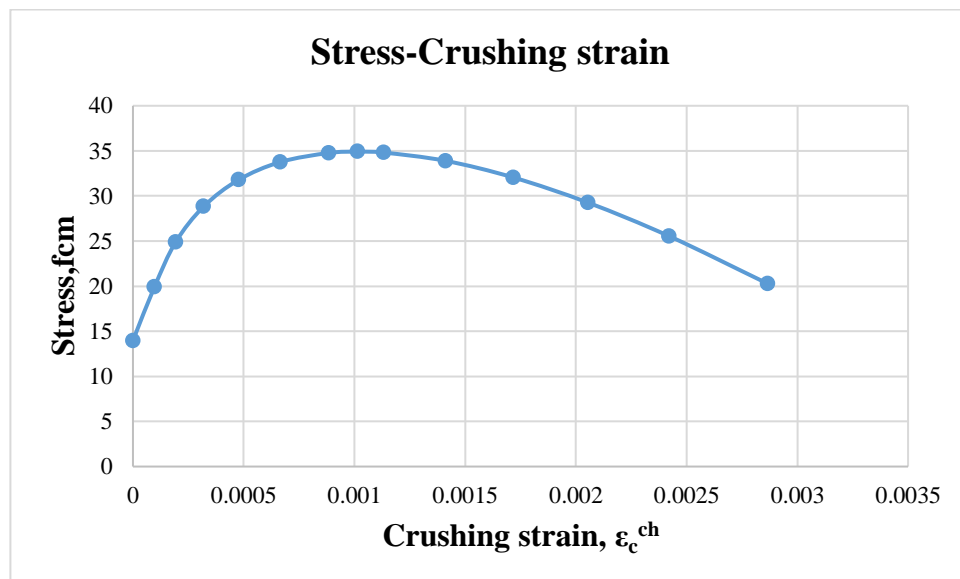


Figure 4.1: Compressive stress-crushing strain diagram of $f_{ck}=26.9$ Mpa concrete

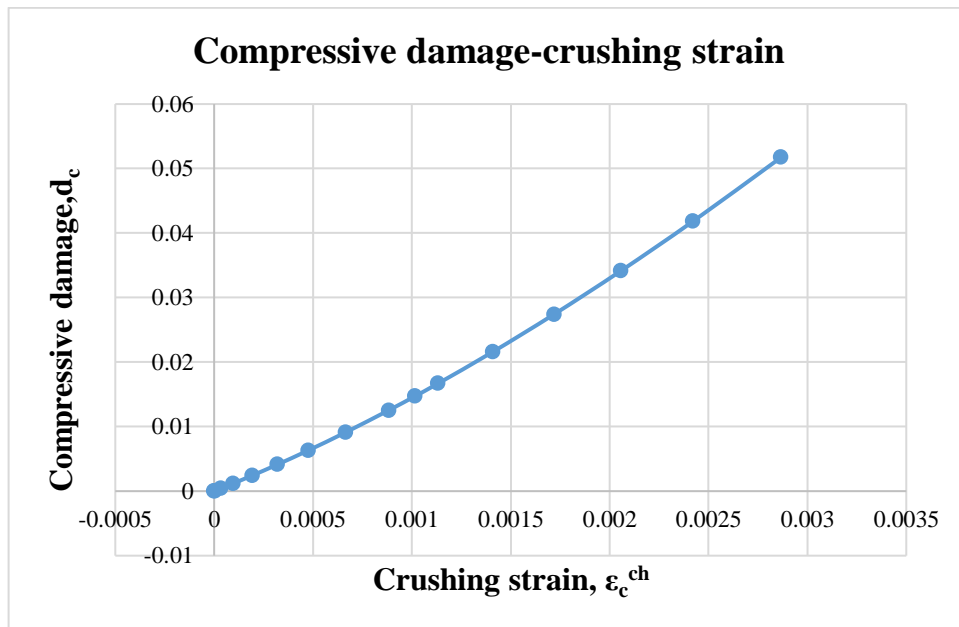


Figure 4.2: Compressive damage-crushing strain diagram of $f_{ck}=26.9\text{Mpa}$ concrete.

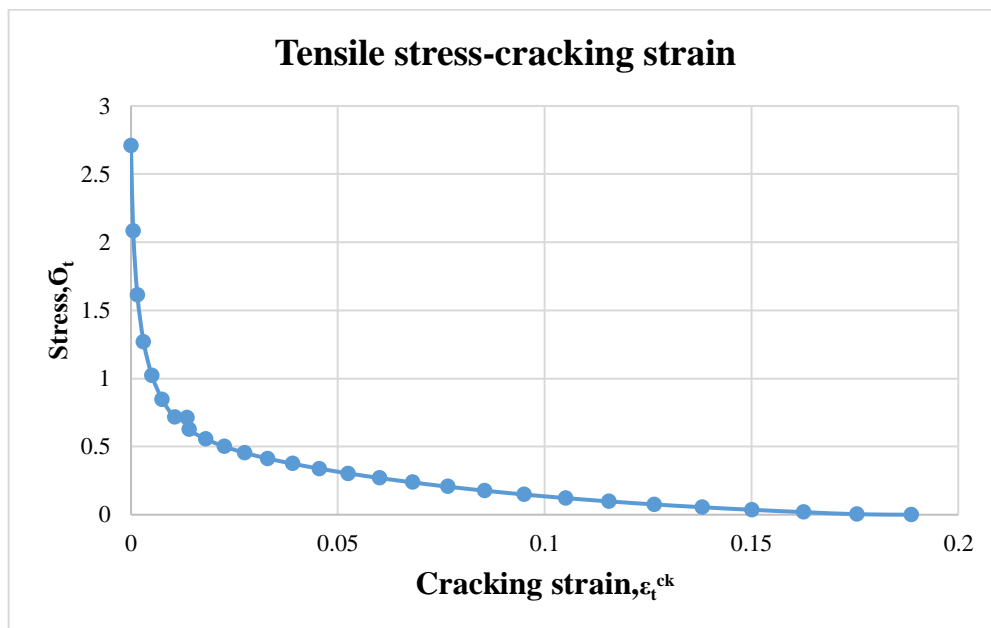


Figure 4.3: Tensile stress-cracking strain diagram of $f_{ck}=26.9\text{Mpa}$ concrete

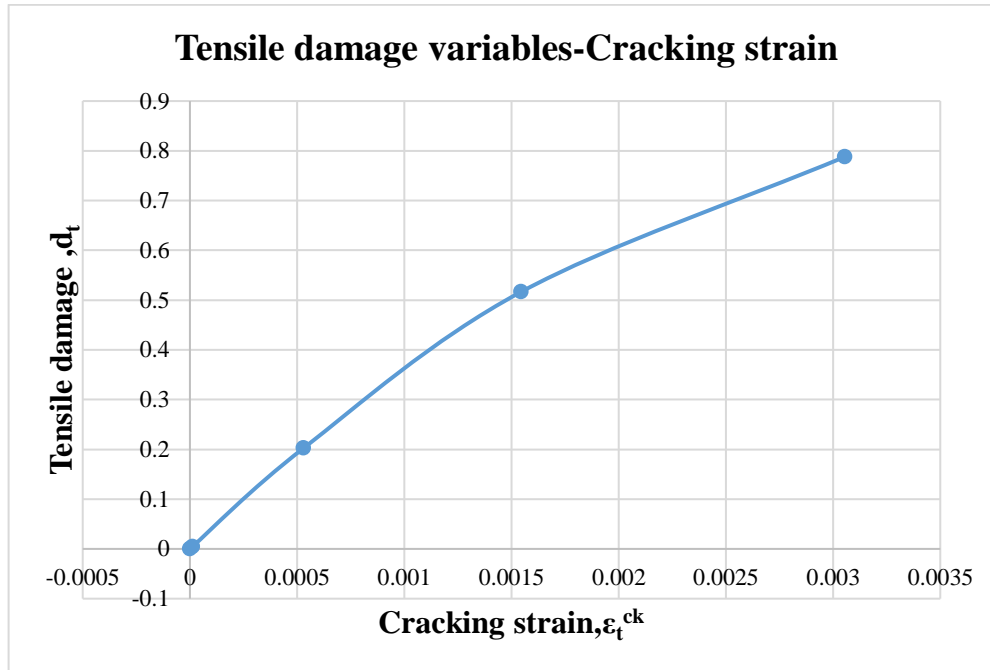


Figure 4.4: Tensile damage variables-cracking strain diagram of $f_{ck}=26.9\text{Mpa}$ concrete

Validation result

The validation work was done before starting modelling of the research specimen in order to decide on different parameters. So, using the method that is described in chapter three, the above-described specimen was modeled. By changing mesh size, different analyses were done and also a load-displacement curve was recorded. For mesh size of 50mm the maximum load was 13.4937kN, for 40mm it is 18.89kN, for 30mm it is 22.67kN and for 20mm it is 29.981kN. As it is shown in Figure 4.5, there is a difference in the ascent of the load-displacement curve between FEA and experimental. Since elastic modulus is the slope of the stress-strain curve, the difference is created due to the difference in elastic modulus of FEA and experimental. The experimental load was 35,763.53N and the maximum finite load was 29986.1N. The ratio of finite element load to experimental load is $29986.1/35,585.6=0.843$, which is 84%. The load displacement curve of finite load, experimental and analytical analysis is shown in Figure 4.5.

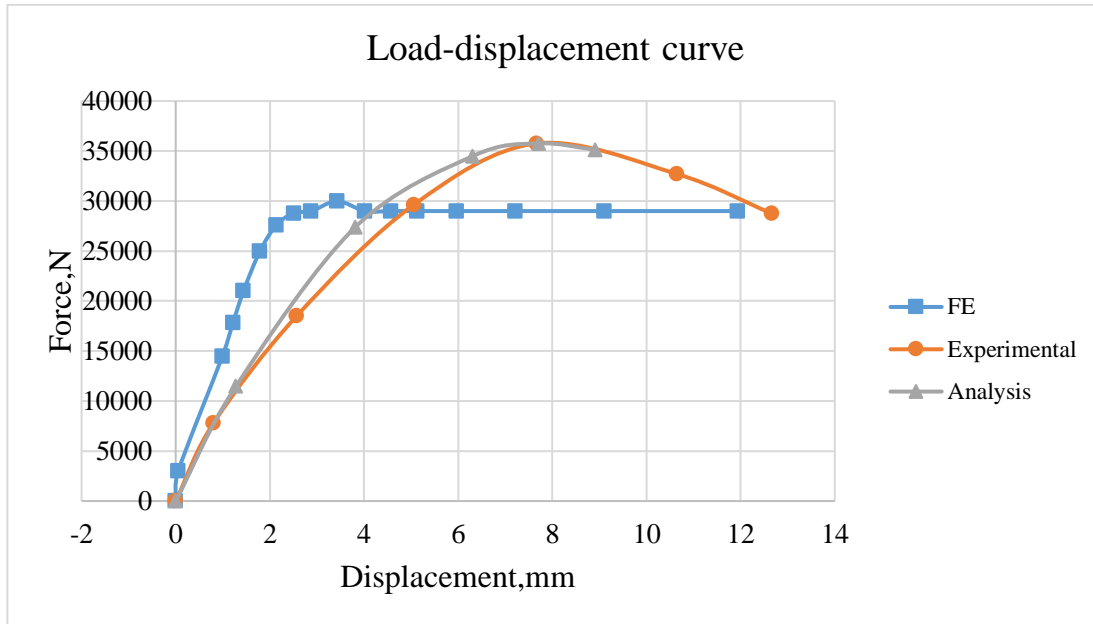


Figure 4.5: Comparison of FE load-displacement curve with experimental and analysis.

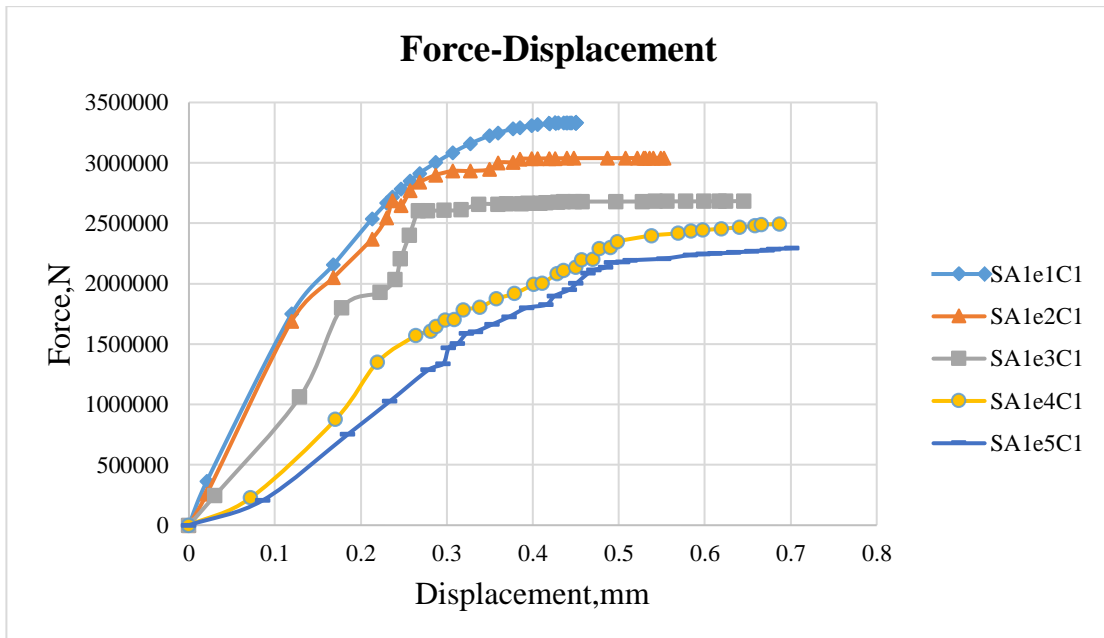
4.2 Results and Discussion

270 specimens were modelled to account for the variation of eccentricity, which is the same in both direction, angle between axis of moment or axis of beam on the column, concrete grade and shape of the column. So the results are discussed below.

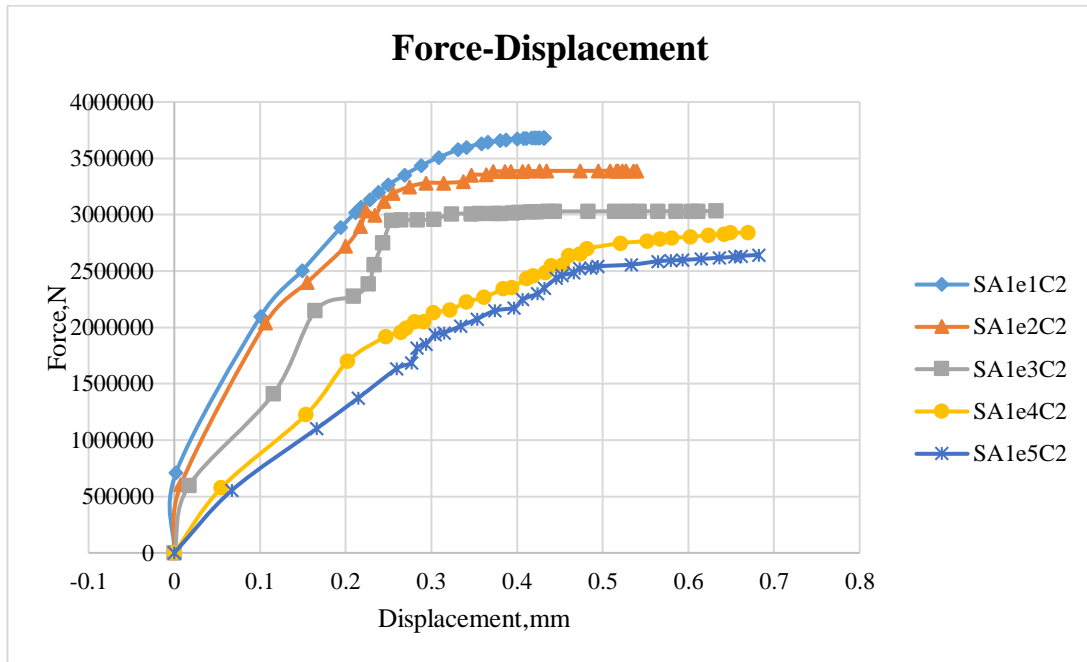
4.2.1 Influence of both directions the same eccentricity on short biaxial non-orthogonal RC column.

As it is shown in Figure 4. 6(a), the maximum load-carrying capacity for a square with a 15-degree angle, a 10-mm eccentricity in both directions, and a concrete cylindrical strength of 20 Mpa (SA1e1C1) is 3332840N, and the corresponding deflection is 0.45044mm. But for SA1e2C1, which is square with 15 degrees, 20mm of eccentricity in both directions and a 20Mpa cylindrical strength of concrete, the maximum load-carrying capacity is 3041520N and its corresponding deflection is 0.55278mm. When we compare SA1e1C1 with SA1e2C1, there is a reduction in the load-carrying capacity of the column by 8.741% compared with SA1e1C1. But the deflection of SA1e2C1 is higher than SA1e1C1 by 22.72%. This is due to the increment of bending moment, which creates higher deformation for 20 mm eccentricity in both directions

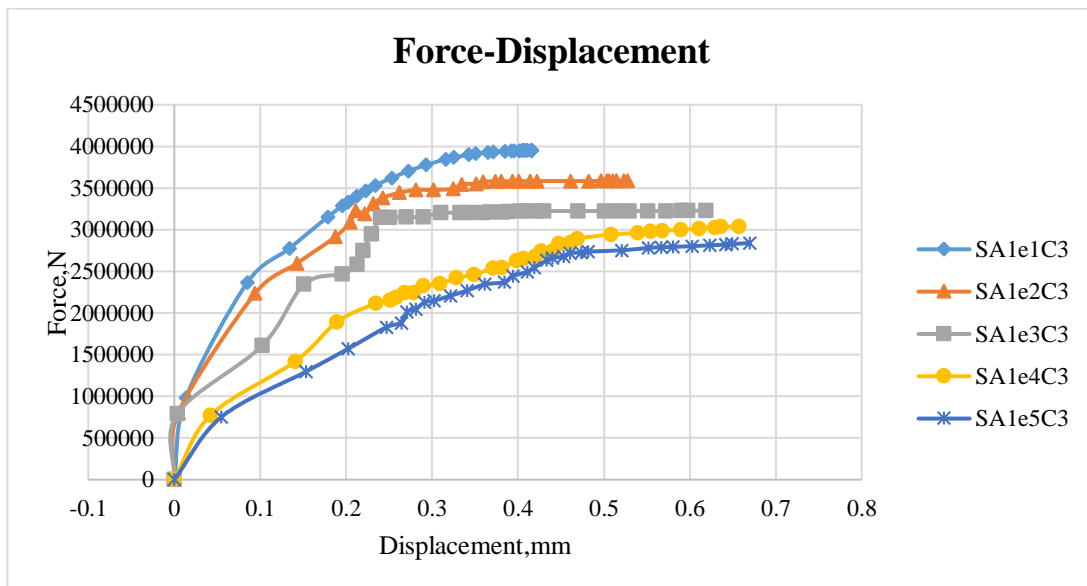
relative to a reinforced concrete column with 10 mm eccentricity in both directions. The maximum load-carrying capacity of column SA1e3C1 is 2683241N with a corresponding deflection of 0.64547mm, and the maximum load-carrying capacity of column SA1e4C1 is 2491257N with a corresponding deflection of 0.68692mm. For the last column, which is SA1e5C1, the maximum load-carrying capacity is 2293741N with a corresponding deflection of 0.7012mm. As a result, the reduction of load-carrying capacity from SA1e2C1 to SA1e3C1 is 11.78%, the reduction of load-carrying capacity from SA1e3C1 to SA1e4C1 is 7.15%, and the reduction of load-carrying capacity from SA1e4C1 to SA1e5C1 is 7.93%. But, the deflection of SA1e3C1 is higher than SA1e2C1 by 16.77%, the deflection of SA1e4C1 is higher than SA1e3C1 by 6.42%, and the deflection of SA1e5C1 is higher than SA1e4C1 by 2.08%. As eccentricity in both directions is increased from the center, the load-carrying capacity of the column is reduced and the deflection of the column increases. The load-displacement curve is presented here for column specimens of 15 degrees, square, eccentricity in both directions (10, 20, 30, 40, 50mm), and all concrete grades (C1=fck=20Mpa, C2=fck=25Mpa, and C3=fck=30Mpa). But for the remaining specimens, which means for squares with angles of 30°, 45°, 60°, 75°, 90°, and for rectangular and circular shapes with angles of 15°, 30°, 45°, 60°, 75°, and 90°, and for all considered concrete grade and eccentricity, is presented in Appendix A.



a) Load displacement curve for square, $f_{ck}=20\text{Mpa}$ ($\alpha=15$ deg.)



b) Load displacement curve for square, $f_{ck}=25\text{Mpa}$ ($\alpha=15$ deg.)



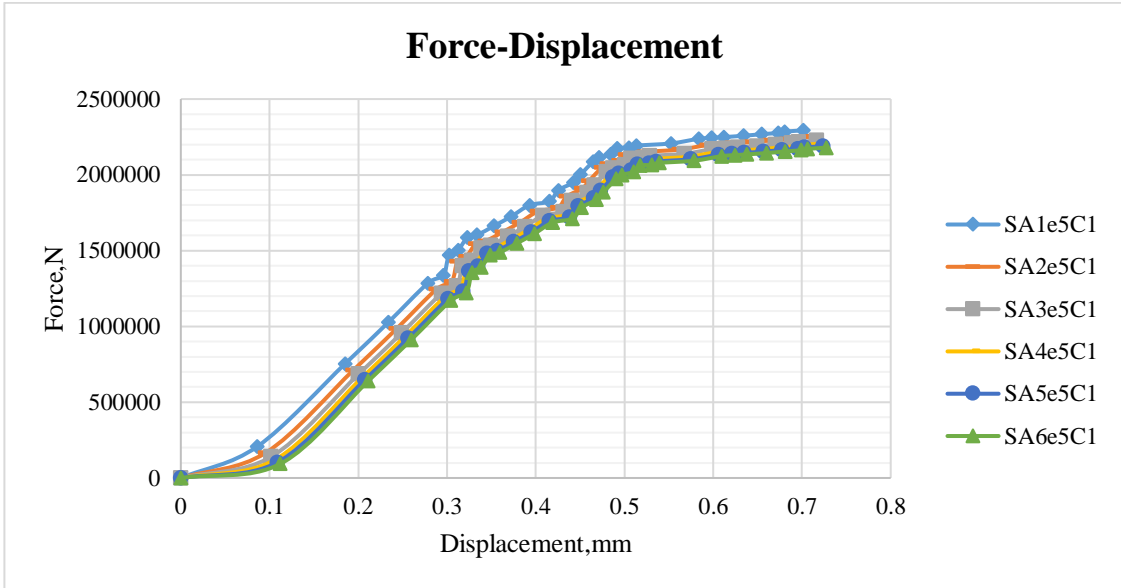
c) Load displacement curve for square, $f_{ck}=30$ Mpa ($\alpha=15$ deg.)

Figure 4.6: Load displacement curve for illustration of eccentricity

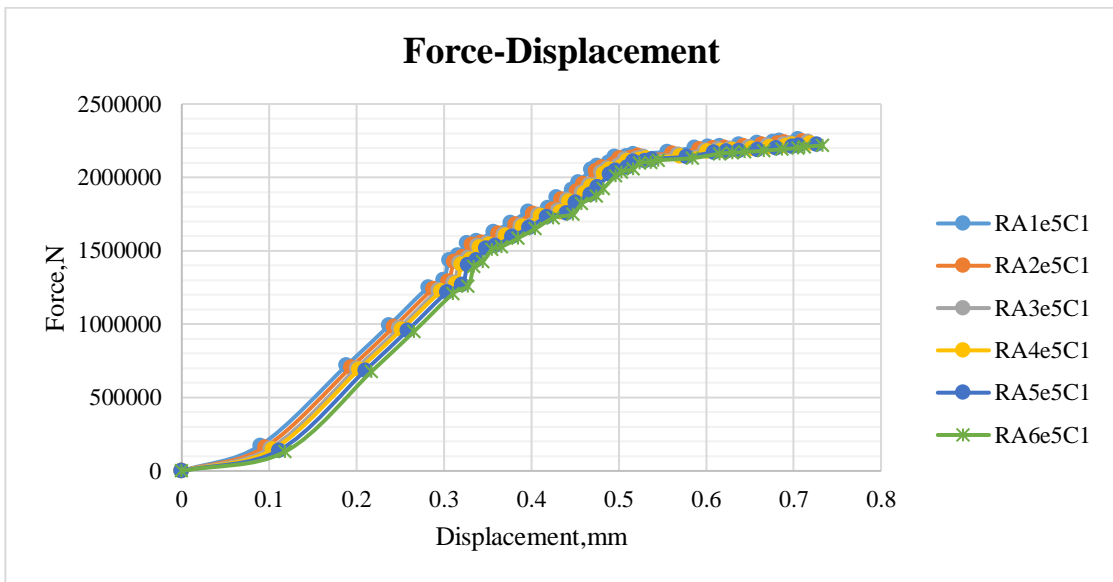
4.2.2 Influence of angle between axis of moment on short biaxial non-orthogonal RC column.

Since the angle between the axis of bending moment is one of the variables of this study, its influence is presented in Figure 4.7. As the angle between the axis increases, the axial load-carrying capacity reduces for the angle from 0° to 90° . This is created due to the tendency of the bending of the column resembles to be uniaxial when the angle between the axis is very small. But when the angle between the axis is large, then the tendency to bend resembles that of a biaxial column. So the column with a small angle can carry a larger load than the column with a larger angle. But the rate of change in the axial load-carrying capacity is small. As it is shown in Figure 4.7 (a), for SA1e5C1, the maximum load-carrying capacity is 2293741N and the corresponding deflection is 0.70128mm, but for SA2e5C1, it is 2252741N with a corresponding deflection of 0.71081mm. So the axial load is reduced by 1.79% with respect to SA1e5C1, but the deflection increases by 1.36%. For SA3e5C1, the maximum load-carrying capacity is 2225741N with a corresponding deflection of 0.71668mm, in which its load is reduced by 1.199% and its deflection increases by 0.83%. For SA4e5C1, the maximum load-carrying capacity is 2205741N with a corresponding deflection of 0.72104mm, in which its load is reduced by 0.899% and its deflection increases by 0.61%.

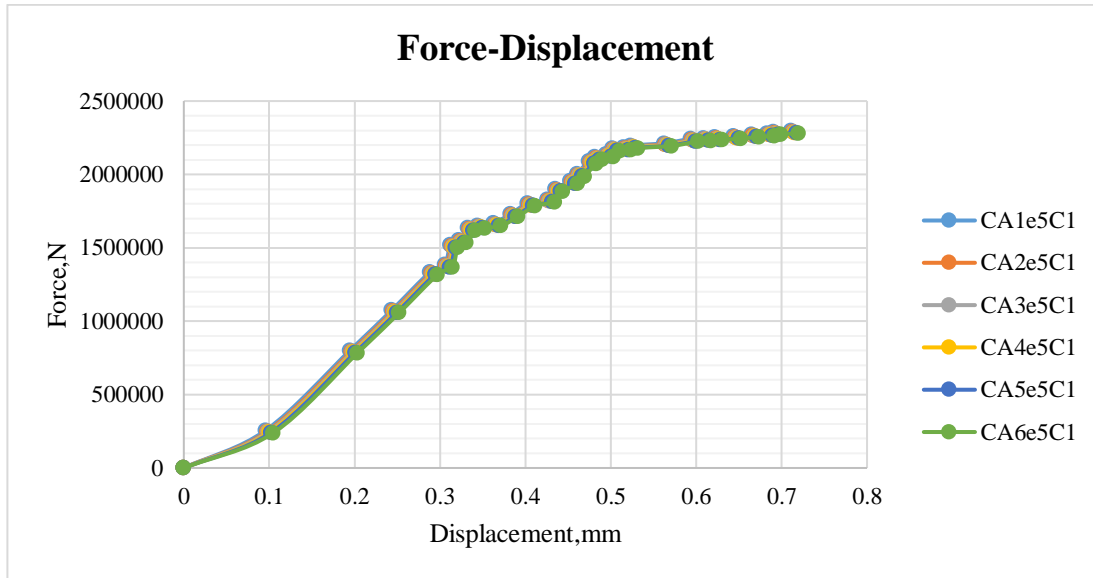
For SA5e5C1, the maximum load-carrying capacity is 2189241 N with a corresponding deflection of 0.7240 mm in which its load is reduced by 0.748% and its deflection increases by 0.411%. For SA6e5C1, the maximum load-carrying capacity is 2179741 N with a corresponding deflection of 0.7273 mm, in which its load is reduced by 0.434% and its deflection increases by 0.46%. The load-displacement curve is provided here in Figure 4.7, for a square with $f_{ck} = 20$ Mpa (C1), with an eccentricity of 50 mm in both directions, and for other specimens is presented in Appendix A.



a) Load displacement curve for square, $f_{ck}=20$ Mpa and $e=50$ mm



b) Load displacement curve for rectangular, $f_{ck}=20$ Mpa and $e=50$ mm



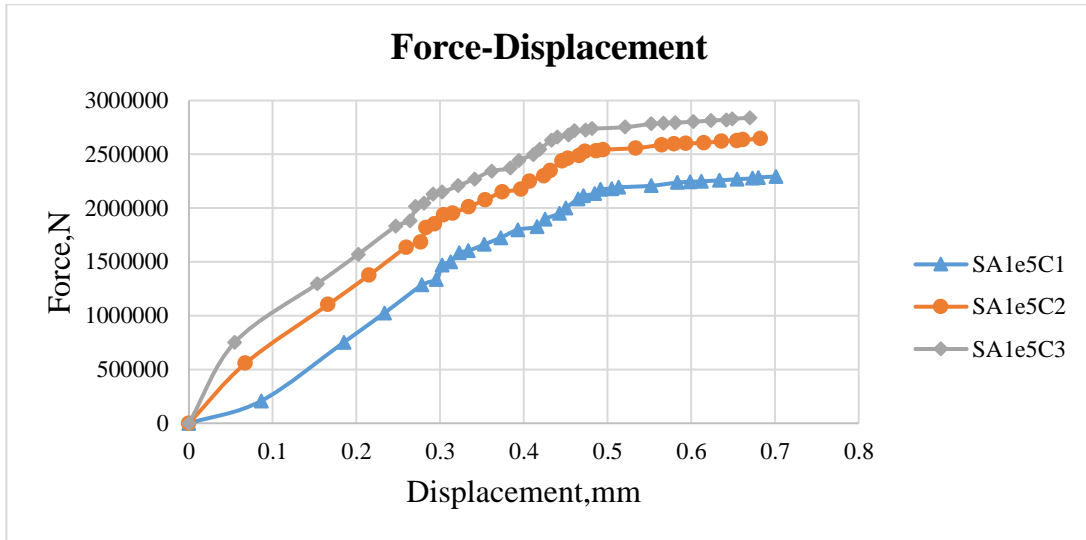
c) Load displacement curve for Circular, $f_{ck}=20$ Mpa and $e=50$ mm

Figure 4.7: Load displacement curve for illustration of angle

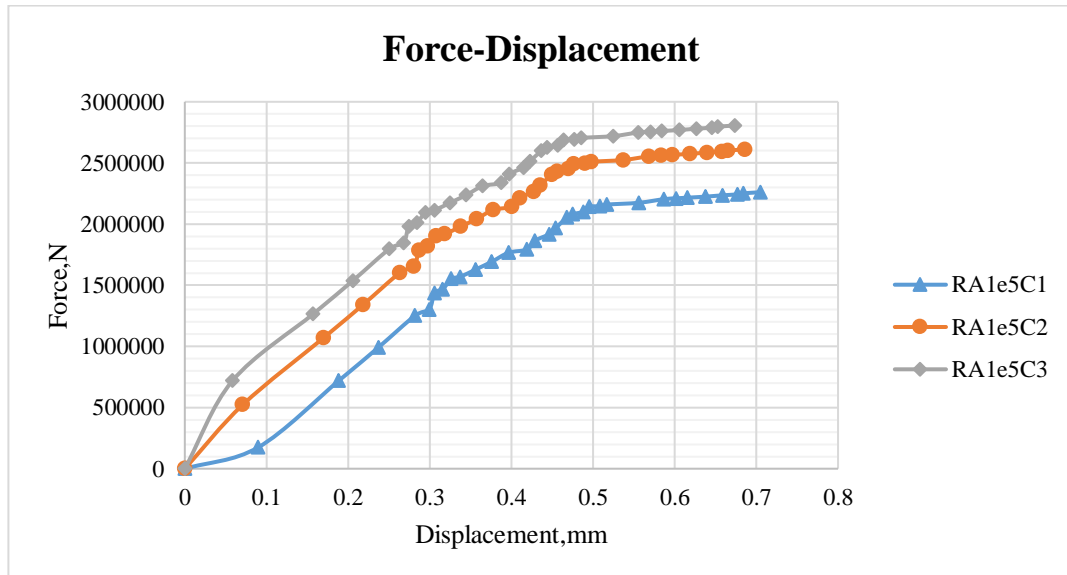
4.2.3 Influence of concrete grade on short biaxial non-orthogonal RC column.

As it is shown in Figure 4.8, the axial load-carrying capacity increases with the increment of concrete grade, but the deflection of the reinforced concrete column reduces with the increment of concrete grade. For a reinforced concrete column specimen of SA1e5C1, which means a square column with an angle of 15 degrees, eccentricity of 50mm in both directions and a concrete grade of $f_{ck}=20$ Mpa, the maximum load-carrying capacity is 2293741N with a corresponding deflection of 0.70128mm, and for SA1e5C2 (square, 15deg., $e=50$ mm and $f_{ck}=25$ Mpa), the maximum load-carrying capacity is 2643236N with a corresponding deflection of 0.68259mm. For SA1e5C3 (square, 15deg., $e=50$ mm, $f_{ck}=30$ Mpa), the maximum load-carrying capacity is 2838741N, with a corresponding deflection of 0.66982mm. The load is increased by 15.24% when the concrete grade increases from $f_{ck}=20$ Mpa to $f_{ck}=25$ Mpa for SA1e5C1 to SA1e5C2, but the deflection is reduced by 2.67%. The change from SA1e5C2 to SA1e5C3, which is from cylindrical strength of 25Mpa to 30Mpa, increases the axial load-carrying capacity by 7.37%, and deflection is reduced by 1.87%. This is due to the behavior of the concrete property, which means as the concrete grade increases, the strength of the concrete increases but the ductility of the concrete reduces. Due to this, the deflection in our specimen

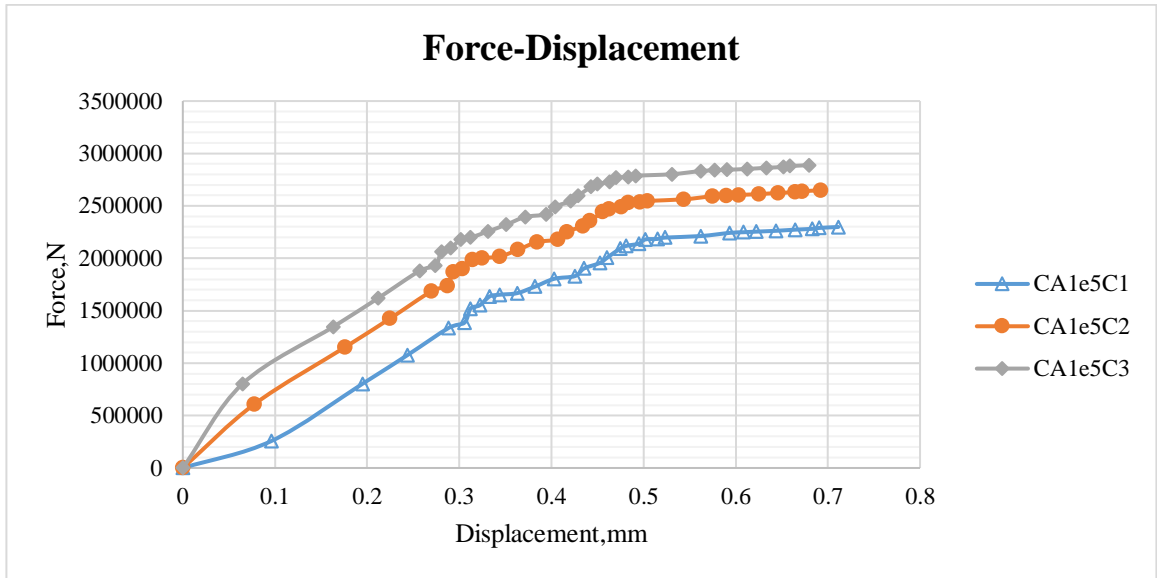
reduces with the increment of the concrete cylindrical strength but increases the axial load-carrying capacity. For rectangular and circular columns, the illustrations are presented in Figure 4.8 (b) and (c), respectively.



a) Load displacement curve for square, 15 deg and e=50mm



b) Load displacement curve for rectangular, 15 deg and e=50mm



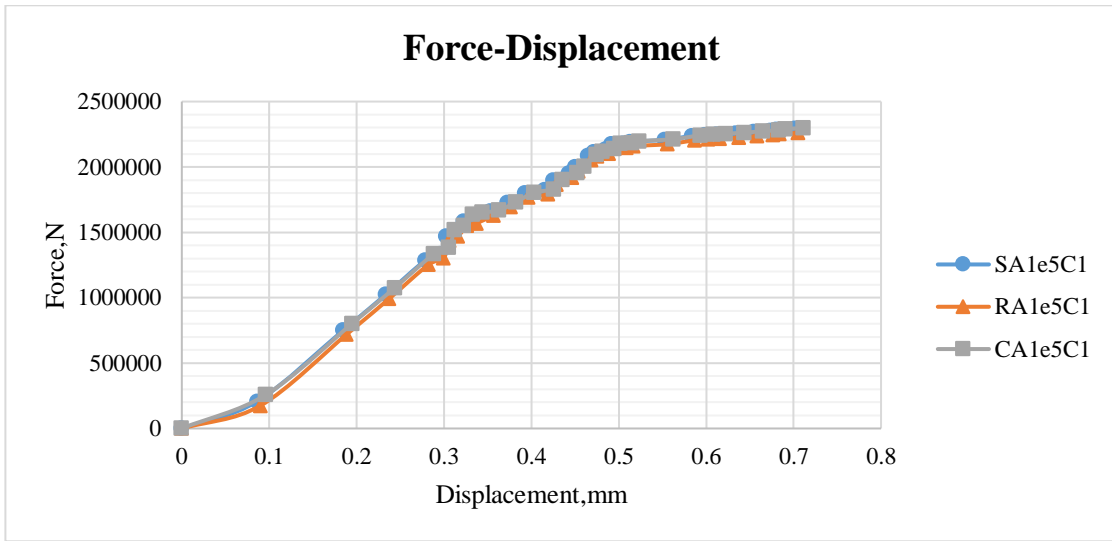
c) Load displacement curve for circular, 15 deg and e=50mm

Figure 4.8: Load displacement curve for illustration of angle

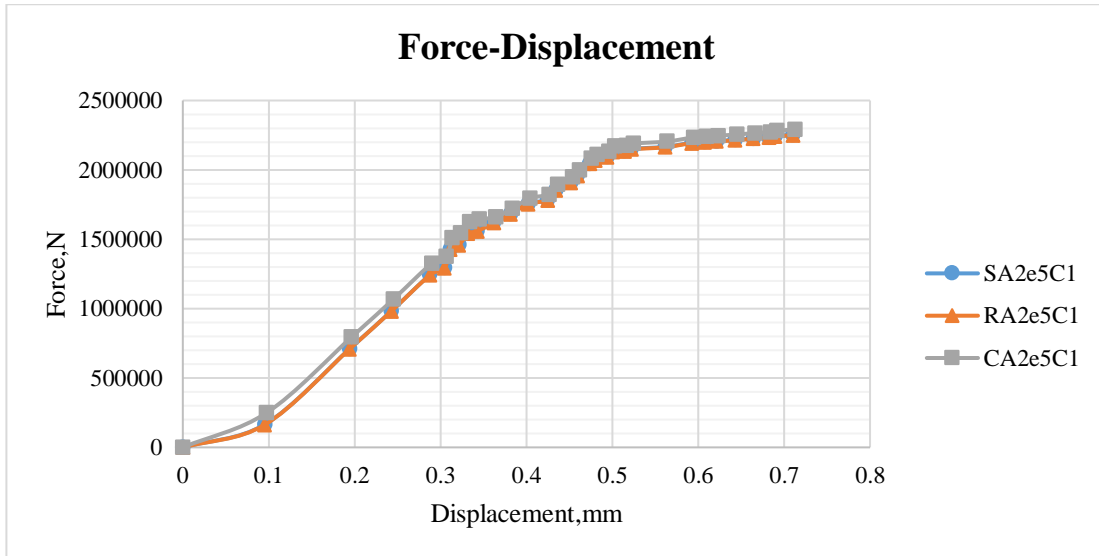
4.2.4 Influence of shape of column on short biaxial non-orthogonal RC column.

The shape of the column is another variable of this study, and it is presented in Figure 4.9. The axial load-carrying capacity of the circular column is higher than the square column, and the axial load-carrying capacity of the square column is higher than the rectangular column. For reinforced concrete column specimen SA1e5C1 (Square, 15 deg., e=50mm and $f_{ck}=20\text{Mpa}$), which is presented in Figure 4.9 (a), the maximum load-carrying capacity is 2293741N with a corresponding deflection of 0.70128mm. But for the rectangular column, RA1e5C1 (rectangular, 15 deg., e=50mm and $f_{ck}=20\text{Mpa}$), which is presented in Figure 4.4 (a), it is 2260675N with a corresponding deflection of 0.7049mm. The axial load-carrying capacity of SA1e5C1 is higher than RA1e5C1 by 1.44%, but the deflection is smaller by 0.516%. For circular reinforced concrete column CA1e5C1 (circular, 15 deg., eccentricity=50mm and $f_{ck}=20\text{Mpa}$), which is presented in Figure 4.4(a), the maximum force is 2298128N with a corresponding deflection of 0.7113mm. The non-orthogonal circular column axial load capacity is higher than square and rectangular by 0.192% and 1.66%, respectively. This is created due to stress concentration around the corner of the square column and rectangular column due to non-orthogonality of the bending moment. The neutral axis of the column will be inclined depending on the orientation of the axis of bending moment, which will create a high stress

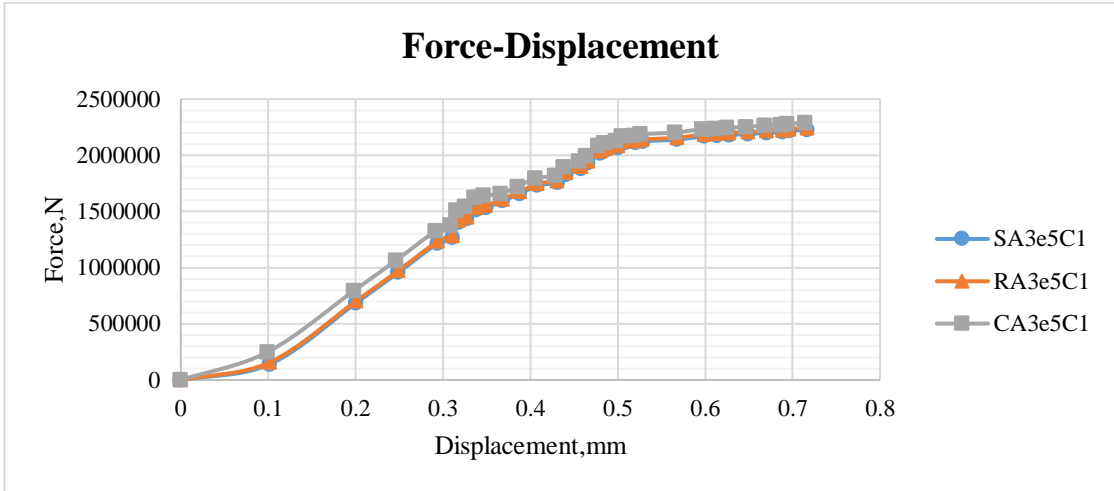
concentration around the square column and the rectangular one. However, the square column has a higher axial load-carrying capacity due to its uniform dimension on both side, which helps to resist bending moments because the column is subjected to biaxial bending moments. Figure 4.9 (b), (c), (d), (e), and (f) show the load displacement curves for the 30 degree (A2), 45 degree (A3), 60 degree (A4), 75 degree (A5), and 90 degree (A6) for all square, rectangular, and circular.



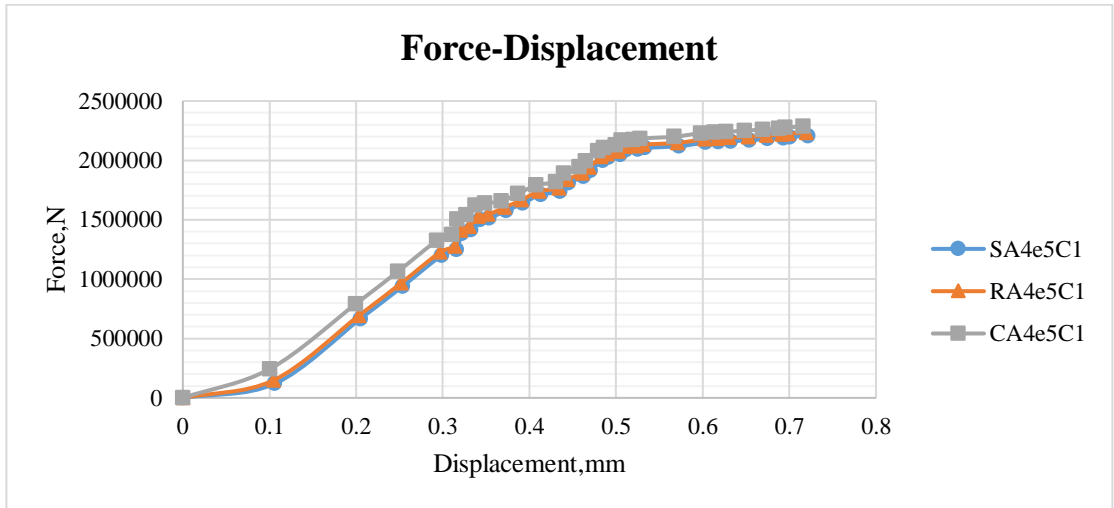
a) Load displacement curve for 15 deg., $e=50\text{mm}$ and $f_{ck}=20\text{Mpa}$



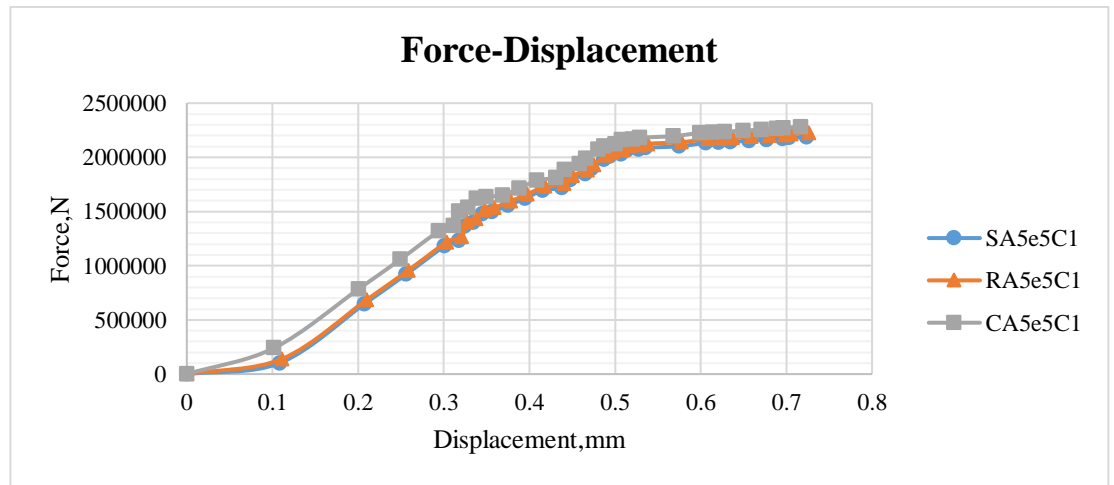
b) Load displacement curve for 30 deg., $e=50\text{mm}$ and $f_{ck}=20\text{Mpa}$



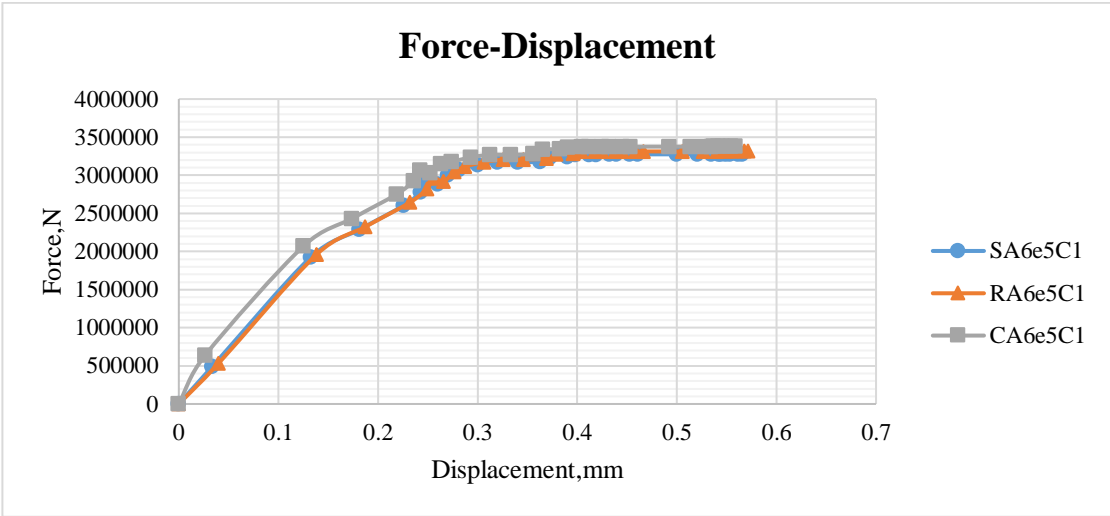
b) Load displacement curve for 45 deg., e=50mm and fck=20Mpa



d) Load displacement curve for 60 deg., e=50mm and fck=20Mpa



e) Load displacement curve for 75 deg., e=50mm and fck=20Mpa



f) Load displacement curve for 15 deg., e=50mm and fck=20Mpa

Figure 4.9: Load displacement curve for illustration of shape of column

CHAPTER FIVE

CONCLUSION AND RECOMMENDATION

5.1 Conclusion

Nowadays, different countries use building structures as a means of communication to deliver the culture of one community. So, to do that, it needs flexibility in terms of keeping the shape of the building in different ways. In this case, a column, which is subjected to non-orthogonal biaxially loaded conditions, may have encountered. However, there has not been enough research into the behavior of short non-orthogonal biaxially loaded RC columns. So the purpose of this research is to study the behavior of a short non-orthogonal biaxially loaded RC column.

ABAQUS Finite element analysis software is used for modelling the specimen. Concrete damage plasticity for concrete and a plastic model for reinforcement steel was used in the modelling. The axis of non-orthogonality was drawn on the steel plate. The steel plate was modelled as a rigid discrete part and plain concrete was modelled as a 3D deformable part, but for the longitudinal reinforcement, 3D deformable wire was used. Tie and embedded region were used in the interaction module. After analysis of the specimen, the result is summarized.

As we increase the eccentricity from 10 -50mm on both direction of the non-orthogonal short RC short column, the axial load-carrying capacity reduces by an average value of 8.9% and deflection increases by an average value of 12%. As we increase the angle between the axis of moment from 15°-90°, the axial load-carrying capacity is reduced by an average value of 1.014% and deflection increases by an average value of 0.7342%. As we increase the concrete grade of non-orthogonal biaxially loaded RC column from $f_{ck} = 20-30\text{MP}$, the axial load capacity of column by an average value of 11.305% but reduce the deflection by an average value of 2.27%. Circular shape is preferable than the square and rectangular for short non-orthogonal biaxially loaded RC column. Square is also better than rectangular one.

5.2 Recommendation

- The finding of this study is recommended to any organization or individuals that participate in the construction industry, for those who participate in the design and construction building structures as a basement to further study.
- Further study could be done by considering the other variables like the curvature of the column.
- Further study could be done by changing the dimension of the column to check the capacity of non-orthogonal biaxially loaded column.

REFERENCES

- Abaqus CAE user guide version 6.13(2013). Pawtucket (RI); Hibbit, Karlsson and Sorensen.
- Abaqus release note version 6.13(2013). Pawtucket (RI); Hibbit, Karlsson and Sorensen.
- Abaqus theory version 6.13(2013). Pawtucket (RI); Hibbit, Karlsson and Sorensen.
- Abaqus analysis-2 user's manual version 6.13(2013). Pawtucket (RI); Hibbit, Karlsson and Sorensen.
- Abaqus analysis-3 user's manual version 6.13(2013). Pawtucket (RI); Hibbit, Karlsson and Sorensen.
- Abdel Rahman M.A., Mohammed F. and Mohammed M.A, (2010). Some parameters affecting the behaviour of reinforced normal strength concrete short columns under centric an eccentric static loading. *Journal of Engineering Sciences*. 38(5): pp. 1119-1157.
- ACI Committee 318. (1989). Commentary on the building code requirements for reinforced concrete (ACI318R-89), American Concrete Institute, Farmington Hills, MI,369pp.
- Afey, H. M. (2012). Ultimate flexural rigidity for stability analysis of RC beam column members. *Structural and Building*, 165, 299–308.
- Afey, H. M., Taher, S. F., & El-Metwally, S. E. (2009). A new design procedure for braced reinforced high strength concrete columns under uniaxial and biaxial compression. *Arabian Journal for Science and Engineering*, KFUPM, KSA, 34, 349–377.
- Ahmad, S. H., and Weerakoon, S. L. (1995). “Model for behavior of slender reinforced concrete columns under biaxial bending.” *ACI Struct. J.*, 92(2), 188–198.
- Al-Ansari M.S. and Afzal M.S. (2020). *Mathematical Model for Analysis of Uniaxial and Biaxial Reinforced Concrete Columns*. Advances in civil Engineering. Hindawi.
- Alfarah B, Lopez-Almense F,Oller S(2017).New methodology for calculating damage variables evolution in plastic damage model for RC structures. *Engineering structures*.132:70-86.
- Barzegar, F., and Erasito, T. (1995). “Concrete sections under biaxial bending: Interactive analysis with spreadsheets.” *ACI Concrete Int.*, 17(12), 28–33.

- Bernardo A.L. (2007). Investigation of Biaxial Bending of Reinforced Concrete Columns through Fiber Method Modeling. *Journal of Research in Science, Computing, and Engineering*. 4(3): pp.61-73.
- Bikhiet, M.M., El-Shafey, N.F., and El-Hashimy, H.M. (2014) Behavior of Reinforced Concrete Short Columns Exposed to Fire", *Alexandria Engineering Journal*. 53(3): PP.643-653.
- Bonet J.L.,Romero M.L. and Miguel P.F. (2011). Effective flexural stiffness of slender reinforced concrete columns under axial forces and biaxial bending.*Engineering Structures*.33:881:893.
- Bonet J.L.,Barros M.H.F.M. and Romero M.L.(2006). Comparative study of analytical and numerical algorithms for designing reinforced concrete sections under biaxial bending. *Computer and Structures*.84:2184-2193.
- Brachmann, I.; Browning, J.; and Matamoros, A. (2004). Drift-Dependent Confinement Requirements for Reinforced Concrete Columns under Cyclic Loading. *ACI Structural Journal*. 101(5): pp. 669-677.
- Brecollotti M., Annibale L.M. and Bruno R.B. (2019). Curvature ductility of biaxially loaded reinforced concrete short columns. *Engineering Structures*.200.
- Bresler, B. (1960). "Design criteria for reinforced columns under axial load and biaxial bending." *ACI J.*, 32(5), 481–490.
- CEN European Committee for Standardization. EN 1992-1-1 Eurocode 2: Design of concrete structures – Part 1–1: General rules and rules for buildings. Brussels: CEN; 2004.
- Cengiz, D. 1990. Concrete Box Sections under Biaxial Bending and Axial Load, *Journal of Structural Engineering* 116(3): 860–865.
- Chan E.C. (1982). Nonlinear geometric, material and time dependent analysis of reinforced concrete shells with edge beams. Report UCB-SESM 82/8, University of California at Berkeley, USA.
- Chang S.Y. (2010). Experimental Studies of Reinforced Concrete Bridge Columns under Axial Load plus Biaxial Bending. *Journal of Structural Engineering*.136 (1).
- Chang, S. Y. (2002). "Explicit pseudo-dynamic algorithm with unconditional stability." *J. Eng. Mech.*, 128(9), 935–947.
- Chang, S.Y. (2001). "Application of the momentum equations of motion to pseudo-dynamic testing." *Philos. Trans. R. Soc., London, Ser. A*, 359(1786), 1801–1827.

- Chen W. F., Lui E. M. (1987). *Structural stability: Theory and implementation*, New York, NY: Elsevier Science Publishing Co., Inc., 483 pp.
- Cranston W. B. (1972). Analysis and design of reinforced concrete columns. *Cement and Concrete Association*. 1(20): 54 p.
- Di Ludovico, M.; Verderame, G. M.; Prota, A.; Manfredi, G.; Cosenza, E. (2012). Experimental Behavior of Nonconforming RC Columns with Plain Bars under Constant Axial Load and Biaxial Bending, *Journal of Structural Engineering* 139(6): 897–914.
- Dundar, C. (1990). “Concrete box sections under biaxial bending and axial load.” *J. Struct. Engrg.*, ASCE, 116(3), 860–865.
- El-Metwally, S. E. (1994). Method of segment length for instability analysis of reinforced concrete beam-columns. *ACI Structural Journal*, 91, 666–677.
- Fafitis, A. (2001). Interaction Surfaces of Reinforced-Concrete Sections in Biaxial Bending, *Journal of Structural Engineering* 127(7): 840–846.
- Furlong, R.W. (1961). Ultimate strength of square columns under biaxially eccentric loads. *Journal ACI*, 57(9), 1129-1140.
- Gouwens, A. J. (1975). “Biaxial bending simplified.” *Reinforced concrete columns*, ACI SP-50. American Concrete Institute, Detroit, 233–261.
- Hamdy M.A. and El-Tony M.E. (2016). Simplified Design Procedure for Reinforced Concrete Columns Based on Equivalent Column Concept. *International Journal of Concrete Structures and Materials*.
- Hamed E. and Lai C. (2016). Geometrically and materially nonlinear creep behaviour of reinforced concrete columns. *Structures*.5:1-12.
- Hashemi S.SH. and Vaghefi M., (2015). Investigation of bond slip effect on the P-M interaction surface of RC columns under biaxial bending. *Scientia Iranica*.22 (2):388-399.
- Hong, H. P. (2001). “Strength of slender reinforced concrete columns under biaxial bending.” *J. Struct. Eng.*, 127(7), 758–762.
- Hordijk DA (1992). Tensile and tensile fatigue behavior of the concrete: experiments, modelling and analysis. *Heron*.37 (1):3-79.
- Hsu, C.-T. T. (1989). “T-shaped reinforced concrete members under biaxial bending and axial compression.” *ACI Struct. J.*, 86(4), 460–468.

- Hsu, C.-T. T. (1986). “Reinforced concrete members subject to combined biaxial bending and tension.” *ACI J.*, 83(1), 137–144.
- Hsu, C. T. (1988). “Analysis and design of square and rectangular columns by equation of failure surface.” *ACI Struct. J.*, 85(2), 167–179.
- Kim J.K and Lee S.S. (2000). The behavior of reinforced concrete columns subjected to axial force and biaxial bending. *Engineering structures*.23:1518-1528.
- Kwak H.G. and Kim J.K. (2006). Nonlinear behavior of slender RC columns (1). Numerical formulation. *Construction and building materials*.20:527:537.
- Li A.Y., Huang Y.T. and Hwang S.J. (2014). Seismic Response of Reinforced Concrete Short Columns Failed in Shear. *ACI structural journal*.111 (4).
- MacGregor J.G, Breen J.E, Pfrang E.O (1970). Design of slender concrete column. *ACI Journal*.67 (2):6-28.
- Mari A.R. (1984). Nonlinear geometric, material and time dependent analysis of three-dimensional reinforced and pre-stressed concrete frames. Report UCB-SESM 84/12, University of California at Berkeley, USA.
- Mavichak, V., and Furlong, R. W. (1976). “Strength and stiffness of reinforced concrete columns under biaxial bending.” Res. Rep.7-2F, Center for Highway Research, Univ. of Texas at Austin, Austin, Tex.
- Meek J.L.(1963). Ultimate strength of columns with biaxially eccentric loads. *ACI Journal*. 57(8):1053–64.
- Moran, F. (1972). Design of reinforced concrete sections under normal loads and stresses in the ultimate limit state. Bulletin information, No. 83, Comite European du Beton, Paris.
- Najmi A. and Tayem A. (1993).Uniaxial bending of columns.*Journal of structural engineering*, 119(4).
- Nguyen GD, Korsunsky A (2008).Development of an approach to constitutive modelling of concrete: damage coupled with plasticity. *International Journal of Solid structures*.45 (20):483-501.
- Nilson, Arthur H. (1997). Design of concrete structures. (12th ed.). McGraw-Hill.
- Pannell, F. N. (1963). “Failure surfaces for members in compression and biaxial bending.” *ACI J.*, 60(1), 129–140.
- Park, H., & Paulay, T. (1975). Reinforced concrete structures. New York, NY: Wiley.

- Parme, A. L., Nieves, J. M., and Gouwens, A. (1966). "Capacity of reinforced rectangular columns subjected to biaxial bending." *ACI J.*, 63(9), 911–923.
- Popa V., Cotofana D. and Vacareanu R. (2014). Effective stiffness and displacement capacity of short reinforced concrete columns with low concrete quality. *Bull Earthquake Eng.*
- Rodriguez, J. A., and Aristozabal-Ochoa, J. D. (1999). "Biaxial interaction diagrams for short columns of any cross section." *J. Struct. Eng.*, 125(6): 672–683.
- Sezen, H., and Moehle, J. P. (2006). Seismic Tests of Concrete Columns with Light Transverse Reinforcement. *ACI Structural Journal*.103 (6): pp. 842-849.
- Thomas Hsu C.T. (1985). Biaxially loaded l-shaped reinforced Concrete columns. *Journal of Structural Engineering*.111 (12).
- Wang, G. G. and Hsu, C. T. (1992). "Complete biaxial load-deformation behavior of RC columns." *J. Struct. Eng.*, 118(9), 2590–2609.
- Yen, J. Y. R. (1991). "Quasi-Newton method for reinforced-concrete column analysis and design." *J. Struct. Eng.*, 117(3), 657–666.
- Z. Xu, Q. Han and C. Huang. (2016). Behavior evaluation for reinforced concrete columns with rectangular hollow section subjected to axial compression and biaxial bending. *The Baltic journal of road and bridge engineering*.11 (1):53-61.

APPENDIX-A

LOAD-DISPLACEMENT CURVE

A-1 Load displacement curve for illustration of eccentricity.

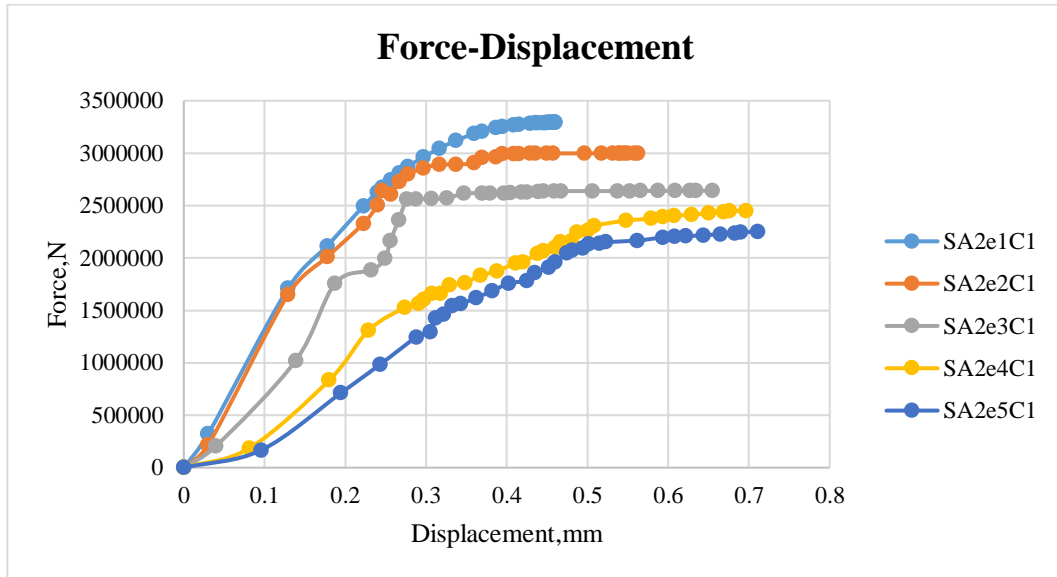


Figure A. 1: Load displacement curve for square, $f_{ck}=20\text{Mpa}$ ($\alpha=30$ deg.)

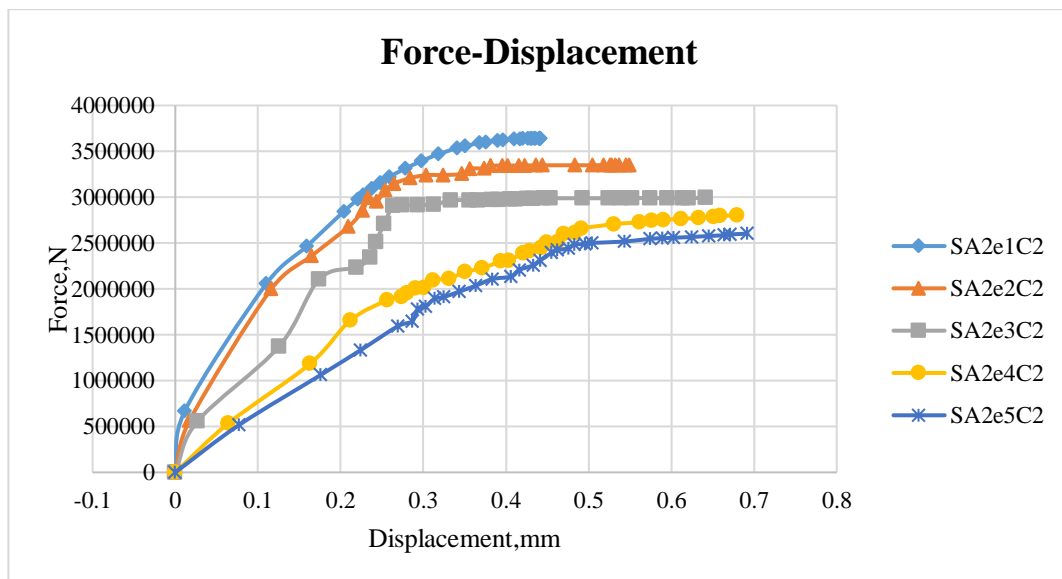


Figure A. 2: Load displacement curve for square, $f_{ck}=25\text{Mpa}$ ($\alpha=30$ deg.)

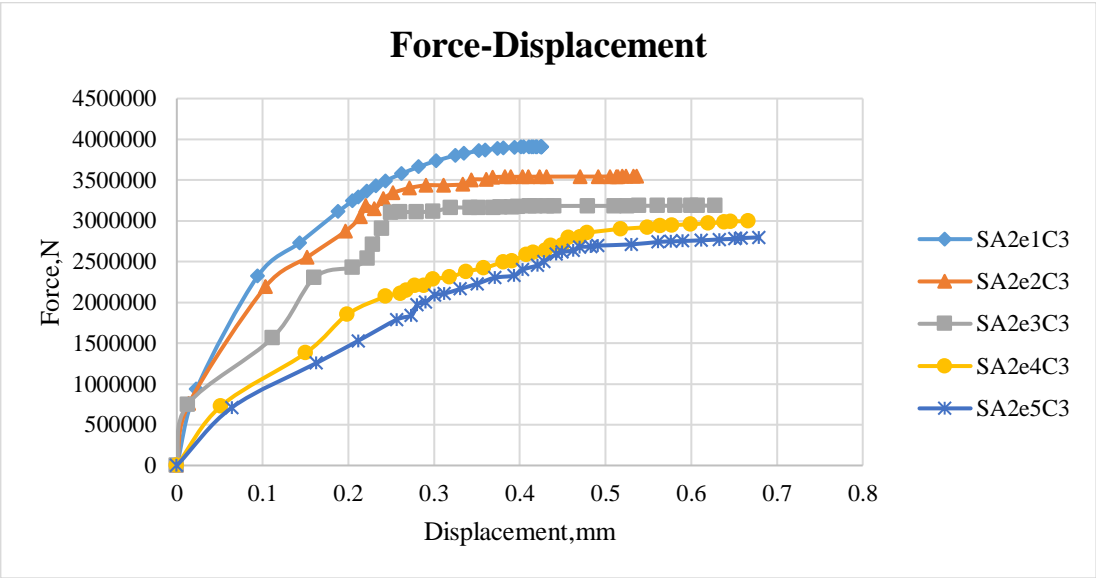


Figure A. 3: Load displacement curve for square, fck=30Mpa ($\alpha=30$ deg.)

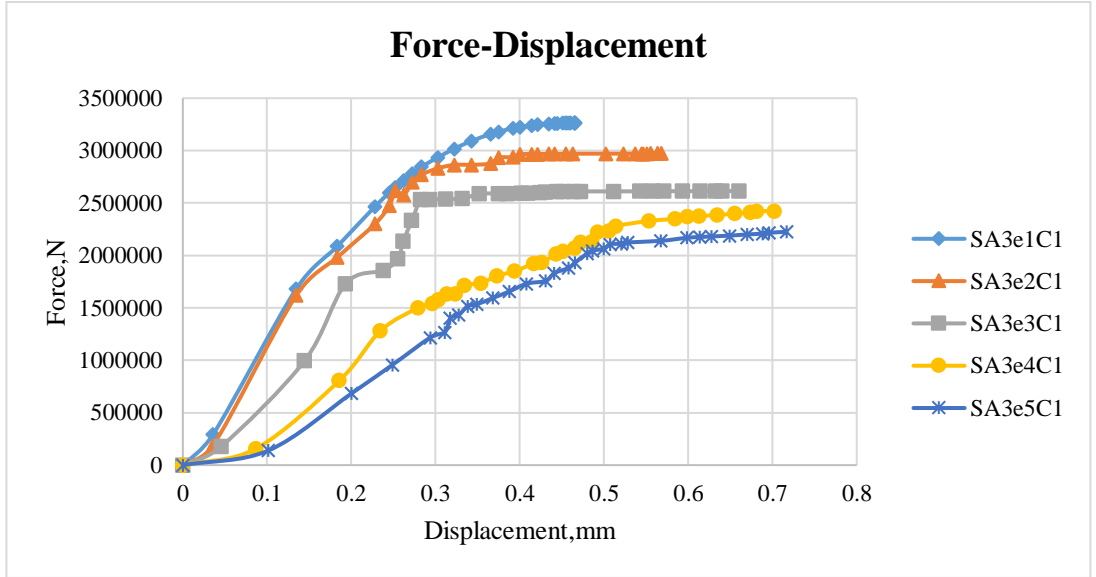


Figure A. 4: Load displacement curve for square, fck=20Mpa ($\alpha=45$ deg.)

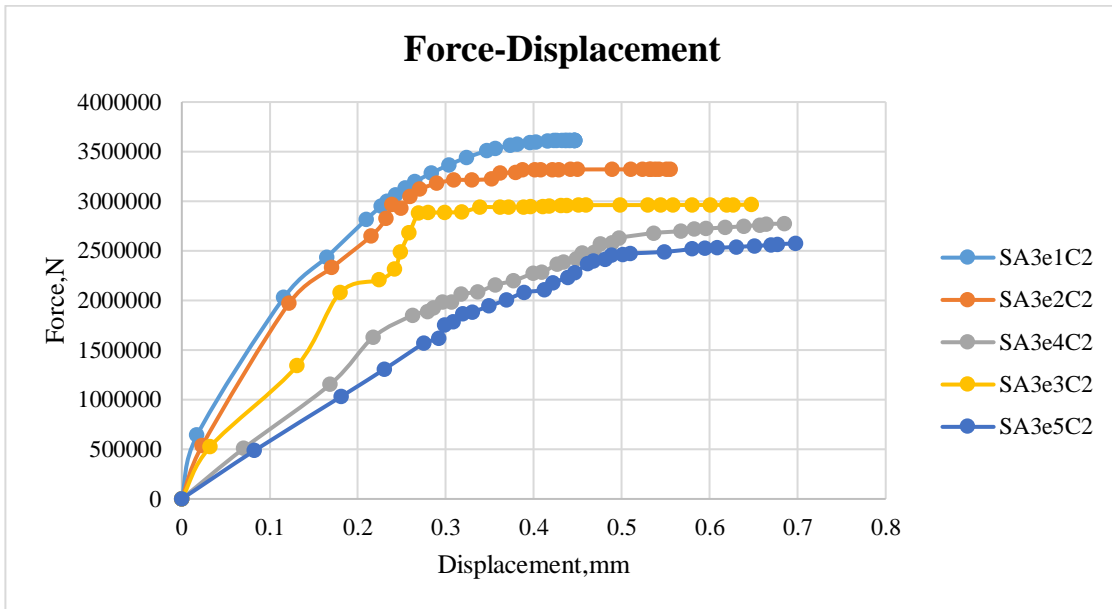


Figure A. 5: Load displacement curve for square, $f_{ck}=25\text{Mpa}$ ($\alpha=45$ deg.)

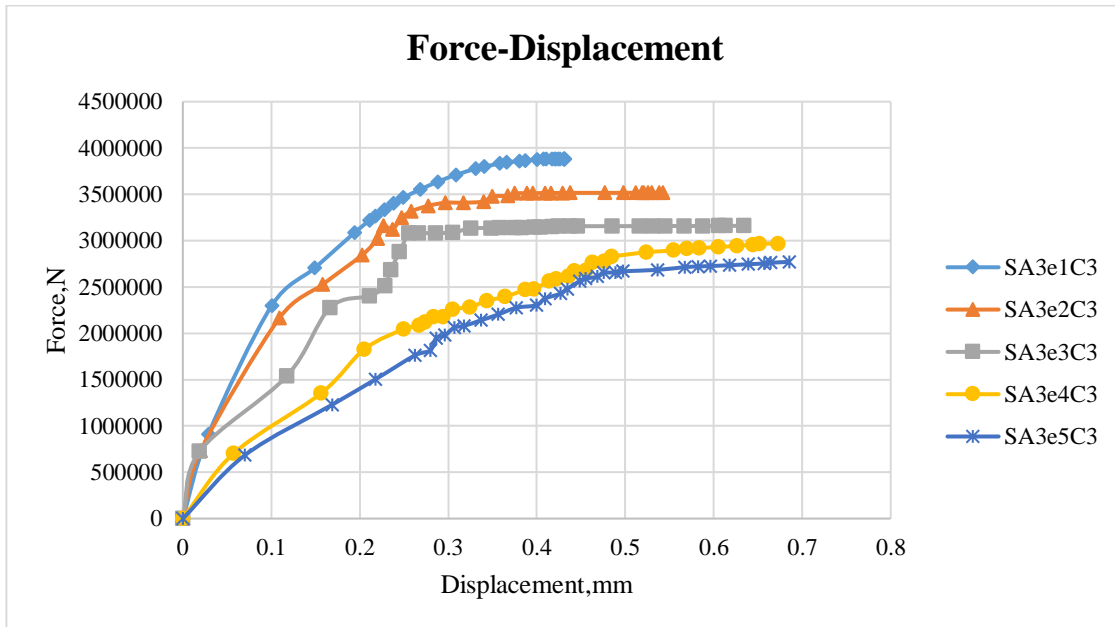


Figure A. 6: Load displacement curve for square, $f_{ck}=30\text{Mpa}$ ($\alpha=45$ deg.)

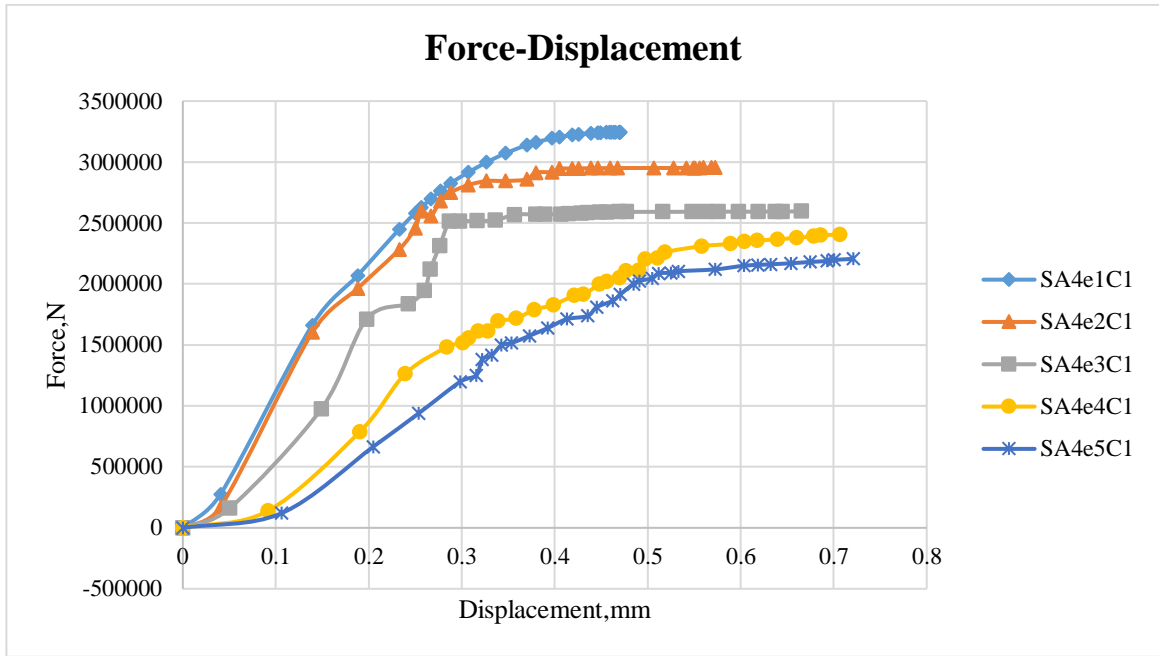


Figure A. 7: Load displacement curve for square, $f_{ck}=20\text{Mpa}$ ($\alpha=60$ deg.)

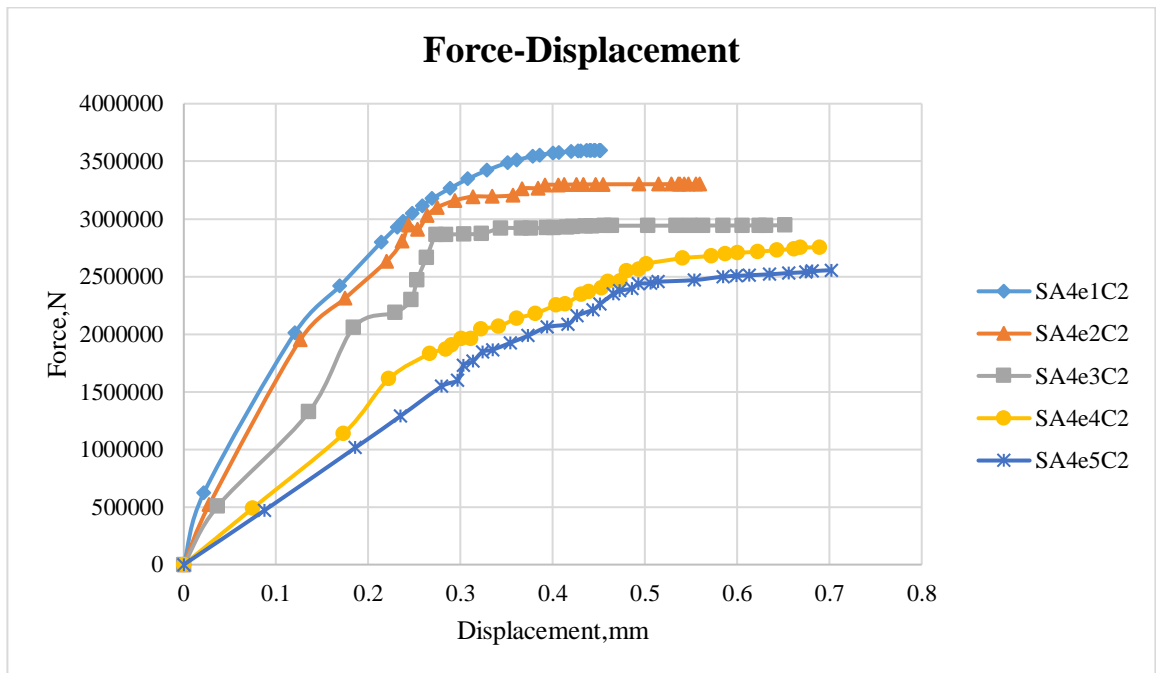


Figure A. 8: Load displacement curve for square, $f_{ck}=25\text{Mpa}$ ($\alpha=60$ deg.)

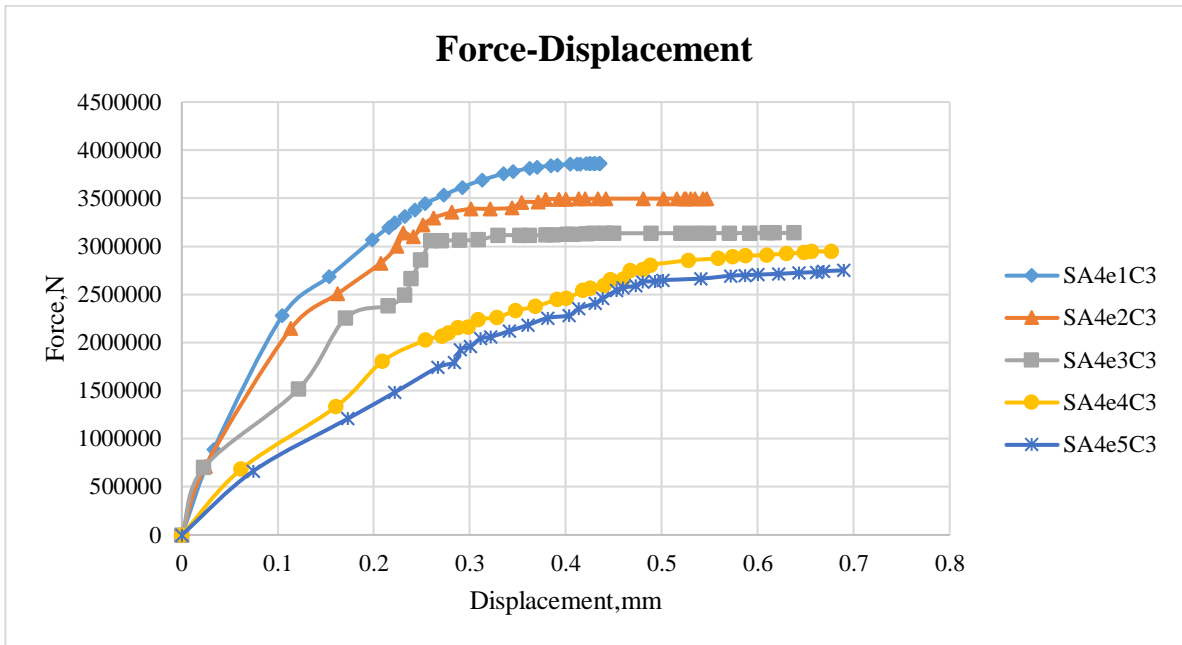


Figure A. 9: Load displacement curve for square, $f_{ck}=30\text{Mpa}$ ($\alpha=60$ deg.)

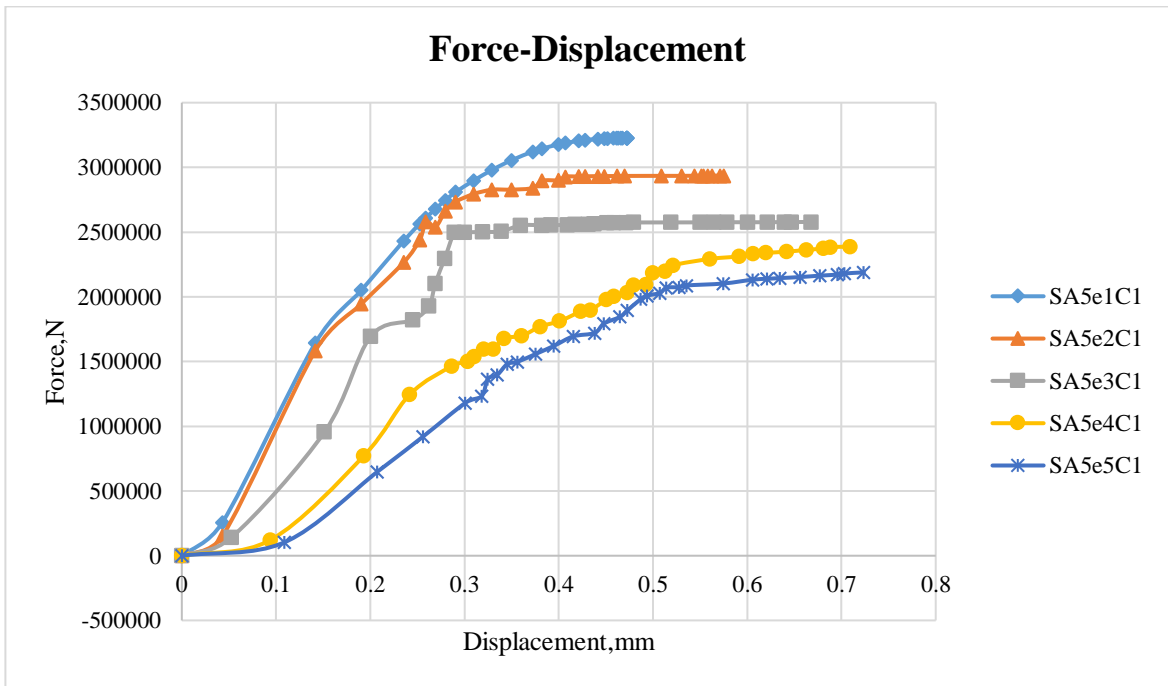


Figure A. 10: Load displacement curve for square, $f_{ck}=20\text{Mpa}$ ($\alpha=75$ deg.)

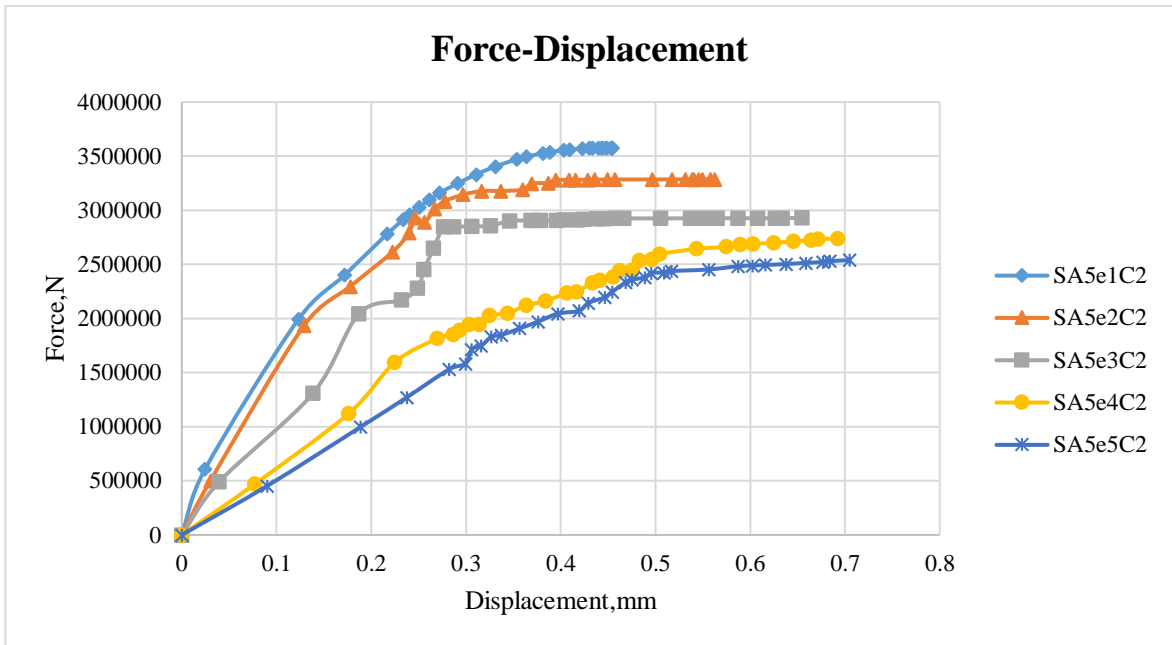


Figure A. 11: Load displacement curve for square, $f_{ck}=25\text{Mpa}$ ($\alpha=75$ deg.)

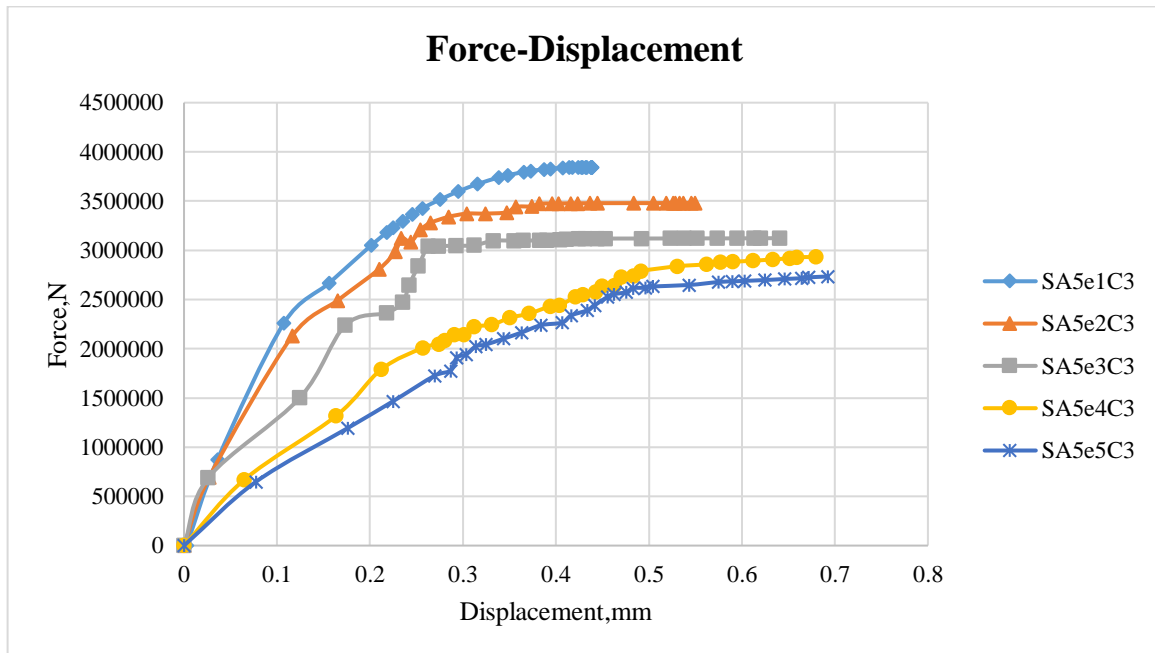


Figure A. 12: Load displacement curve for square, $f_{ck}=30\text{Mpa}$ ($\alpha=75$ deg.)

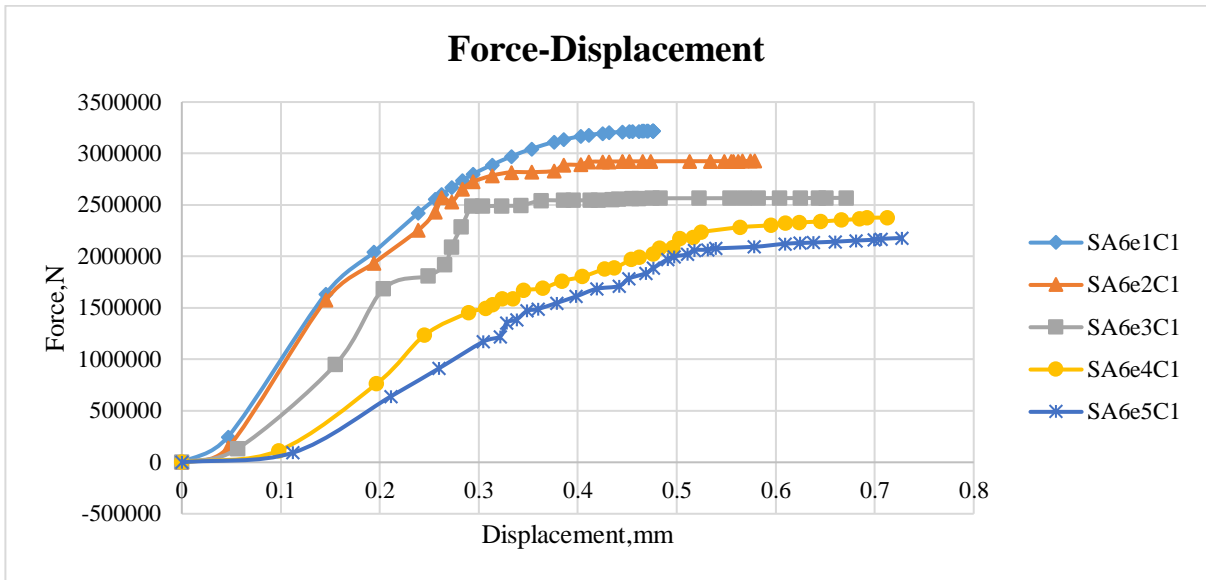


Figure A. 13: Load displacement curve for square, $f_{ck}=20\text{Mpa}$ ($\alpha=90$ deg.)

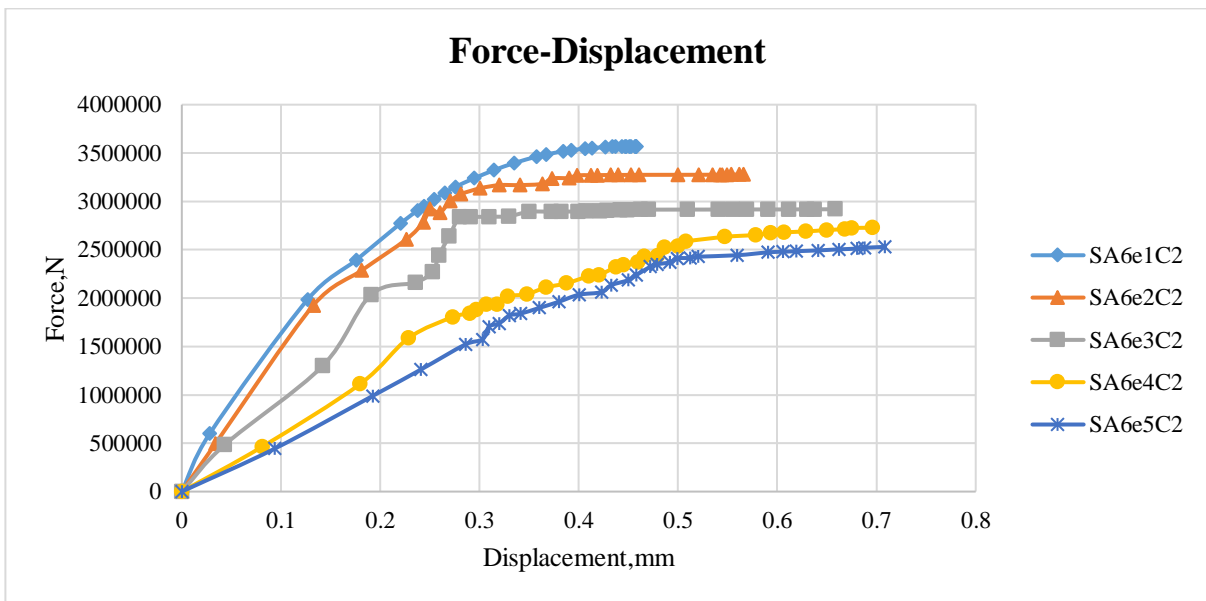


Figure A. 14: Load displacement curve for square, $f_{ck}=25\text{Mpa}$ ($\alpha=90$ deg.)

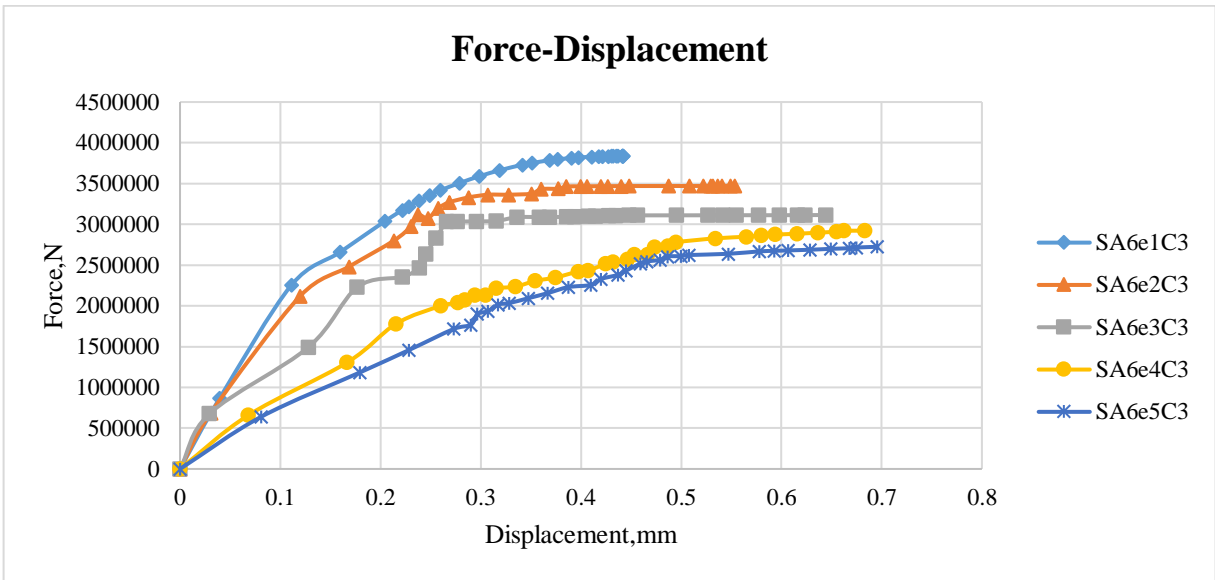


Figure A. 15: Load displacement curve for square, $f_{ck}=30\text{Mpa}$ ($\alpha=90$ deg.)

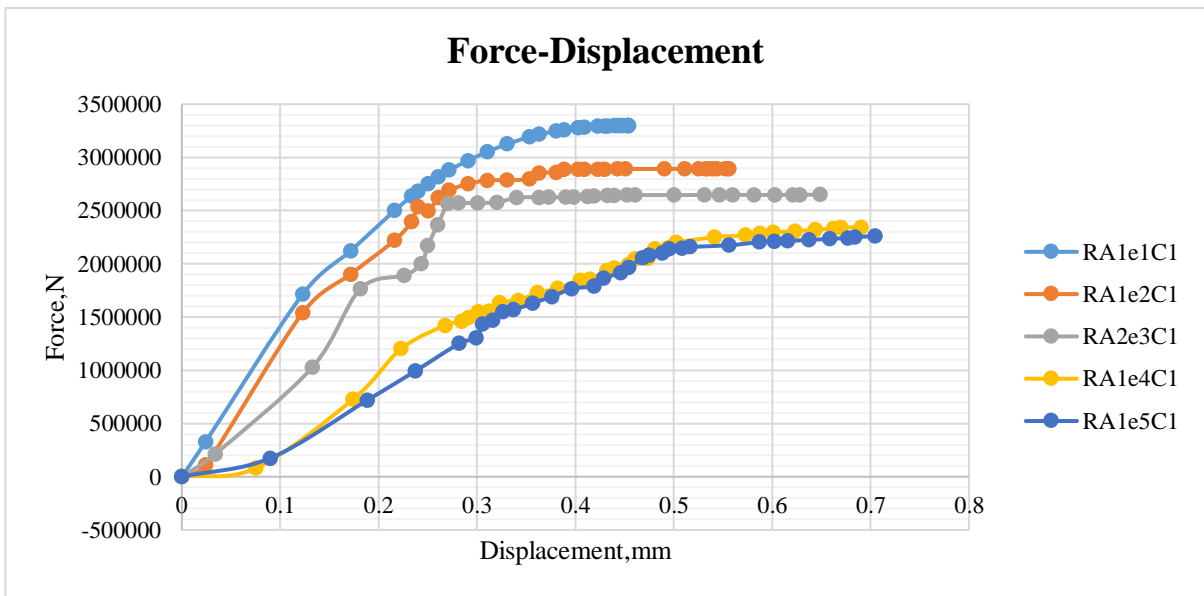


Figure A. 16: Load displacement curve for rectangle, $f_{ck}=20\text{Mpa}$ ($\alpha=15$ deg.)

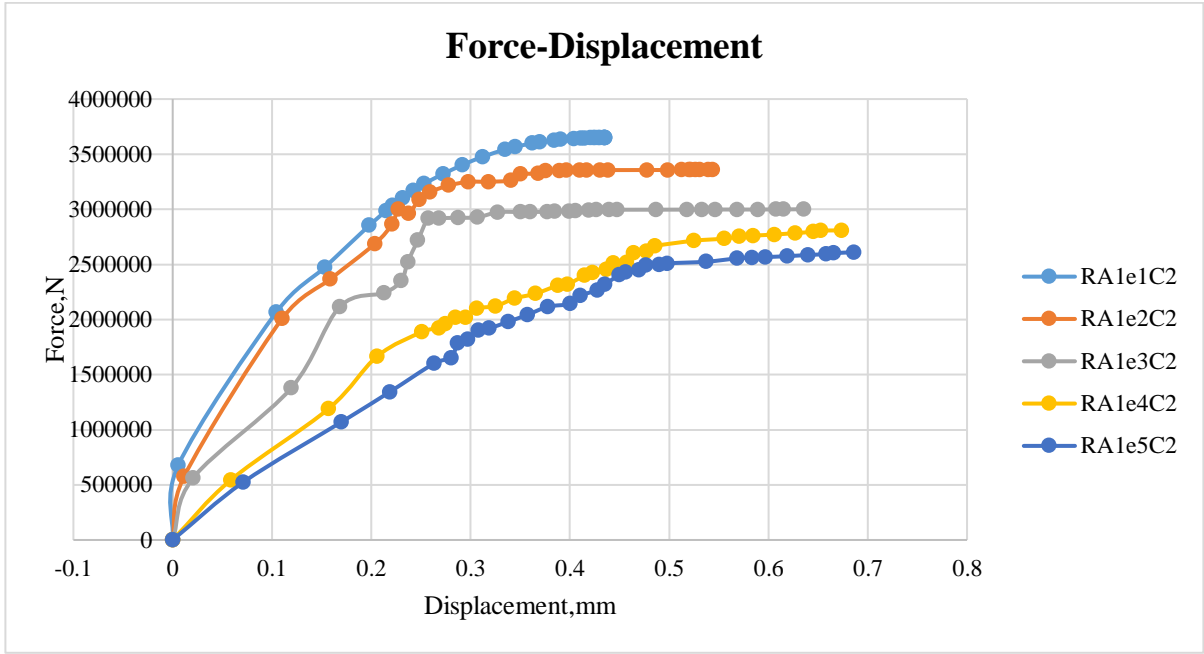


Figure A. 17: Load displacement curve for rectangle, $f_{ck}=25\text{Mpa}$ ($\alpha=15^\circ$)

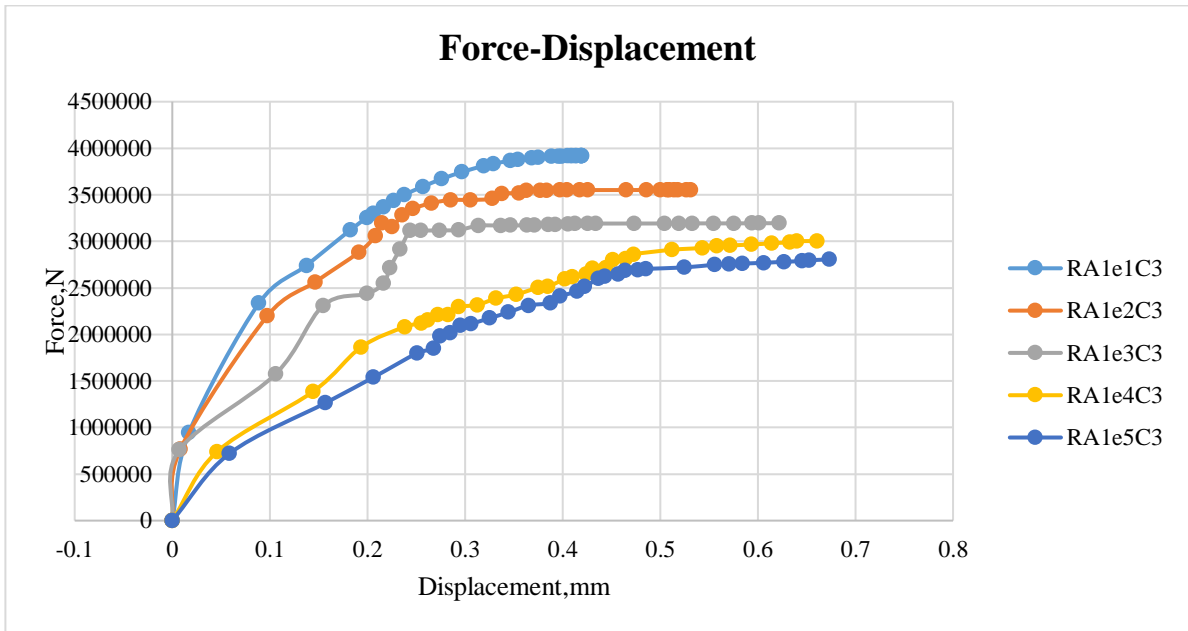


Figure A. 18: Load displacement curve for rectangle, $f_{ck}=30\text{Mpa}$ ($\alpha=15^\circ$)

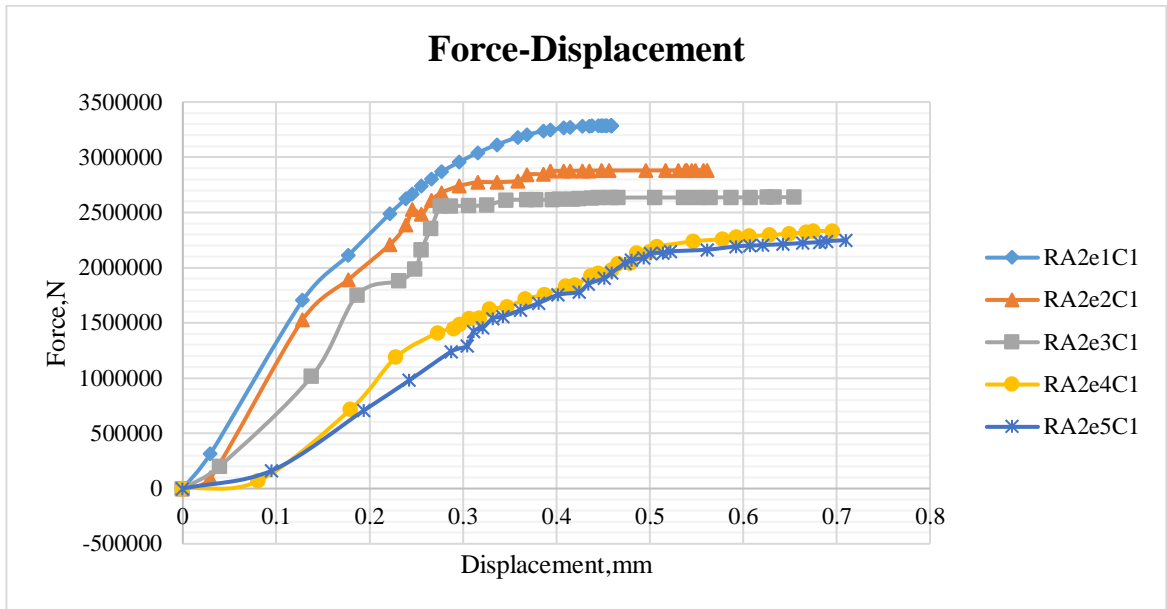


Figure A. 19: Load displacement curve for rectangle, $f_{ck}=20\text{Mpa}$ ($\alpha=30$ deg.)

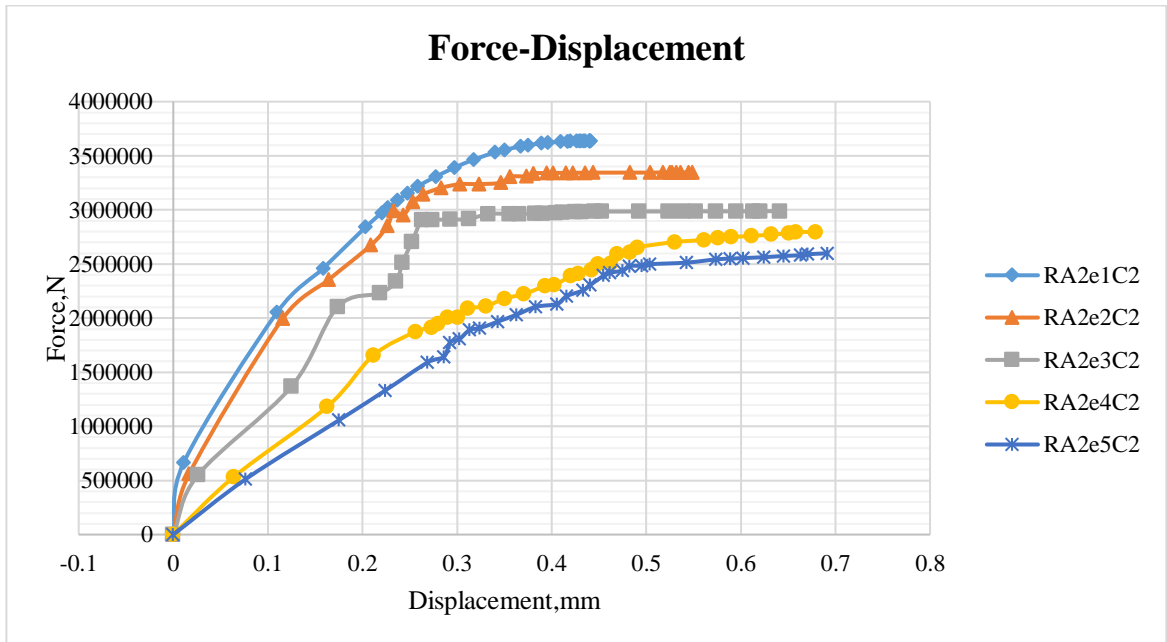


Figure A. 20: Load displacement curve for rectangle, $f_{ck}=25\text{Mpa}$ ($\alpha=30$ deg.)

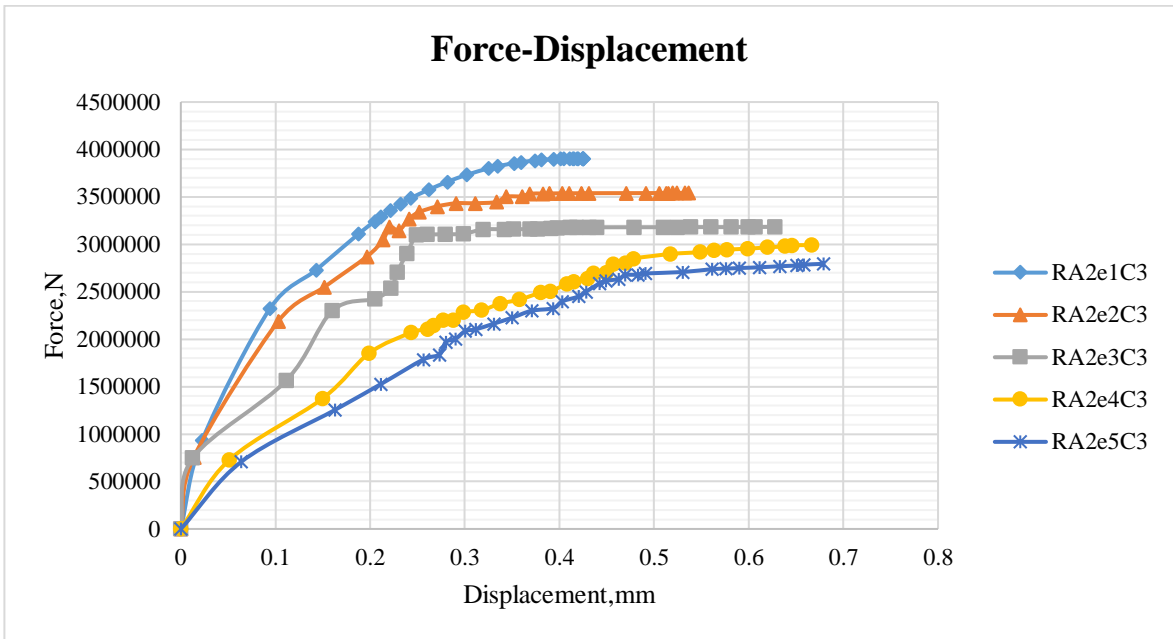


Figure A. 21: Load displacement curve for rectangle $f_{ck}=30\text{Mpa}$ ($\alpha=30$ deg.)

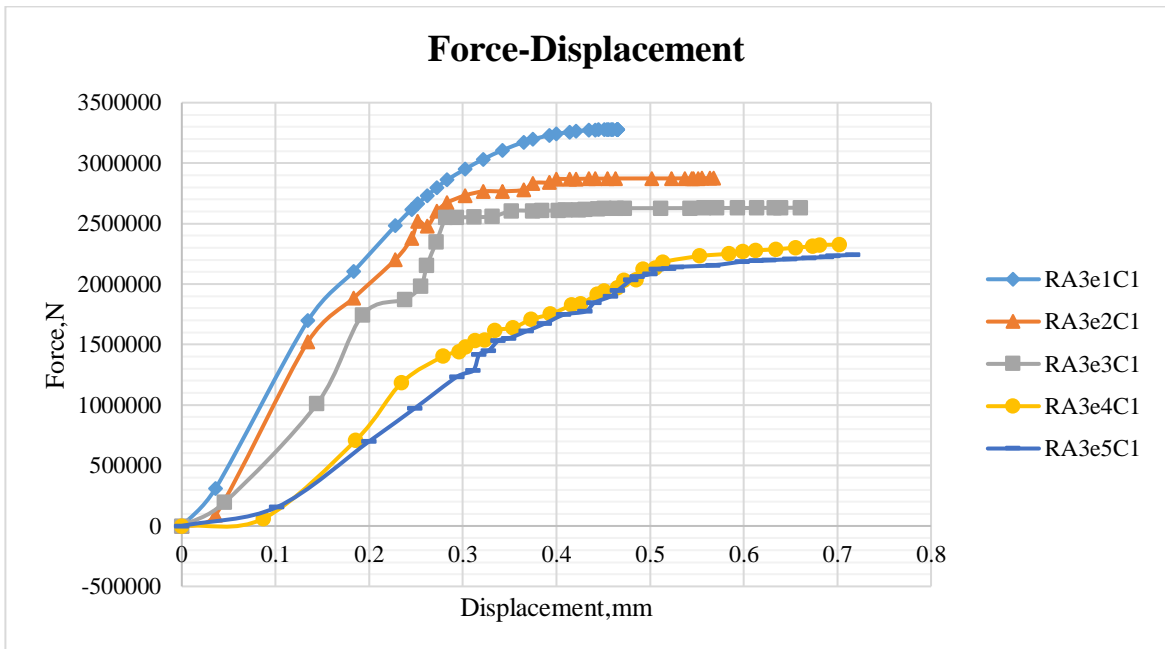


Figure A. 22: Load displacement curve for rectangle, $f_{ck}=20\text{Mpa}$ ($\alpha=45$ deg.)

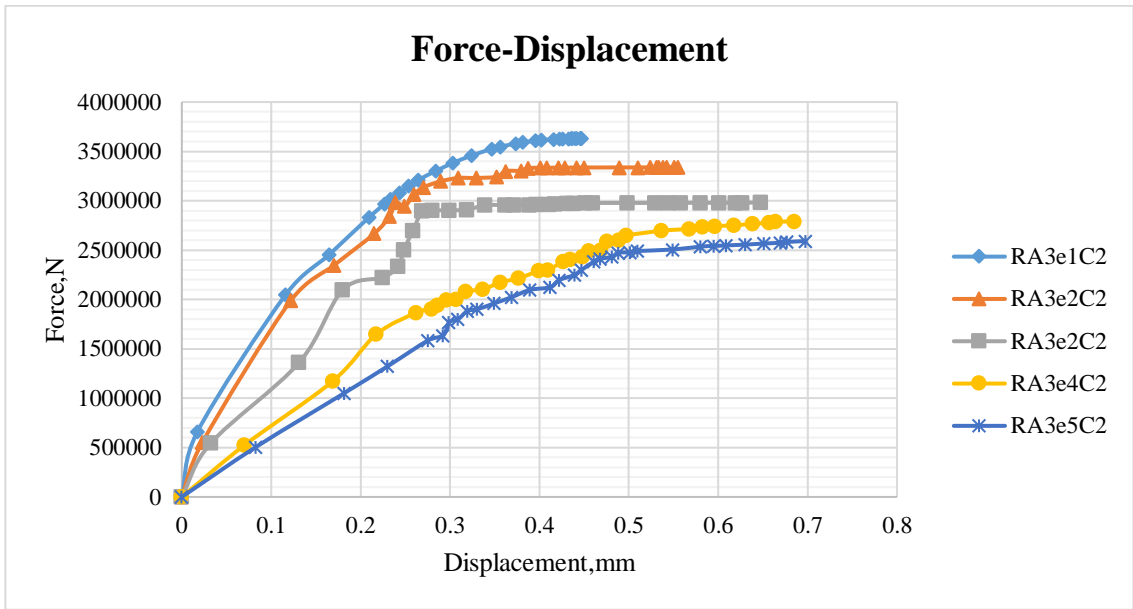


Figure A. 23: Load displacement curve for rectangle, $f_{ck}=25\text{Mpa}$ ($\alpha=45$ deg.)

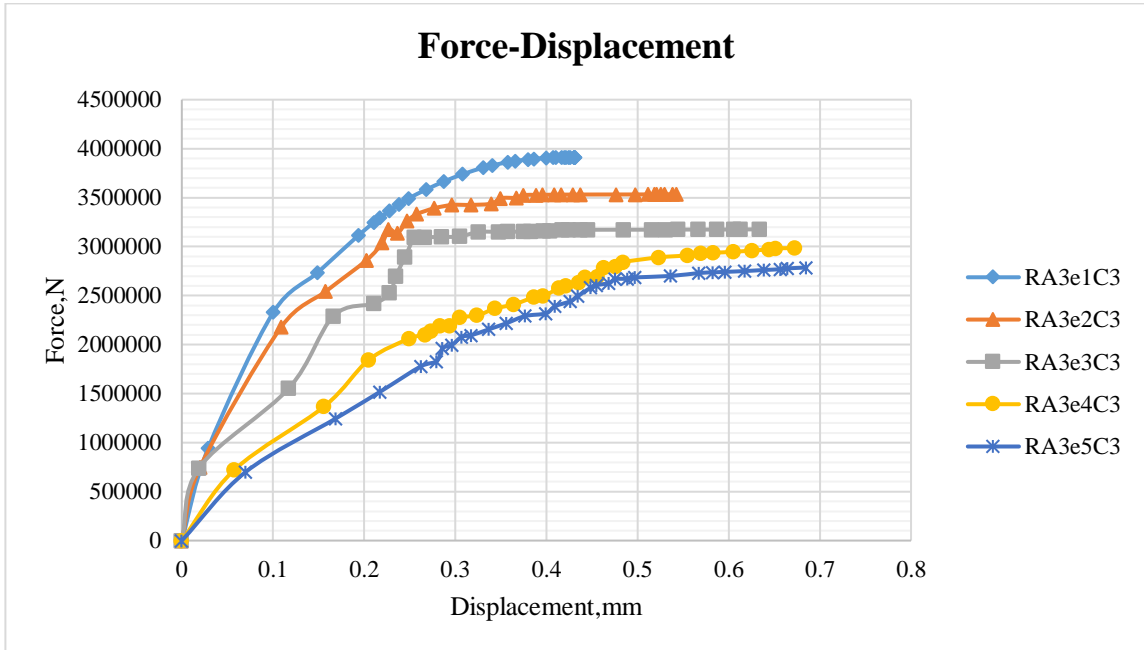


Figure A. 24: Load displacement curve for rectangle, $f_{ck}=30\text{Mpa}$ ($\alpha=45$ deg.)

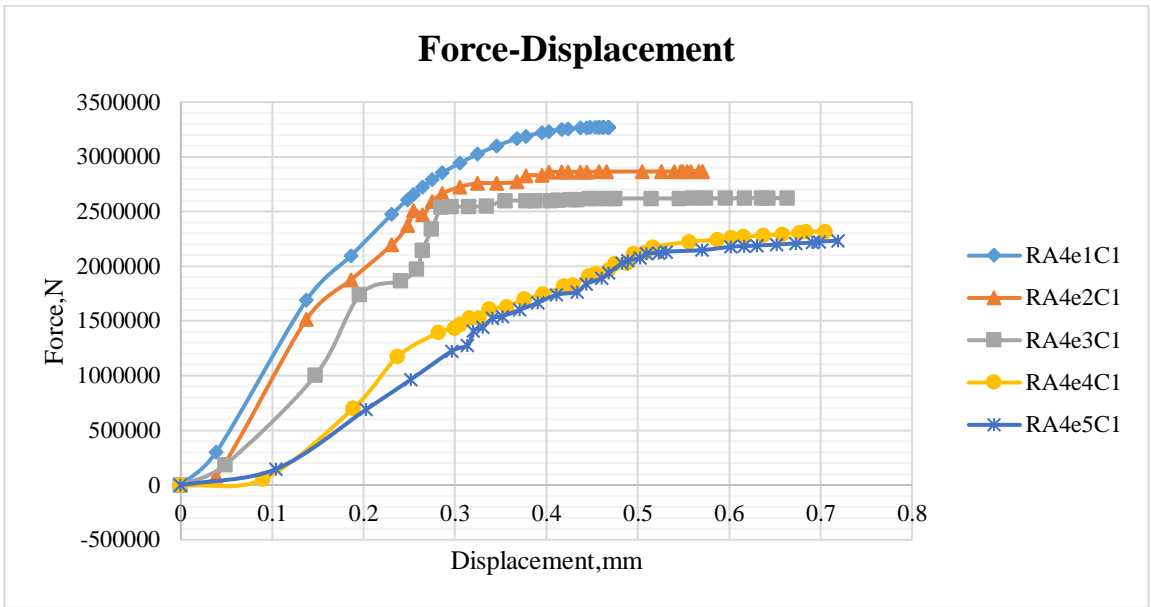


Figure A. 25: Load displacement curve for rectangle, fck=20Mpa ($\alpha=60$ deg.)

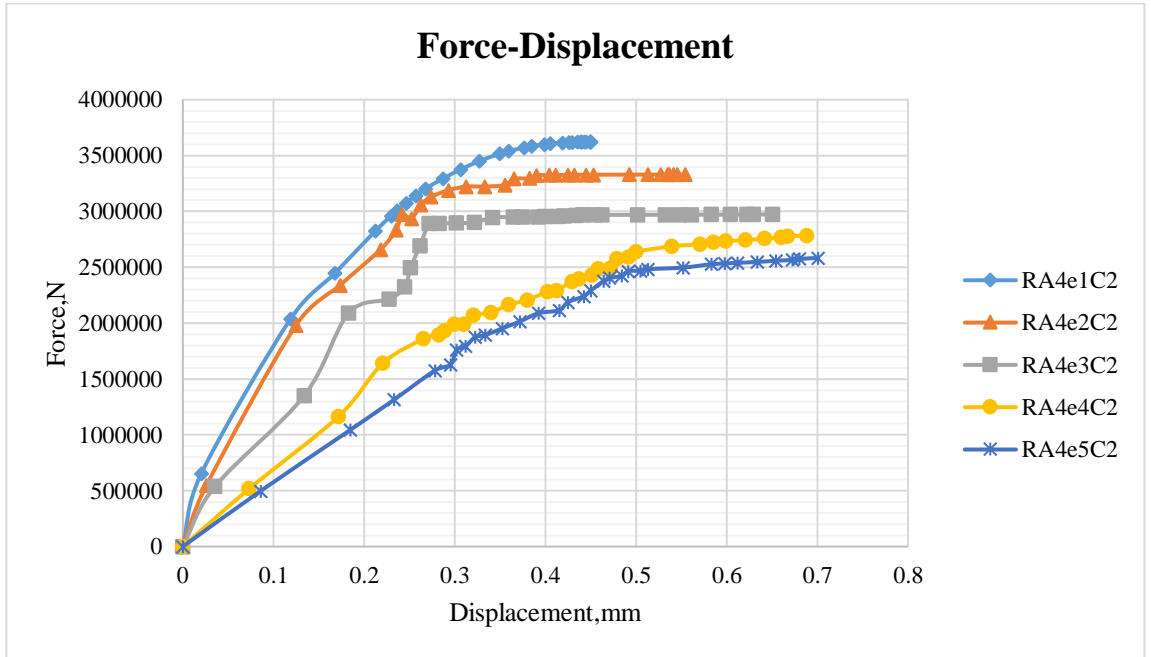


Figure A. 26: Load displacement curve for rectangle, fck=25Mpa ($\alpha=60$ deg.)

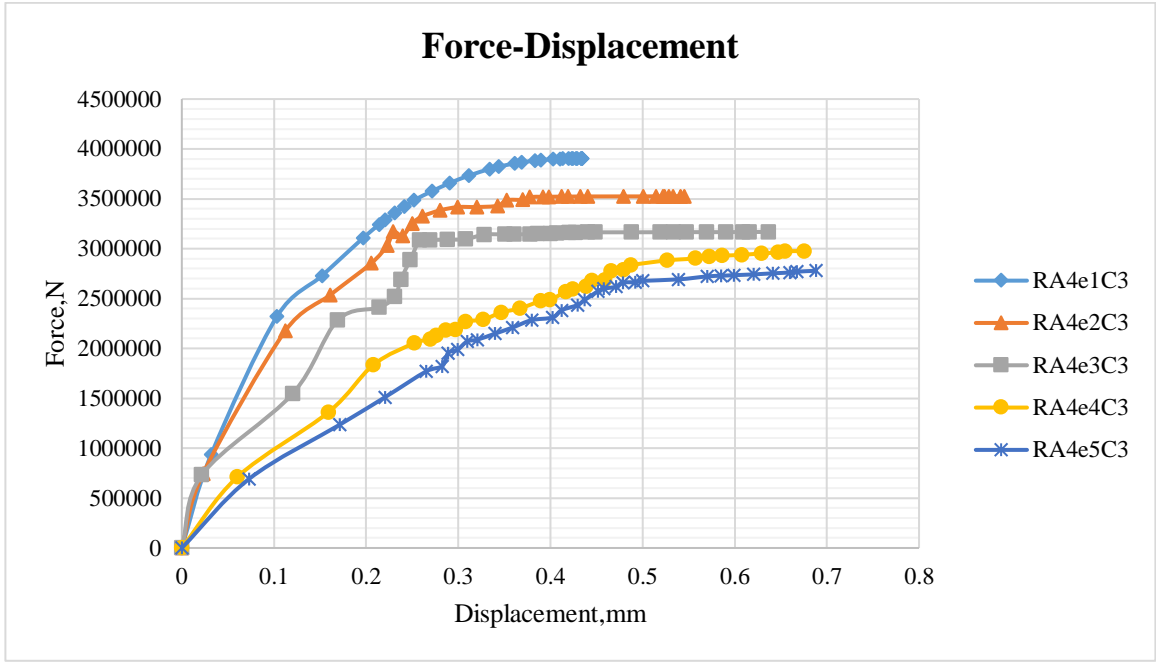


Figure A. 27: Load displacement curve for rectangle, $f_{ck}=30\text{Mpa}$ ($\alpha=60$ deg.)

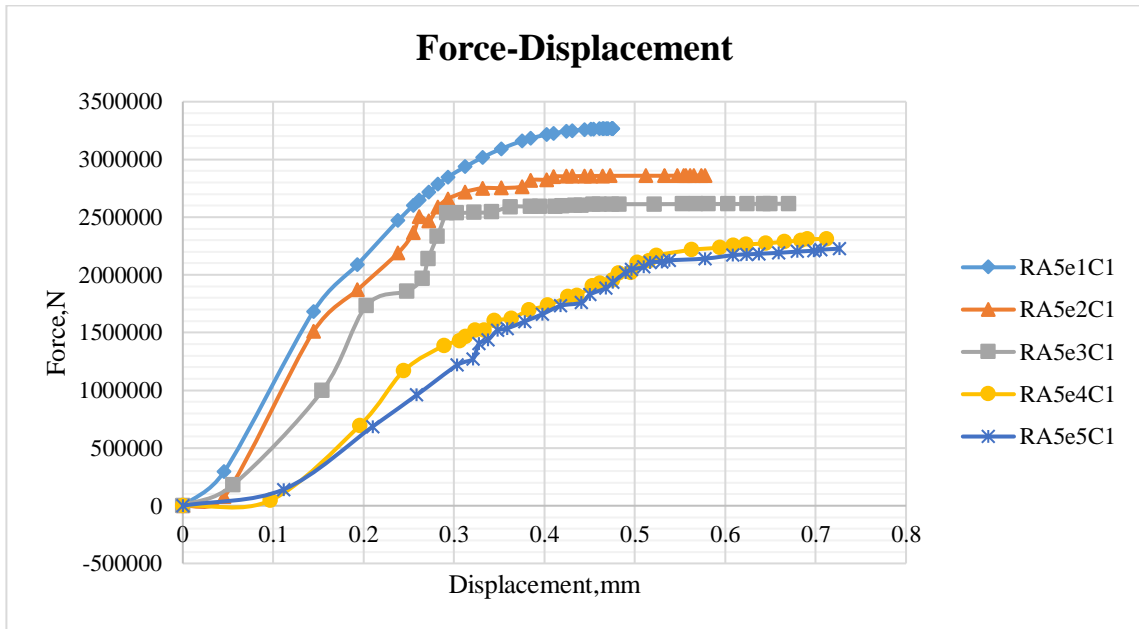


Figure A. 28: Load displacement curve for rectangle, $f_{ck}=20\text{Mpa}$ ($\alpha=75$ deg.)

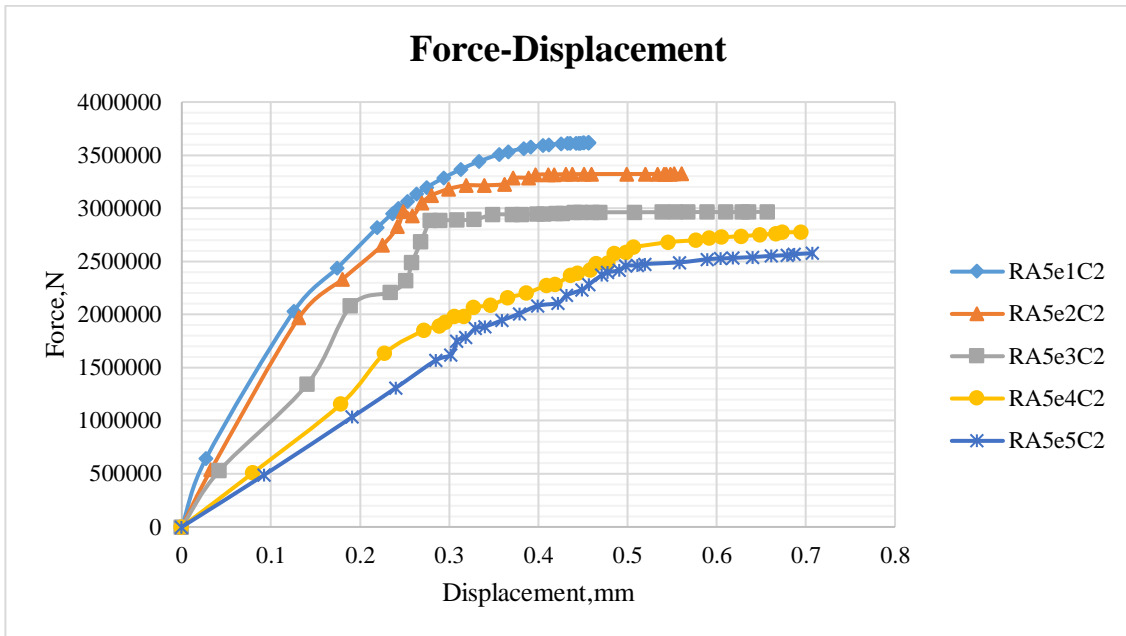


Figure A. 29: Load displacement curve for rectangle, $f_{ck}=25\text{Mpa}$ ($\alpha=75^\circ$ deg.)

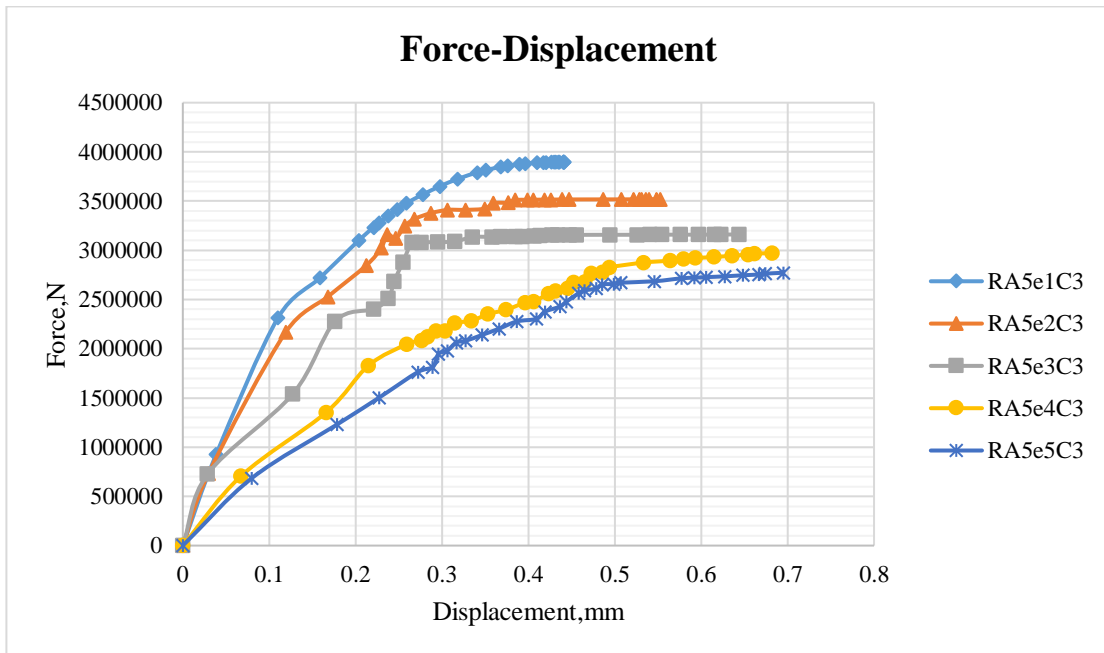


Figure A. 30: Load displacement curve for square, $f_{ck}=30\text{Mpa}$ ($\alpha=75^\circ$ deg.)

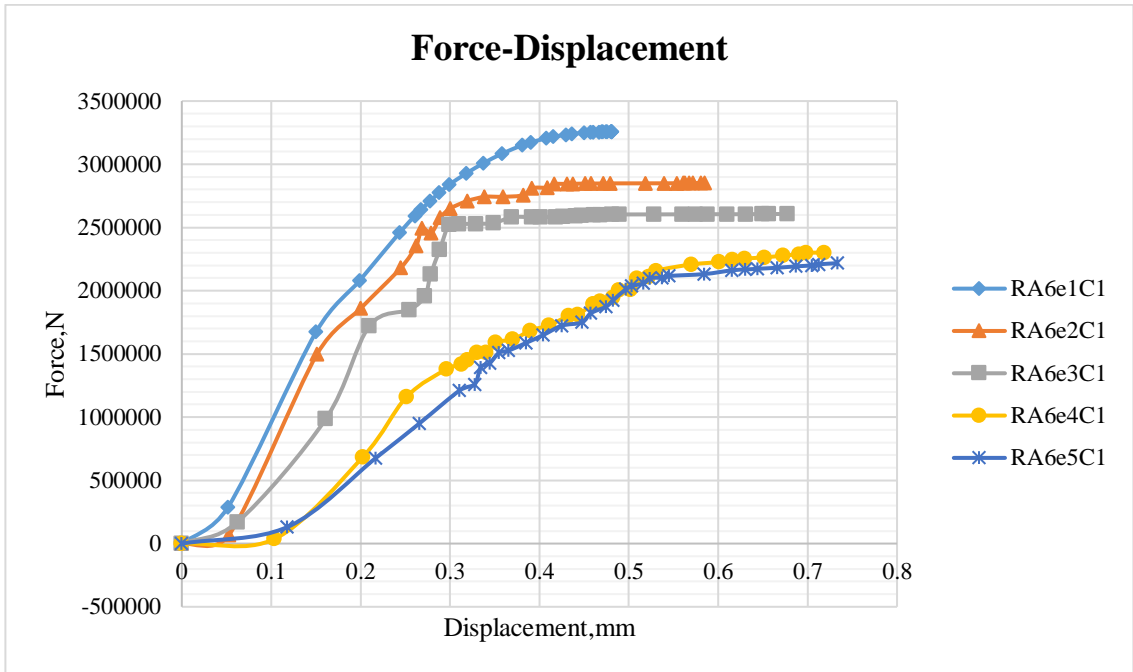


Figure A. 31: Load displacement curve for rectangle, $f_{ck}=20\text{Mpa}$ ($\alpha=90$ deg.)

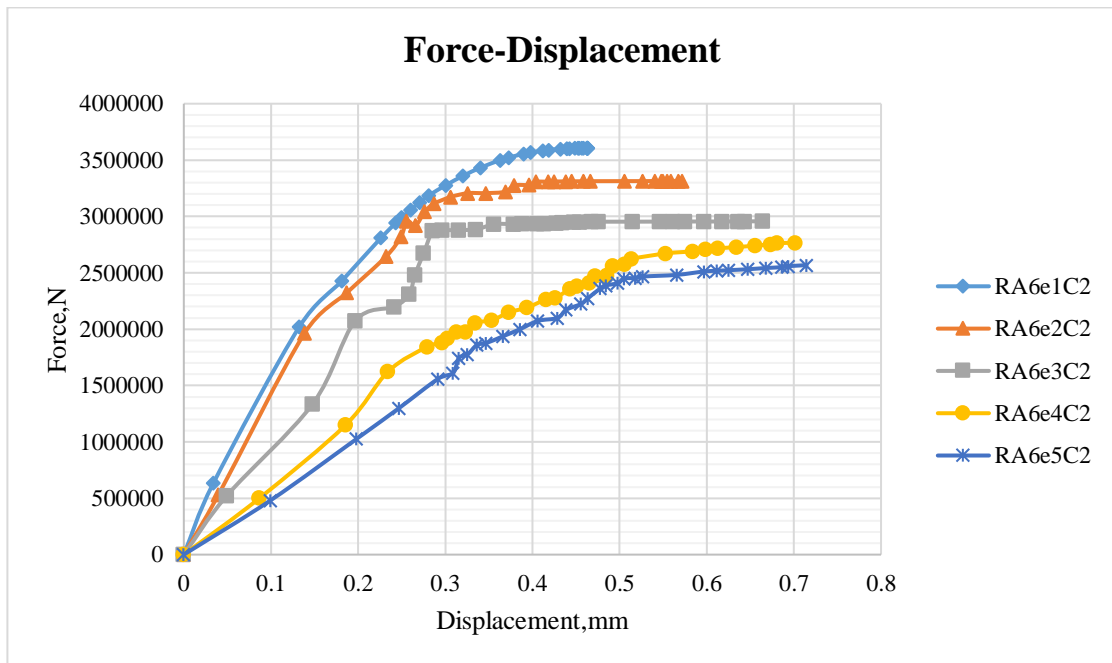


Figure A. 32: Load displacement curve for rectangle, $f_{ck}=25\text{Mpa}$ ($\alpha=90$ deg.)

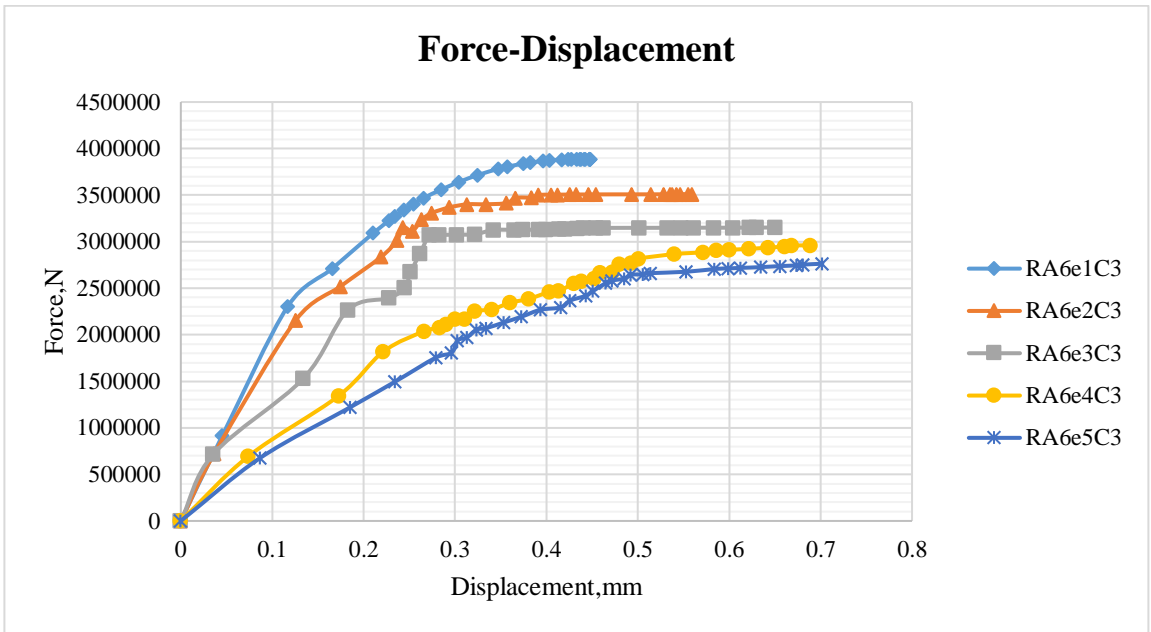


Figure A. 33: Load displacement curve for rectangle, $f_{ck}=30\text{Mpa}$ ($\alpha=90$ deg.)

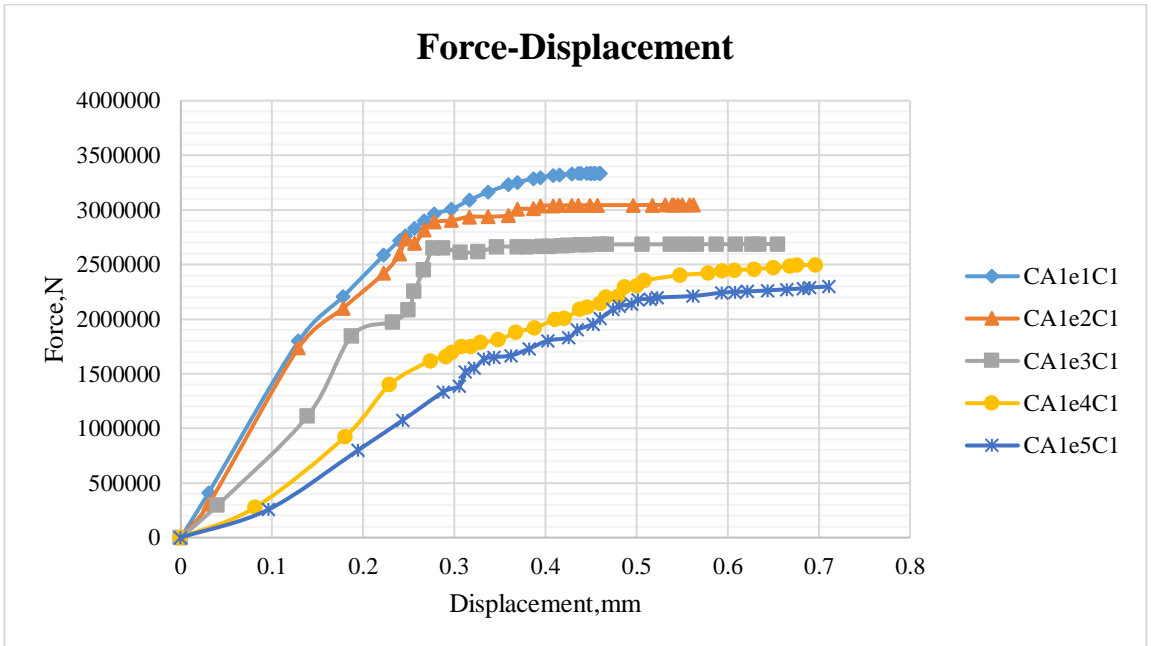


Figure A. 34: Load displacement curve for rectangle, $f_{ck}=20\text{Mpa}$ ($\alpha=15$ deg.)

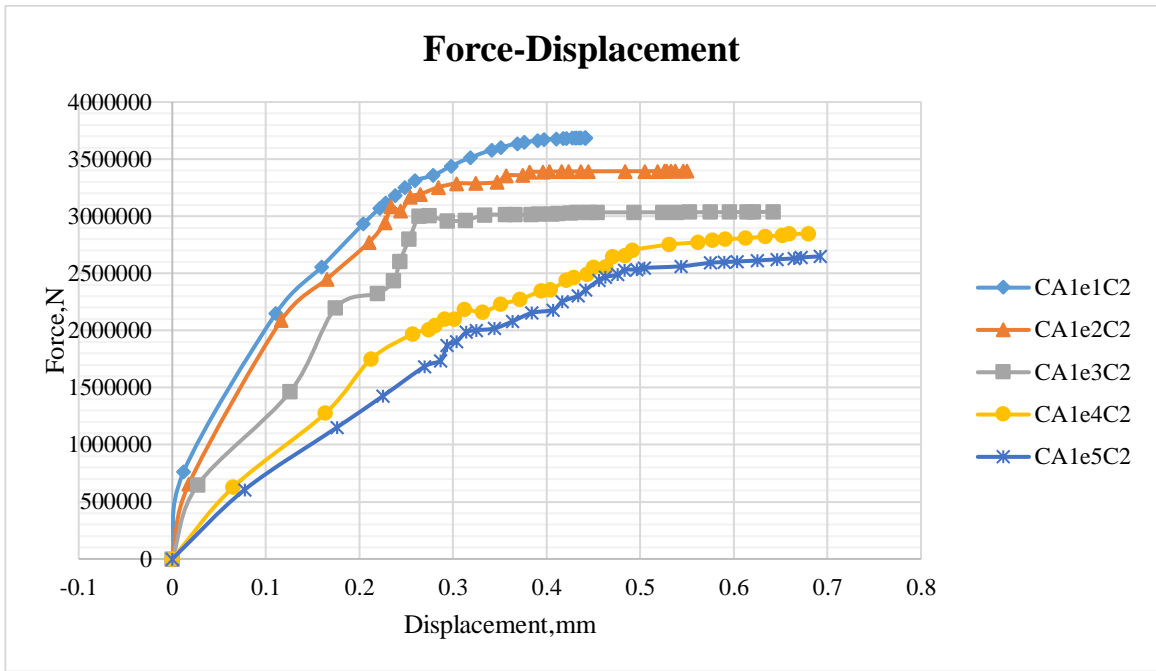


Figure A. 35: Load displacement curve for circle, $f_{ck}=25\text{Mpa}$ ($\alpha=15$ deg.)

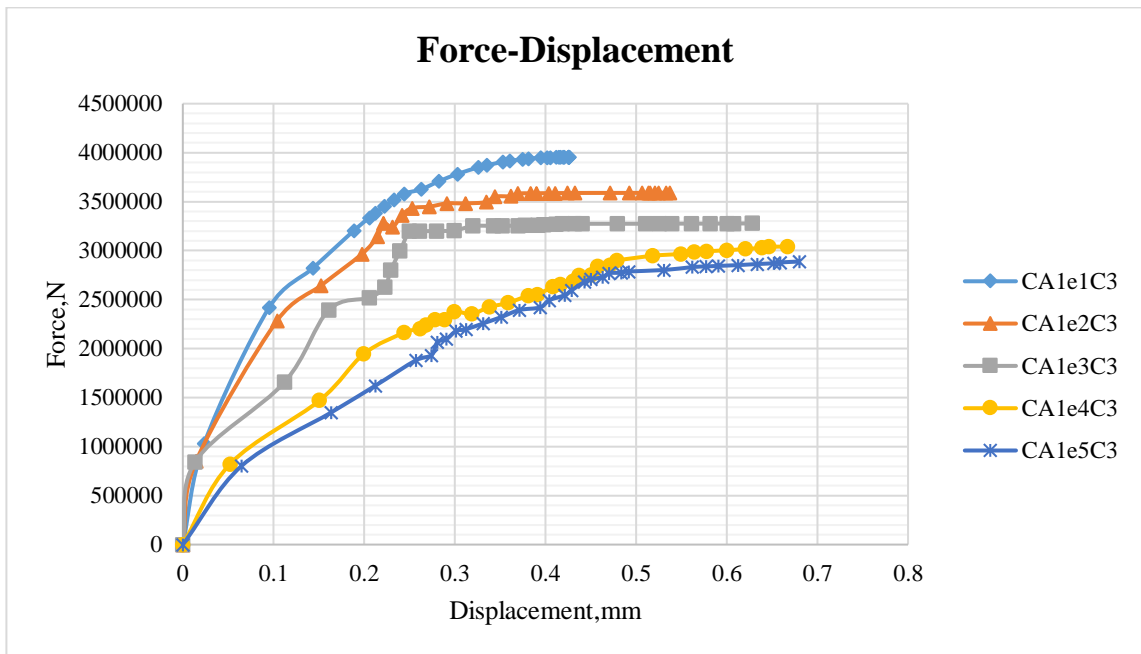


Figure A. 36: Load displacement curve for circle, $f_{ck}=30\text{Mpa}$ ($\alpha=15$ deg.)

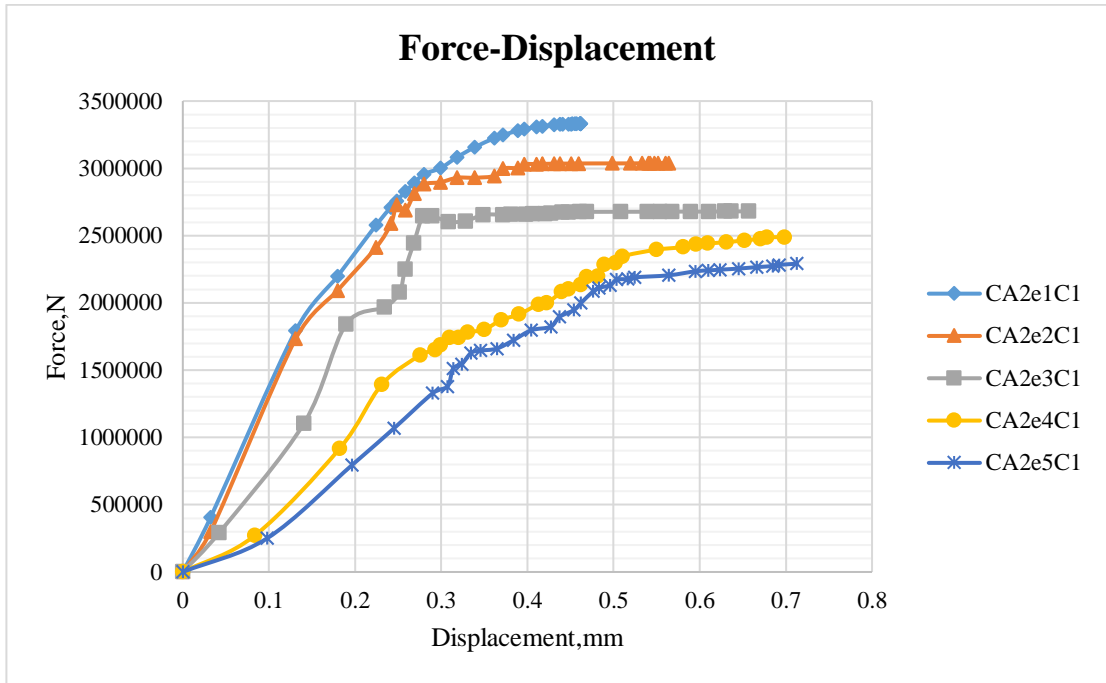


Figure A. 37: Load displacement curve for circle, $f_{ck}=20\text{Mpa}$ ($\alpha=30$ deg.)

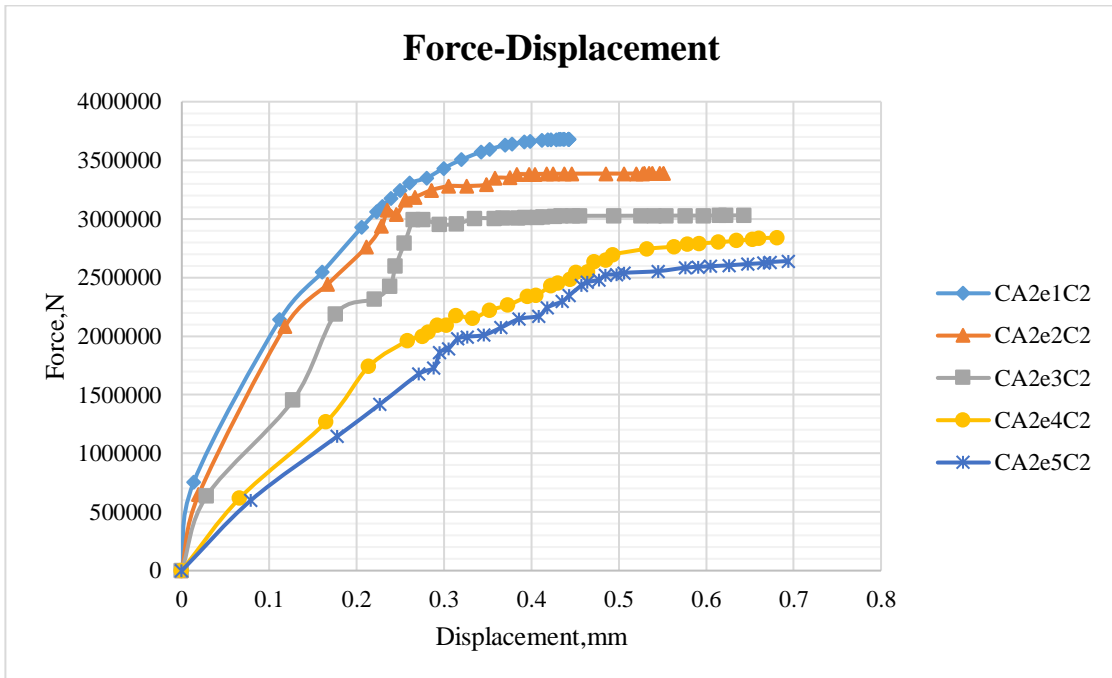


Figure A. 38: Load displacement curve for circle, $f_{ck}=25\text{Mpa}$ ($\alpha=30$ deg.)

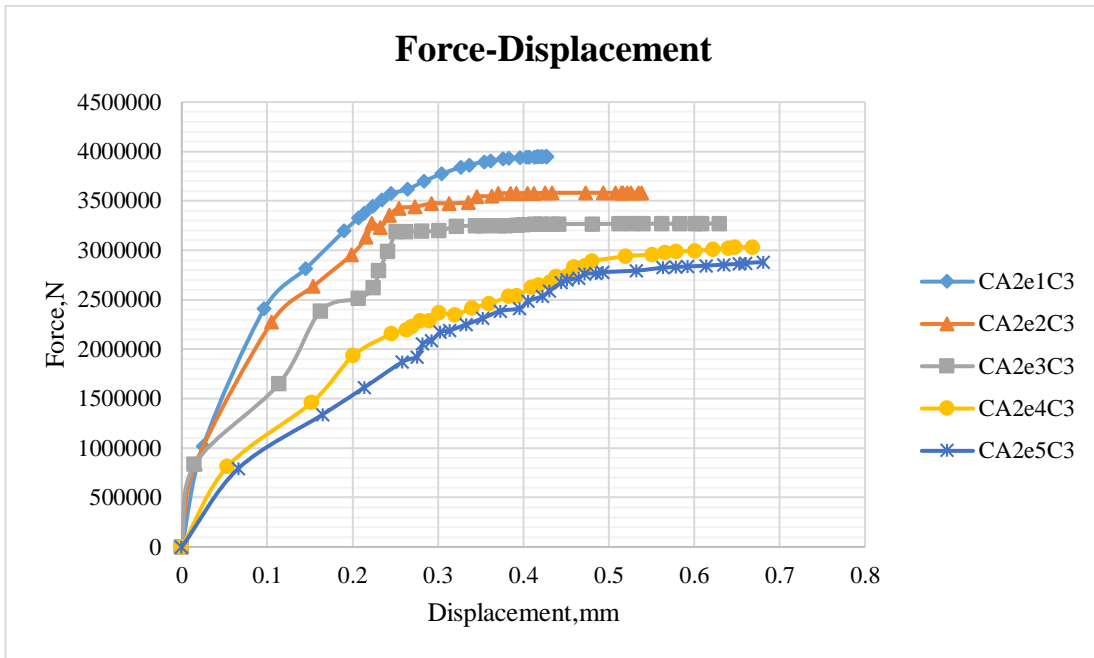


Figure A. 39: Load displacement curve for circle, $f_{ck}=30\text{Mpa}$ ($\alpha=30$ deg.)

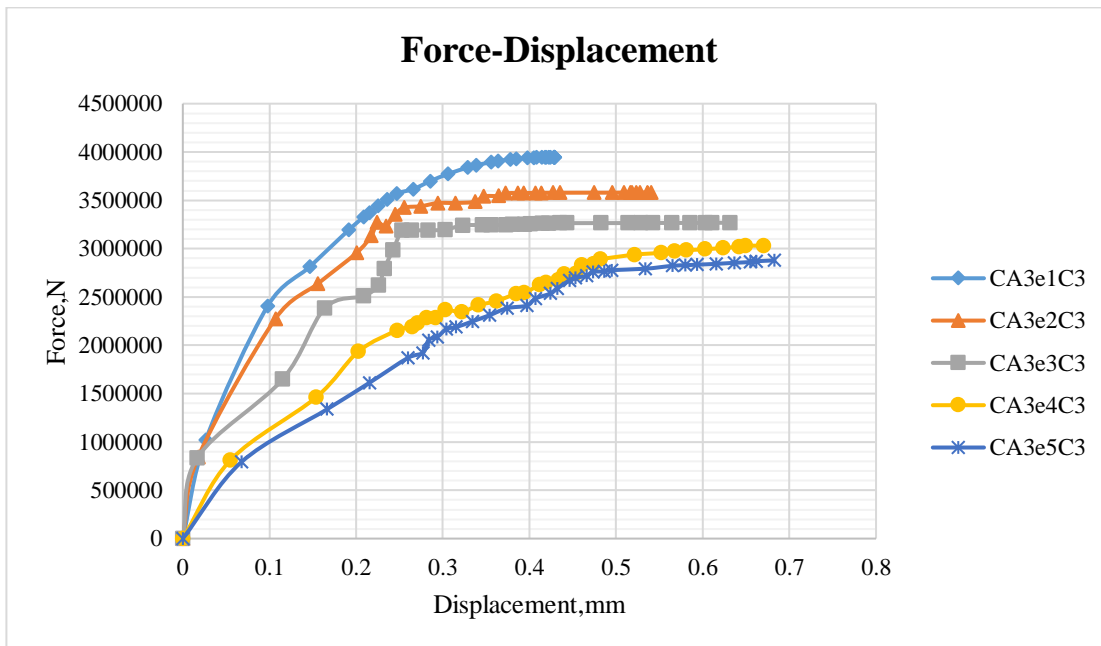


Figure A. 40: Load displacement curve for circle, $f_{ck}=30\text{Mpa}$ ($\alpha=45$ deg.)

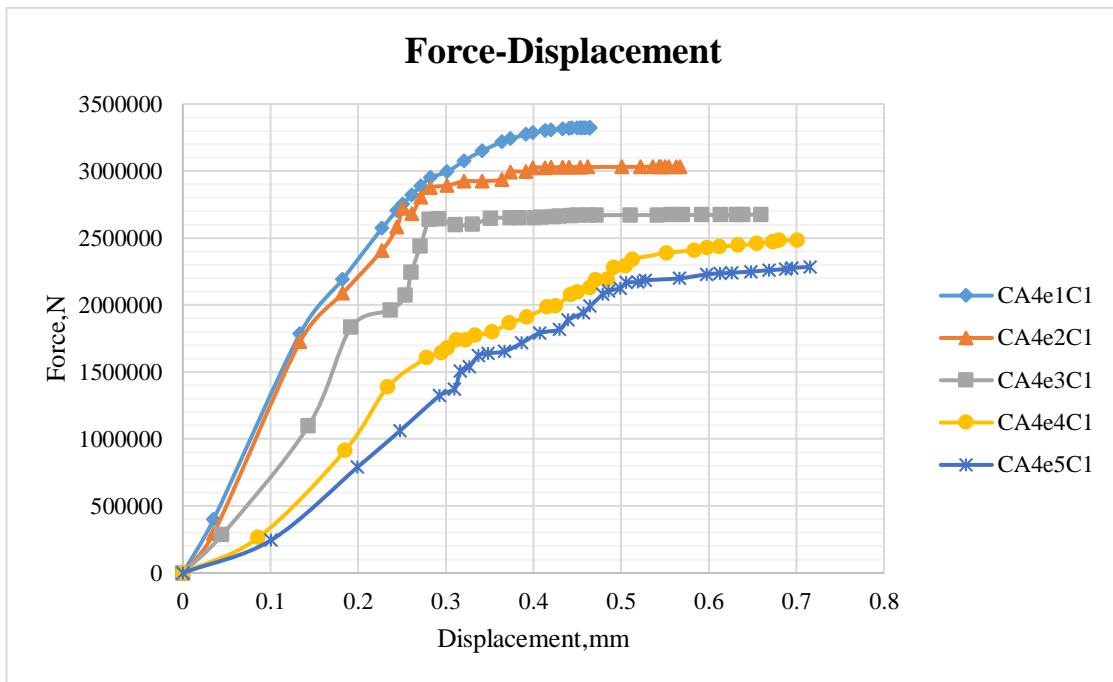


Figure A. 41: Load displacement curve for circle, $f_{ck}=20\text{Mpa}$ ($\alpha=60$ deg.)

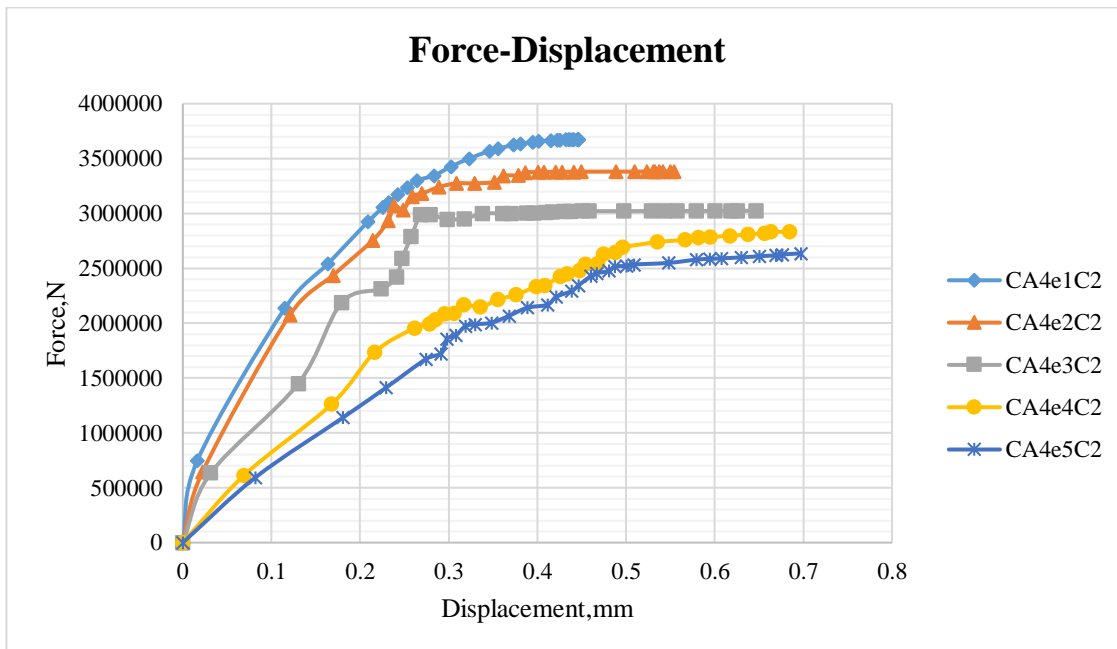


Figure A. 42: Load displacement curve for circle, $f_{ck}=25\text{Mpa}$ ($\alpha=60$ deg.)

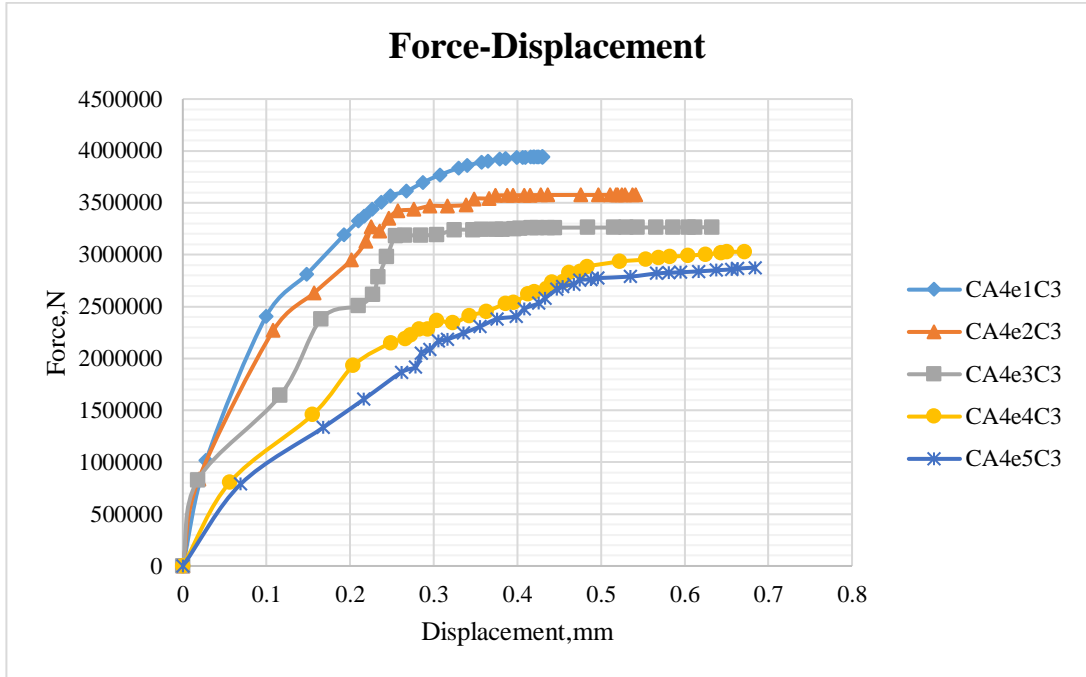


Figure A. 43: Load displacement curve for circle, $f_{ck}=30\text{Mpa}$ ($\alpha=60^\circ$)

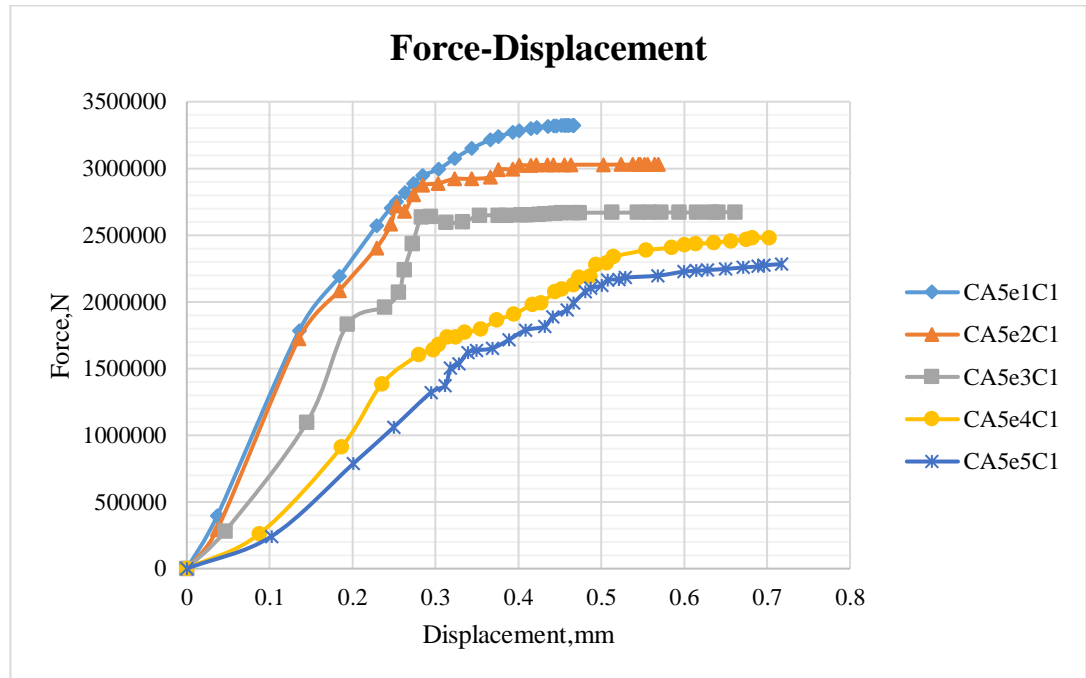


Figure A. 44: Load displacement curve for circle, $f_{ck}=20\text{Mpa}$ ($\alpha=75^\circ$)

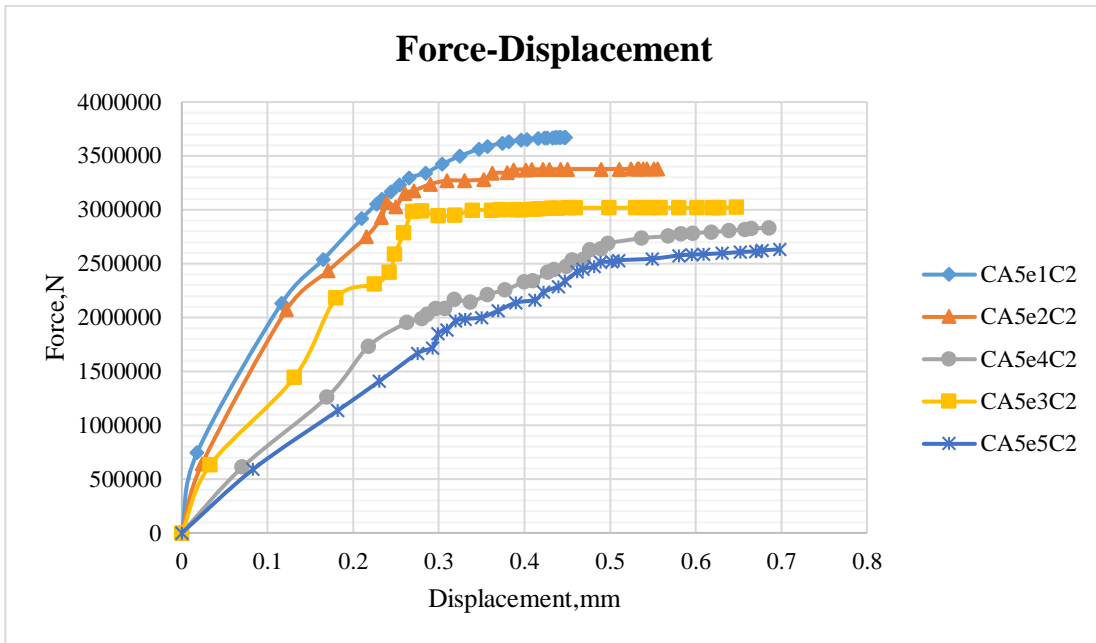


Figure A. 45: Load displacement curve for circle, $f_{ck}=25\text{Mpa}$ ($\alpha=75\text{ deg.}$)

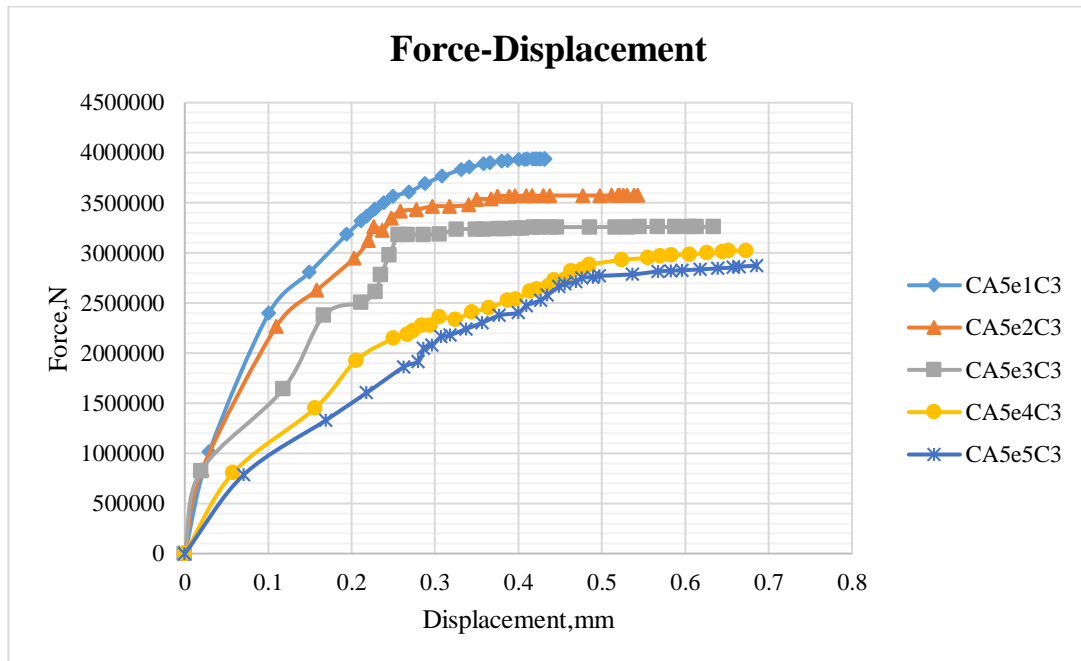


Figure A. 46: Load displacement curve for circle, $f_{ck}=30\text{Mpa}$ ($\alpha=75\text{ deg.}$)

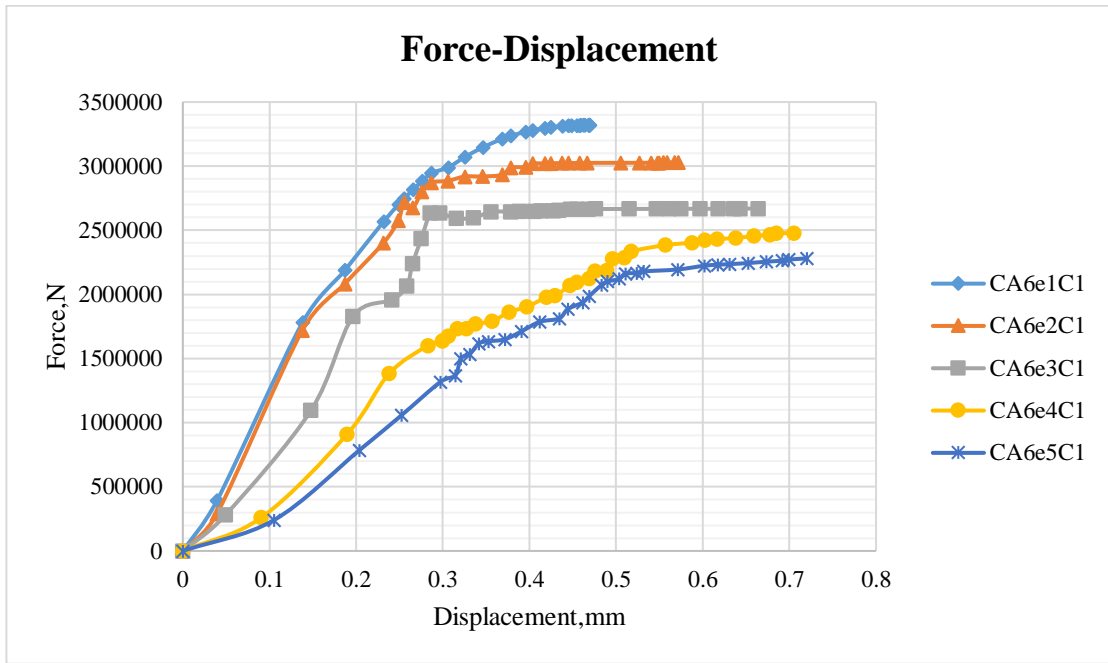


Figure A. 47: Load displacement curve for circle, $f_{ck}=20\text{Mpa}$ ($\alpha=90^\circ$ deg.)

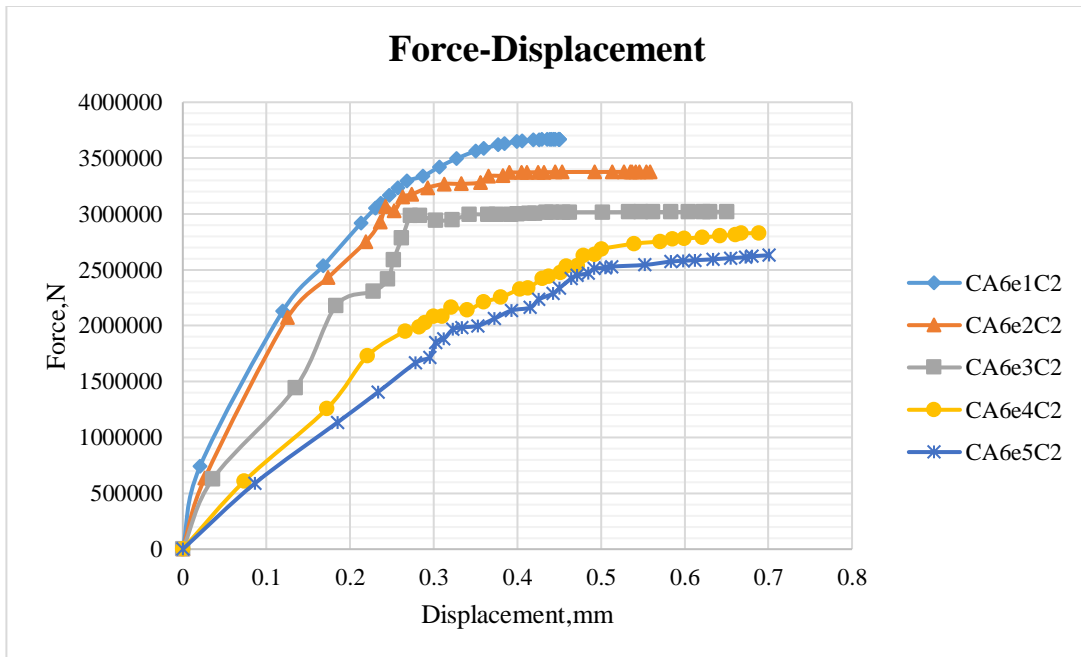


Figure A. 48: Load displacement curve for circle, $f_{ck}=25\text{Mpa}$ ($\alpha=90^\circ$ deg.)

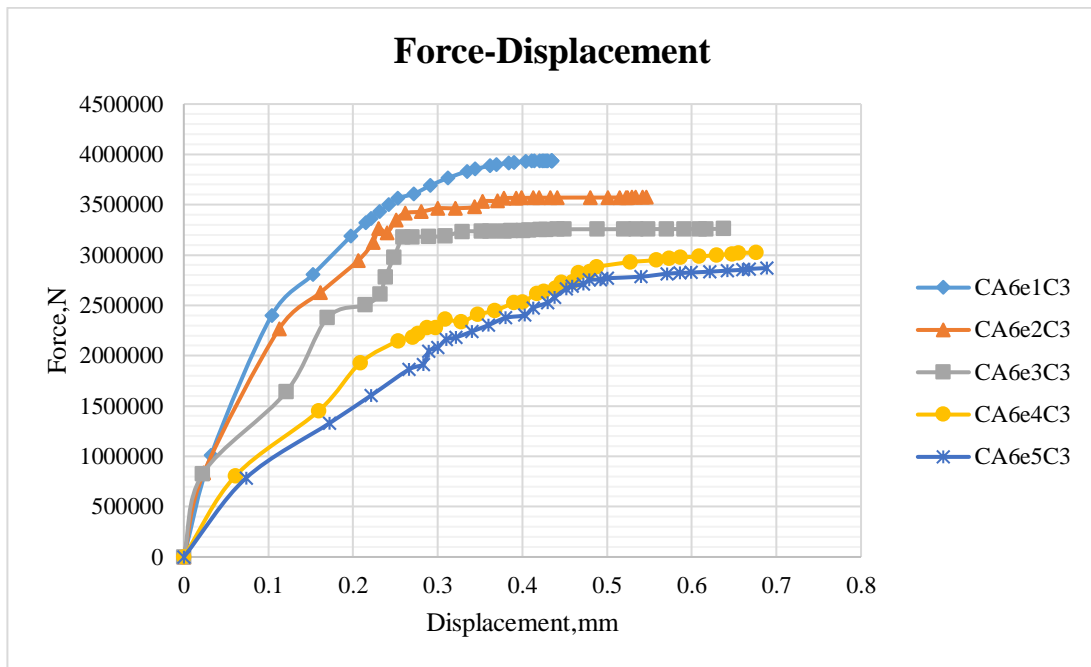


Figure A. 49: Load displacement curve for circle, $f_{ck}=30\text{Mpa}$ ($\alpha=90$ deg.)

APPENDIX-B

INPUT DATA OF MATERIAL PROPERTY

Table B. 1: Material properties for Longitudinal and lateral reinforcement

σ_{true}	ϵ_{pl}
509.2906	0
512.5644	0.012503
526.5894	0.017875
538.669	0.022058
549.7499	0.026694
555.1166	0.031336
561.5753	0.035258
571.6448	0.040297
578.1816	0.044174
580.3108	0.047839
584.8473	0.053068
587.38	0.057377
587.7519	0.060543
617.5162	0.109795
Stirrup	
f_y	E
350MPa	203Gpa
351.116	0

Table B. 2: Material properties for concrete fck 20Mpa

σ_c	ε_{in}	dc	ε_{in}	σ_t	ε_{cr}	dt	ε_{cr}
11.85196	0	0	0	2.222208	0	0	0
16.98421	0.000122	0.00011	9.02E-06	1.77362	0.000526	0.003867	1.16E-05
21.04514	0.000236	0.000526	4.3E-05	1.422671	0.001538	0.172753	0.000526
24.11078	0.000384	0.001512	0.000122	1.152845	0.003047	0.455038	0.001538
26.2501	0.000563	0.003	0.000236	0.948097	0.005054	0.72675	0.003047
27.52587	0.00077	0.005011	0.000384	0.794042	0.007559		
27.9953	0.001004	0.007577	0.000563	0.678445	0.010562		
28	0.001032	0.010736	0.00077	0.673486	0.013588		
27.71066	0.001264	0.014524	0.001004	0.591305	0.014065		
26.71979	0.001547	0.014989	0.001032	0.524712	0.018067		
25.06658	0.001852	0.01898	0.001264	0.472591	0.022569		
22.79135	0.002178	0.024136	0.001547	0.430403	0.027571		
19.9312	0.002523	0.030019	0.001852	0.39486	0.033072		
15.60236	0.002979	0.03665	0.002178	0.363653	0.039073		
		0.044044	0.002523	0.33522	0.045574		
		0.054327	0.002979	0.30856	0.052575		
				0.28307	0.060075		
				0.25843	0.068076		
				0.234503	0.076577		
				0.211272	0.085578		
				0.188786	0.095079		
				0.167123	0.105079		
				0.146371	0.11558		
				0.126612	0.126581		
				0.107908	0.138081		
				0.090306	0.150082		
				0.073827	0.162582		
				0.058476	0.175583		
				0	0.190965		

Table B. 3: Material properties for concrete fck 25Mpa

σ_c	ε_{in}	dc	ε_{in}	σ_t	ε_{cr}	dt	ε_{cr}
13.19998	0	0	0	2.578644	0	0	0
18.97448	0.000101	5.81E-05	4.95E-06	2.000683	0.00053	0.00433	1.15E-05
23.71899	0.0002	0.000406	3.44E-05	1.563457	0.001543	0.194828	0.00053
27.45947	0.000331	0.001209	0.000101	1.239596	0.003053	0.501071	0.001543
30.22102	0.000494	0.002443	0.0002	1.003256	0.005061	0.773365	0.003053
32.02791	0.000686	0.004142	0.000331	0.832111	0.007566		
32.9036	0.000908	0.006348	0.000494	0.707982	0.01057		
33	0.001021	0.009111	0.000686	0.70274	0.013595		
32.8708	0.001159	0.012487	0.000908	0.616716	0.014073		
31.95149	0.001439	0.014271	0.001021	0.547711	0.018075		
30.16693	0.001745	0.016533	0.001159	0.493306	0.022576		
27.53774	0.002079	0.021309	0.001439	0.448166	0.027578		
24.08385	0.002439	0.02687	0.001745	0.408728	0.033079		
18.94994	0.002898	0.033269	0.002079	0.37273	0.03908		
		0.040552	0.002439	0.338831	0.045581		
		0.050382	0.002898	0.306321	0.052582		
				0.274893	0.060083		
				0.244489	0.068084		
				0.215184	0.076585		
				0.187113	0.085586		
				0.160418	0.095087		
				0.135225	0.105088		
				0.111626	0.115588		
				0.089673	0.126589		
				0.069381	0.13809		
				0.050731	0.15009		
				0.033671	0.162591		
				0.018131	0.175591		
				0	0.189244		

Table B. 4: Material properties for concrete fck 30Mpa

σ_c	ϵ_{in}	d_c	ϵ_{in}	σ_t	ϵ_{cr}	d_t	ϵ_{cr}
14.86167	0	0	0	2.911916	0	0	0
21.16115	8.77E-05	1.98E-05	1.87E-06	2.202727	0.000532	0.004609	1.11E-05
26.48328	0.000176	0.000315	2.96E-05	1.682376	0.001548	0.214537	0.000532
30.81471	0.000294	0.000943	8.77E-05	1.309809	0.003059	0.539806	0.001548
34.14188	0.000442	0.001917	0.000176	1.047298	0.005067	0.808825	0.003059
36.45094	0.000622	0.00327	0.000294	0.863387	0.007572		
37.72782	0.000833	0.005046	0.000442	0.733488	0.010576		
38	0.001005	0.007295	0.000622	0.728059	0.013601		
37.95817	0.001076	0.010077	0.000833	0.63933	0.014079		
37.12736	0.001351	0.012445	0.001005	0.567925	0.018081		
35.22053	0.00166	0.013461	0.001076	0.510443	0.022583		
32.22249	0.002001	0.017519	0.001351	0.461161	0.027584		
28.1178	0.002376	0.022327	0.00166	0.416587	0.033085		
22.47459	0.002816	0.027967	0.002001	0.374758	0.039087		
		0.034518	0.002376	0.334711	0.045588		
		0.042638	0.002816	0.296098	0.052589		
				0.258917	0.06009		
				0.223329	0.068091		
				0.189552	0.076592		
				0.157784	0.085593		
				0.128178	0.095094		
				0.10082	0.105095		
				0.075735	0.115595		
				0.052889	0.126596		
				0.032201	0.138097		
				0.013555	0.150097		
				-0.00319	0.162598		
				-0.01819	0.175598		
				0	0.187998		

Table B. 5: Material properties of concrete with fck 26.9Mpa for validation

ein	σ_c	ein	dc	ϵ_{cr}	σ_t	ecr	dt
0	13.96402	0	0	0	2.708365	0	0
9.72357E-05	19.9247	3.67E-06	4.46E-05	0.000531	2.080458	1.14E-05	0.004457
0.00019259	24.87516	3.34E-05	0.000408	0.001545	1.611106	0.000531	0.202601
0.000319197	28.82515	9.72E-05	0.001202	0.003055	1.268048	0.001545	0.516611
0.000476758	31.78428	0.000193	0.002425	0.005063	1.021135	0.003055	0.787998
0.000664976	33.76204	0.000319	0.004117	0.007568	0.844679		
0.000883558	34.76778	0.000477	0.006327	0.010572	0.718093		
0.001015236	34.9	0.000665	0.009114	0.013597	0.712771		
0.001132215	34.81078	0.000884	0.012544	0.014075	0.625637		
0.001410661	33.90015	0.001015	0.014707	0.018077	0.555753		
0.001718616	32.04492	0.001132	0.016688	0.022579	0.500284		
0.002055801	29.25399	0.001411	0.021618	0.02758	0.453699		
0.002421941	25.53616	0.001719	0.027407	0.033082	0.412426		
0.002866626	20.27533	0.002056	0.034125	0.039083	0.374292		
		0.002422	0.041835	0.045584	0.33809		
		0.002867	0.051734	0.052585	0.303242		
				0.060086	0.269562		
				0.068087	0.237084		
				0.076588	0.205948		
				0.085589	0.176323		
				0.09509	0.148366		
				0.105091	0.122196		
				0.115591	0.097887		
				0.126592	0.075464		
				0.138093	0.054908		
				0.150093	0.036165		
				0.162594	0.019151		
				0.175594	0.003762		
				0.188725	0		